PONTIFICIA UNIVERSIDAD CATOLICA DE CHILE

ESCUELA DE INGENIERIA

HYDRODYNAMIC MODELLING OF TIDAL CURRENTS AT CHACAO CHANNEL FOR A PRELIMINARY ENERGY RESOURCE ASSESSMENT

NILS ERIK MIGUEL LINDEEN DE LA FUENTE

Thesis submitted to the Office of Research and Graduate Studies in partial fulfillment of the requirements for the Degree of Master of Science in Engineering

Advisor:

RODRIGO CIENFUEGOS

Santiago de Chile, January, 2012

PONTIFICIA UNIVERSIDAD CATOLICA DE CHILE
ESCUELA DE INGENIERIA

HYDRODYNAMIC MODELLING OF TIDAL CURRENTS AT CHACAO CHANNEL FOR A PRELIMINARY ENERGY RESOURCE ASSESSMENT

NILS ERIK MIGUEL LINDEEN DE LA FUENTE

Members of the Committee:

RODRIGO CIENFUEGOS

CRISTIAN ESCAURIAZA

CRISTOPHER AIKEN

VLADIMIR MARIANOV

Thesis submitted to the Office of Research and Graduate Studies in partial fulfillment of the requirements for the Degree of Master of Science in Engineering

Santiago de Chile, March, 2012

To my family, teachers and Postgraduate colleagues who accompanied me through this process.

ACKNOWLEDGEMENTS

First of all I would like to thank my family for having supported my decision to enter the Master's degree, over immediately getting in the labor life. It was definitely a good decision.

Next, I want to thank Rodrigo Cienfuegos for his patience and lessons, and Cristopher Aiken for his constant willingness and support in the learning process of ROMS model, both helping me overcome all the obstacles that appeared on the way. Without them this process would have been much harder. As well, a great acknowledgement to Domenico Sciolla and Cristian Escauriaza for sharing their knowledge and discoveries in the flow-turbine interaction area of the project, which was a tremendous help to understand certain large scale phenomena.

I would also like to congratulate and thank the renewable energies company Hydrochile for the scholarship they gave me to develop my thesis, which is part of an R&D project they are managing and financing. Not many companies take these initiatives, which are definitely necessary for the development of sustainability and innovation.

Last but not least, I would like to thank all the students, teachers and staff at the Hydraulics and Environmental Engineering Department at the "Universidad Católica", for two very entertaining and enriching years as a Postgraduate student, which I will never forget without a doubt.

CONTENTS

Page

TABLES INDEX

Page

FIGURES INDEX

Page

RESUMEN

La distribución del flujo de las mareas en el espacio y el tiempo es modelada y analizada en la región de los fiordos del sur de Chile y el Canal de Chacao, que une el Océano Pacífico y el Golfo de Ancud, separando la isla de Chiloé del continente en su lado norte. Las ondas mareales ingresan por el sur de la isla de Chiloé, presentando un comportamiento resonante en su viaje hacia el norte, con variaciones de hasta 6 metros en el Seno del Reloncavi. En consecuencia, las diferencias de altura de mareas significativas entre las entradas Este (Golfo de Ancud) y Oeste (Océano Pacífico) del Canal, producen velocidades de más de 3 [m/s] en algunos lugares de su extensión. De esta manera, este trabajo busca realizar una evaluación preliminar del recurso energético de las corrientes de marea para la extracción de energía renovable.

El modelo Regional Ocean Modelling System (ROMS) se utilizó para crear un modelo regional 2D que reproduce el desplazamiento de la onda mareal alrededor de la isla de Chiloé, y a su vez genera condiciones de entrada para un modelo de mayor resolución del Canal. Las mareas modeladas en el modelo regional se validan (y calibran) con las mediciones de mareas existentes en cuatro puntos ubicados a lo largo del Canal (Manao, Tique, Pihuio y Carelmapu). El modelo regional tiene un tamaño de grilla de 5 kilómetros, adecuado para reproducir los fenómenos de marea en la región, y la grilla del Canal, un tamaño de 300 metros, lo que permite crear un mapa de alta resolución de las corrientes a lo largo del Canal, para el estudio de sus características y distribución.

Las turbinas deben ser distribuidas adecuadamente y su cantidad limitada, para permitir la extracción óptima de energía a partir de un flujo de agua y mantener los impactos al mínimo. Este estudio describe el comportamiento de las mareas y los correspondientes flujos del Canal en 2D, con el objetivo de avanzar hacia la creación de un modelo 3D que incorpora la presencia de turbinas. Por último, se hacen sugerencias para la futura ubicación de equipos de medición, del proyecto de Investigación y Desarrollo en el que está enmarcado esta tesis.

Palabras Clave: marea, turbinas, recurso energético, modelo, ROMS, Canal de Chacao.

ABSTRACT

Tidal flow distribution in space and time is modeled and analyzed for the southern fjords region of Chile and the Chacao Channel, one that joins the Pacific Ocean and the Ancud Gulf, and also separates the island of Chiloé from the continent on its northern side. Tidal waves enter south of Chiloé island and show a resonant behavior as they travel north, reaching tidal variations of around 6 meters in Reloncavi Sound. Consequently, the Chacao Channel has a significant tidal height difference between its eastern side (Ancud Gulf) and its western side (Pacific Ocean), which produce velocities of over 3 [m/s] at certain locations along its length. The latter motivates this work as a preliminary energetic resource assessment of tidal currents for renewable energy extraction.

For the modeling process the Regional Ocean Modeling System (ROMS) is used to create a 2D regional model which reproduces tidal wave advance surrounding Chiloé Island, and creating input information for a nested 2D model of the Chacao Channel with finer resolution. Modeled tides in the regional model are validated with tidal measurements at four points located along the Channel (Manao, Tique, Pihuio, and Carelmapu), which allow a proper calibration of both models. The regional model has a grid size of 5 kilometers, enough to properly reproduce tidal phenomena in the region, and the Chacao Channel grid, a size of 300 meters, allowing creating a rather fine map of currents along the Channel as a way of studying it´s characteristics.

Tidal turbines should be properly distributed and their amount limited, to permit the optimal energy extraction from a water flow and maintain impacts at its least. This study does a deep description of sea surface and 2D flow behaviors in the fjords region, and specifically the Chacao Channel, as a long run objective of advancing towards creating a future 3D model which incorporates the presence of turbines. Finally, suggestions for installation of measurement equipments in the R&D project are made, for future optimal model calibration.

Key Words: tide, turbines, energetic resource, Model, ROMS, Chacao Channel.

1. INTRODUCTION

This first chapter is an introduction to the context in which this thesis is developed. It also points out the main and specific objectives behind the investigation done, in order for the reader to understand the general structure and procedures followed through it.

1.1 Context

The raise in carbon emissions and oil prices, added to a coupled energy demand and country development rate, have forced researchers and developers to search for new sources of renewable energies. Although nowadays these energies present reasonably higher costs and lower plant factors than traditional energies (large hydroelectric dams and thermoelectric plants), it is only a matter of time before they become competitive. Wind power has undergone a rapid development; within the past years its global installed capacity has increased from approximately 2.5 GW in 1992 to a little below 40 GW at the end of 2003, with an annual growth rate of around 30% (Morthorst, 2004). In the same manner, Geothermal, Thermo Solar, Solar PV, Biomass, Wave and Tidal energies are all expected to decrease their costs, as their installed capacities (and experience) increases.

Tidal energy exploits the natural ebb and flood of coastal tidal waters, caused principally by the interaction of the gravitational fields of the Earth, Moon and Sun. These tidal currents are magnified by topographical features, such as headlands, inlets and straits, or by the shape of the seabed when water is forced through narrow channels (Rosenfeld, Shulman, Cook, Paduan, & Shulman, 2009). In Chile, going south from the island of Chiloé, an abnormal geography composed by islands and channels or narrows is found, which is strongly marked by glacial action during previous ice ages (Borgel, 1970). These regions present a tremendous potential for the development of tidal energy, which could be used for small population energy supply, or even pumping energy to the main electric grids, in a few particular cases. One of these is the Chacao Channel, presenting currents around 3–5 [m/s], and categorized by Garrad Hassan Partners (an international consulting company with experience in the field of marine energy resource assessment)

as one of the best places worldwide for the development of a tidal farm (Garrad-Hassan, 2009).

Based on these backgrounds, a public-private research and development project, entitled "Assessment of the Tidal Energy Resource in the Chacao Channel, for the Selection and Implementation of Energy Extracting Devices", is being developed under the University's management. One of the main products of the aforementioned project is to develop hydrodynamic models that should allow determining hot spots along the Channel, and the effect that a device or an array of devices may induce on the flow hydrodynamics. One of the potential outputs being to develop tools that support the efficient and optimal design of energy extraction farms. In order to advance in that item, this thesis searches to implement a gross (5 km grid) 2D regional model of the whole Southern Fjords and Chiloé region (also called Chilean Inland Sea) in ROMS, and nest a finer model (300 m grid) of the Chacao Channel in it. This way, a better resolution of the Chacao Channel is obtained, in order to comprehend the medium scale hydrodynamic processes that occur. Finally, recommendations of locations for tide gauges and ADCP's are made, in order to obtain optimal input information for future models, which are a part of the aforementioned investigation project.

1.2 Objectives

Given that this thesis aims to advance in a specific area of the project afore mentioned, its objectives are linked with the objectives of that project. Therefore, the goals of this thesis are:

- Main Objectives:

Implement a model that properly reproduces tidal travel through the northern Chilean Inland Sea, and nest a smaller one that estimates the energetic resource available in the Chacao Channel.

- Specific Objectives:
  - Build and implement a 2D regional model of the complete southern fjords and Chiloé region of Chile, which can reproduce real tidal phenomena and

therefore create good boundary conditions for a nested model.

- Study the tidal phenomenon existent in the Chilean Inland Sea (all around Chiloé Island), and particularly the resonance effect which causes large tide variations at Ancud Gulf and Reloncaví Sound.
- Create a hydrodynamic modeling tool with ROMS, which is applicable to Chacao Channel and nested in the larger scale regional model.
- Determine the space-time 2D flow distribution in Chacao Channel.
- Analyze results in the Channel as a 1D model, as an easy method of behavior analysis.
- Estimate potential energy that could be extracted and generated with tidal turbines in Chacao Channel.
- Recommend proper locations for tide gauges and ADCP's, to obtain optimal real data generation, which allows good calibration of hydrodynamic models in Chacao Channel.

2. BASIC FUNDAMENTS AND REVISION

The first step was to carry out a detailed revision of the basic concepts involved in this thesis and papers and studies done to the date. Firstly an introductory revision of the main concepts behind tides and their operation will be revised and discussed, which will be based on information provided by the chapter on tides from the texts "Introduction to Coastal Processes & Geomorphology" by Masselink, G. and Hughes, M (2003), and "Tides, Surges and Mean Sea-Level" by Pugh, D. (1987). Once having explained the basic concepts behind tides, a revision of tidal models and tidal farms design will be addressed, in order to clear out for readers the status of investigation in the area. Finally, this chapter will close with a brief explanation of the area of study, together with a revision of main studies done up until now, which support the need for this specific thesis.

2.1 Tides

2.1.1 Basic Concepts and Astronomic Forcing

Tides are an effect of the gravitational force the Moon and Sun have over the Earth, which cause a rise and fall of the oceanic surface. This variation of the ocean´s surface is only noticeable in regions where it takes contact with land, along coastlines or shallow continental shelves, because in the open ocean its effect is very mild. The basis to tidal existence is explained by Newton´s law of universal gravitation which states that "every particle in the Universe attracts every other particle with a force that is directly proportional to the product of their masses and inversely proportional to the square of the distance between them" (Serway & Jewett, 2010), and is resumed in equation (2.1). This way, all planets in the Universe have some kind of gravitational effect over the Earth, yet they are insignificant in comparison to the Moon and Sun, because of their size or distance (Masselink & Hughes, 2003).

$$F = \frac{\mathrm{G}\times\mathrm{m}_1\times\mathrm{m}_2}{\mathrm{r}} \qquad (2.1)$$

Where G is the universal gravitation constant, m is the mass of the two bodies interacting, and R is the distance between the centers of mass of them.

The Moon and Sun are the main tidal drivers, given their close proximity to the Earth and large size, respectively. It is their relative positions that determine the advance of tidal waves around the globe. First, the Earth rotates over its own axis in around 23.93 hours, which is called a solar day. At the same time, the Earth and Moon form a system that rotates anticlockwise around their common centre of mass or also called barycenter (located inside the Earth). One rotation of this paired system takes around 27.32 days, which is called a sidereal month. Finally, the Earth-Moon system barycenter rotates around the Sun, in approximately 365.24 days, called a year (Masselink & Hughes, 2003).

The tidal waves are formed by the interaction of two main forces, centripetal and gravitational, that give place to the tide generating force. The first provides the acceleration every particle of mass on the Earth requires to maintain its orbital motion, and particularly to maintain the Earth-Moon system rotating in a stable manner. It is resumed in equation (2.2), it does not depend on location on the Earth's surface, and its direction is always parallel to the plane of rotation of the Earth-Moon system. The second, the local gravitational force, depends on location and is given by equation (2.3). This way, on the Moon facing side of the Earth the gravitational force will be larger than the force experienced on the opposing side. The average centripetal force per unit of mass must equal the average gravitational force per unit of mass, in order to maintain the rotation of the Earth-Moon system stable. Otherwise, they would accelerate towards each other (Masselink & Hughes, 2003).

$$F_c = \frac{\mathrm{G}\times\mathrm{m_E}\times\mathrm{m_M}}{\mathrm{R}^2} \tag{2.2}$$

$$F_{lg} = \frac{\mathrm{G}\times\mathrm{m_E}\times\mathrm{m_M}}{(\mathrm{R}\pm\mathrm{r})^2} \tag{2.3}$$

Where r is the distance between the Earth's center and the point of interest on the Earth's surface, m_E is the mass of the Earth, and m_M is the mass of the Moon.

A small acceleration is experienced in different locations of the Earth, due to the local gravitational force differences, which is applied and observed over the ocean mass. This way, the vector resultant from the addition of both forces is called the tide-generating force, which causes these local accelerations, and is expressed in equation (2.4). It will be positive on the Moon facing side (towards), and negative on the opposing side (away from). Finally, the Ocean surface is drawn towards two points at opposing sides of the Earth (Masselink & Hughes, 2003).

$$F_t = \frac{(\pm r)\times 2\times G\times m_E\times m_M}{R^3} \tag{2.4}$$

Although one might tend to think that the local variation of this force causes the ocean water on the Earth's surface to be drawn towards opposite sides of it, this ignores that this force is very small compared to the Earth's own attractive force acting upon the ocean and directed to its centre at every point. Therefore, it is actually the vector component of the tide-generating force, which is tangential to the Earth's surface that draws the ocean into two bulges on either side. This tangential component of the tide-generating force is known as the tractive force, and is shown in equation (2.5) (Masselink & Hughes, 2003)

$$F_t = \frac{3m_M r^3}{2m_E R^3} g \sin 2\theta \tag{2.5}$$

In this case, θ is the angle between the point of interest on the Earth's surface and the line joining the centers of the Earth and Moon. Finally, one can observe how the phenomena explained works in reality, and the effect these have over the Earth surface. It is seen how bulges at both sides of the Earth are formed, and how the forces applied over it affect the tide propagation. Figure 2-1 summarizes the interactions explained recently.

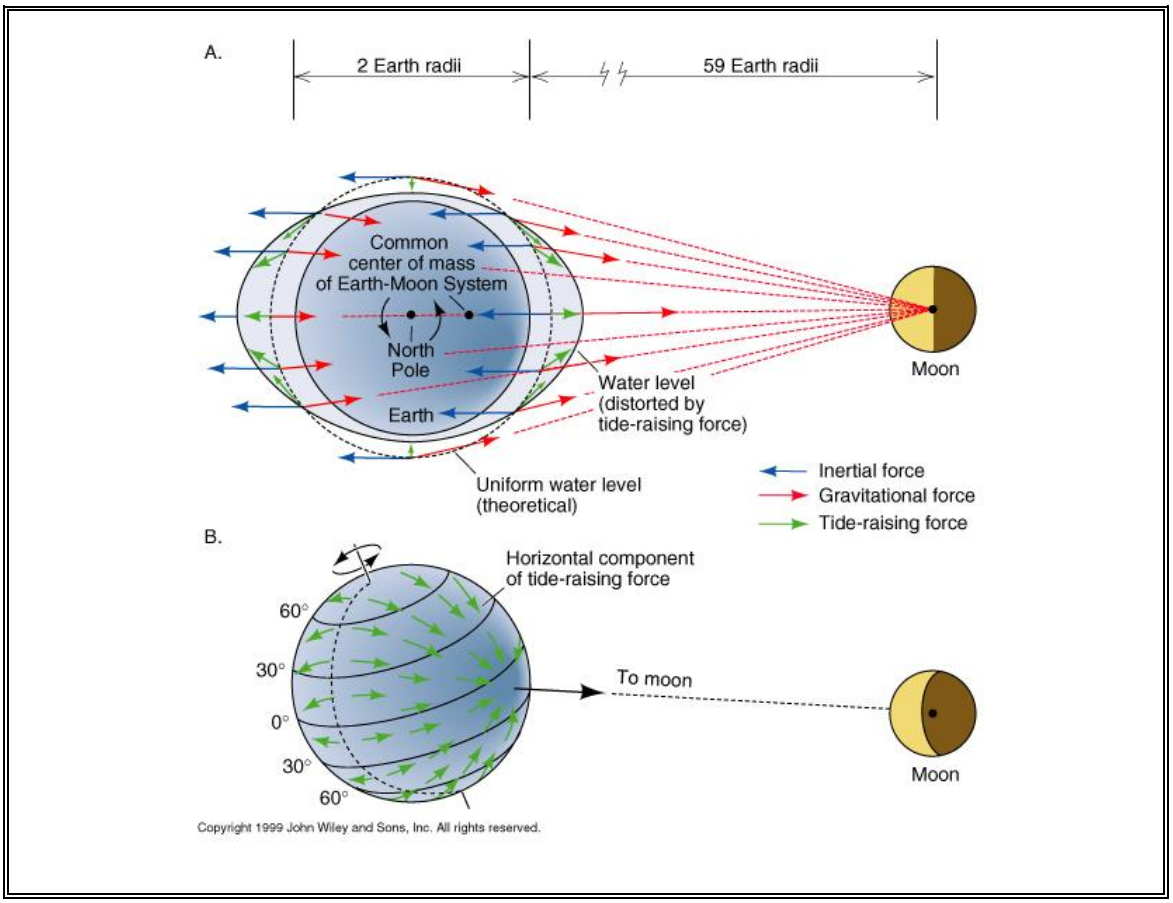

Figure 2-1: Tidal astronomical forcing interaction.[1]

2.1.2 Tidal Reference Levels

Tides are a variation of the level of the sea, which makes it extremely important to understand how these levels are measured and the references that are used in Chile to define their variation. Figure 2-2 sketches the different tidal levels considered.

[1] University of Victoria, http://web.uvic.ca/~rdewey/eos110/webimages.html.

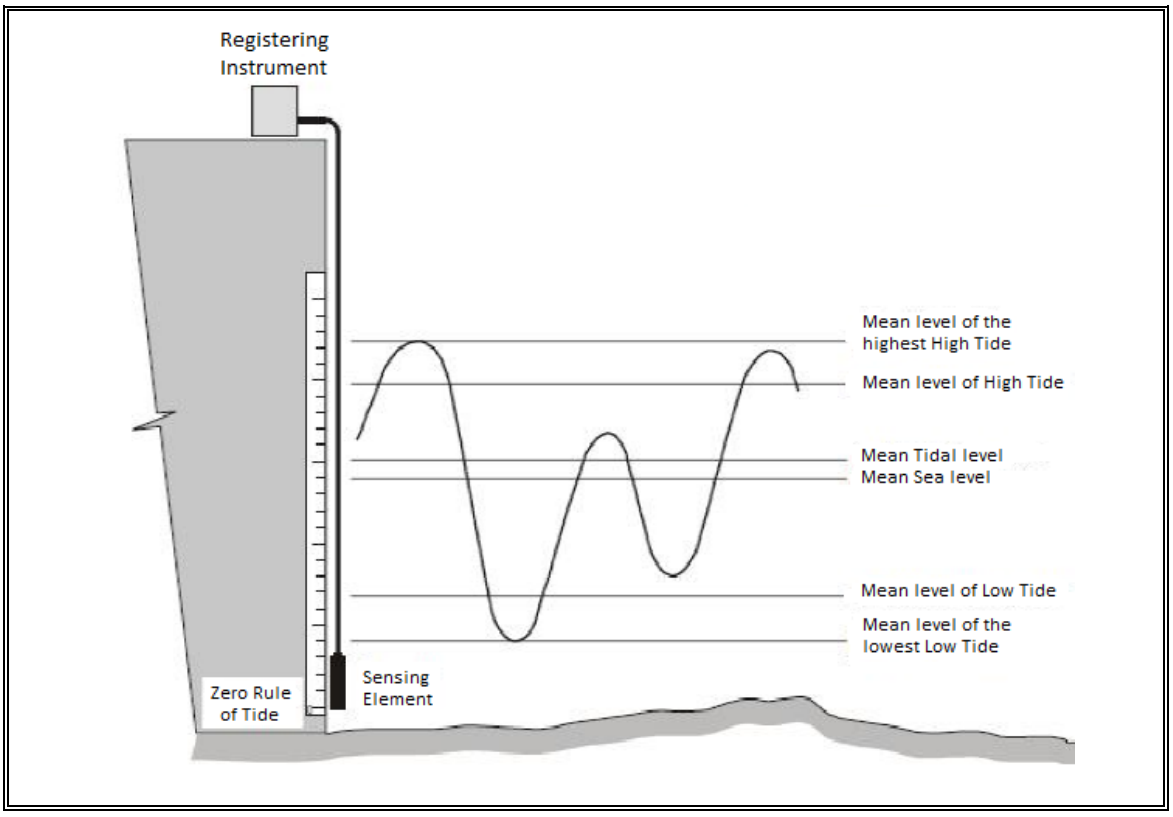

Figure 2-2: Main tidal reference levels, according to Chilean Navy rules.
(SHOA, Glosario de Mareas y Corrientes (Publicación SHOA N° 3013), 1992)

Previous to mentioning the different reference levels, concepts of low and high tide must be defined:

- High Tide: Maximum sea level attained by a flood tide (increasing sea level or tidal wave travelling from open sea towards land). This can be caused either exclusively by periodic astronomic tides, or meteorological conditions could also be involved (SHOA, Glosario de Mareas y Corrientes (Publicación SHOA N° 3013), 1992).
- Low tide: Minimum sea level attained by an ebb tide (decreasing sea level or tidal wave travelling from land towards open sea) (SHOA, Glosario de Mareas y Corrientes (Publicación SHOA N° 3013), 1992).

Reference levels adopted in Chile and sketched in the last figure are explained next (SHOA, Instrucciones Oceanográficas N° 2, Método Oficial para el Cálculo de los Valores No Armónicos de la Marea (Publicación SHOA N° 3202), 1999):

- Mean Tidal Level: equidistant plane between mean high tides and mean low tides, for a long period of observations.
- Mean Sea Level (M.S.L.): it corresponds to the mean level of sea level movements, which would be equivalent to the level sea would have is tides did not exist. To obtain this level, all hourly data of an observation period must be averaged.
- Mean Level of High Tide: is equivalent to the average of all high tides registered during the observation period.
- Mean Level of the highest High Tide: given Chile's geographical location, both high tides seen in a day, have a significant height difference. Therefore the daily highest high tide is defined as so, and all highest high tides of an observation period are then averaged to obtain this level.
- Mean Level of Low Tide: is equivalent to the average of all low tides registered during the observation period.
- Mean Level of the lowest Low Tide: as for high tides, low tides in Chile also present two peaks with different levels in a day. Therefore the daily lowest low tide is defined as so, and all lowest low tides of an observation period are then averaged to obtain this level.
- Probe Reduction Level (P.R.L.): it is the plane for which probes or depths are referred to at a certain location. Navigational necessities require that nautical charts show the lowest depth able to be found at a certain point; therefore usually probes in a chart are referred to some level related to low tides.

2.1.3 The Equilibrium Theory of Tides

The equilibrium theory of tides has three main assumptions (Pugh, 1987):

i) The Earth is covered entirely by an ocean of uniform depth, meaning there are no continental land masses.

ii) There is no inertia in the system, meaning the oceans respond immediately to the tide-generating force.

iii) The Coriolis and friction effects can be neglected.

Basically this theory assumes that under the lack inertia in the system, the tidal bulges will follow the Moon around the Earth. Figure 2-3 shows the comparative position of both bulges with respect to lunar position, at different moments of the month.

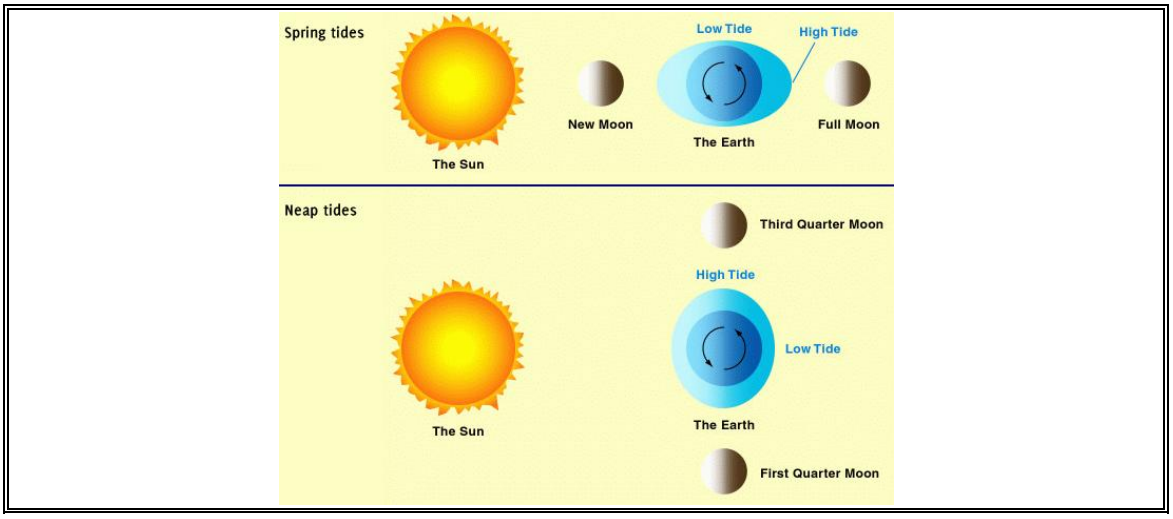

Figure 2-3: Solar-Lunar interaction as a tidal generator.[2]

As mentioned before, not only does the Earth and Moon rotate together around their barycenter, also the Earth spins in an anticlockwise direction on the axis that goes through its poles in 24 hours. Therefore an observer at a certain point will experience two high tides and two low tides in a day or complete spin of the Earth. At the same time, the Moon also rotates around the Earth, and advances 12.2 degrees per day, therefore shifting the tidal bulges by the same amount every day. This explains the variation of tidal peaks from one day to another.

[2] http://mail.colonial.net/~hkaiter/Moon_Phases_Tides.html.

The assumption used up until now, where Moon is aligned with the Earth's equator, is actually not completely real and produces certain changes over the system. In reality the Earth-Moon system is tilted by angle of approximately 28.5°with respect to the Earth's equatorial plane, also known as the lunar declination. This means that tidal bulges formed around the Earth are also tilted with respect to the equatorial plane. This means that an observer located at a certain point above or below the Equator will experience a daily variation between both high tides and low tides. The largest daily variation will occur when at the times in the month when the Moon is positioned over the tropics, called tropical tides. On the contrary, the smallest daily variation (or null variation) will occur at the times in the month when the Moon is positioned above the Equator, called equatorial tides. Both of these usually occur twice a month (Pugh, 1987).

Not only does the Moon produce a tide-generating force over the Earth, the Sun has the exact same effect yet a 46 % of that produced by the Moon. This difference is due to the closer proximity of the Moon to Earth, and even though the Sun's mass is much larger, it is not enough to compensate for distance. The presence of the Sun is traduced in a moderating or amplifying effect of tides, which depends on its relative position with the Moon and Earth. When the Moon is new or full the Earth, Moon and Sun are aligned, so are their bulges, which yield tidal bulges that are the sum of the individual contributors. This moment of the month is called syzygy. On the other hand, when the Moon is in at a right-angle to the Earth with respect to the Sun, so are their bulges, which yield tidal bulges that constructively interfere with each other. This moment of the month is called quadrature. In summary, tides during syzygy are largest and are called spring tides, whereas tides during quadrature are smallest and are called neap tides. Each occurs approximately every 15 days (Pugh, 1987).

The Moon and Sun orbit shapes also have an effect over tides. Until now, circular paths were considered, yet in reality paths are elliptical, which means distances between bodies differ at different moments of the path. The Moon is closest to the Earth at perigee (357,000 km), and furthest at apogee (407,000 km), meaning tide-generating force will be larger at perigee than apogee. As a result, one of the spring-neap tides in a

given month is larger than the other. As well, there will be an occasion when the new moon coincides with perigee and one when full moon does so, usually March and September. In the same way, the orbit of the Earth-Moon system is also elliptical, therefore the Sun is closest to the Earth at perihelion (148,500,000 km), and furthest at aphelion (152,200,000 km), producing a stronger effect over tides at perihelion. Thus the tides are marginally larger in the 6 months centered on January, and marginally smaller in those centered on July (Pugh, 1987).

Finally, the Sun's position over the Earth varies between the Tropic of Cancer (latitude 23.5°North) and the Tropic of Capricorn (latitude 23.5°South), and back again in the course of a year or 365.25 days. When it is over the tropics, during solstices, the solar tidal bulge will add a small amount to the diurnal inequalities in tide range produced by the lunar declination; whereas over the Equator, during equinoxes, it will not. In the long run, there is a precession of the lunar declination with respect to the solar declination, which produces an 18.6 year periodicity in the tides (Pugh, 1987). Figure 2-4 shows the contribution of some components to the time series at Longyearbyen, allowing clear understanding of the dynamics of tidal time series (Gjevik, 2006).

Even though it seems as if this theory can explain most of the observed features of tides, there are four shortcomings (Masselink & Hughes, 2003):

i) The predicted tide range is typically smaller than the observed range.

ii) The predicted tidal range is not constant, but varies with location around the globe.

iii) The timing of high water is generally several hours before or after the time of transit of the Sun and Moon.

iv) The timing of spring and neap tides does not always coincide with syzygy or quadrature, but is typically a day or more different.

These make one conclude that there is some sort of preferential response to the tide generating force, determined by local characteristics, and assumptions of zero inertia and friction are too restrictive. This is why Equilibrium Theory cannot be used in any precise way to predict the tide at a given location.

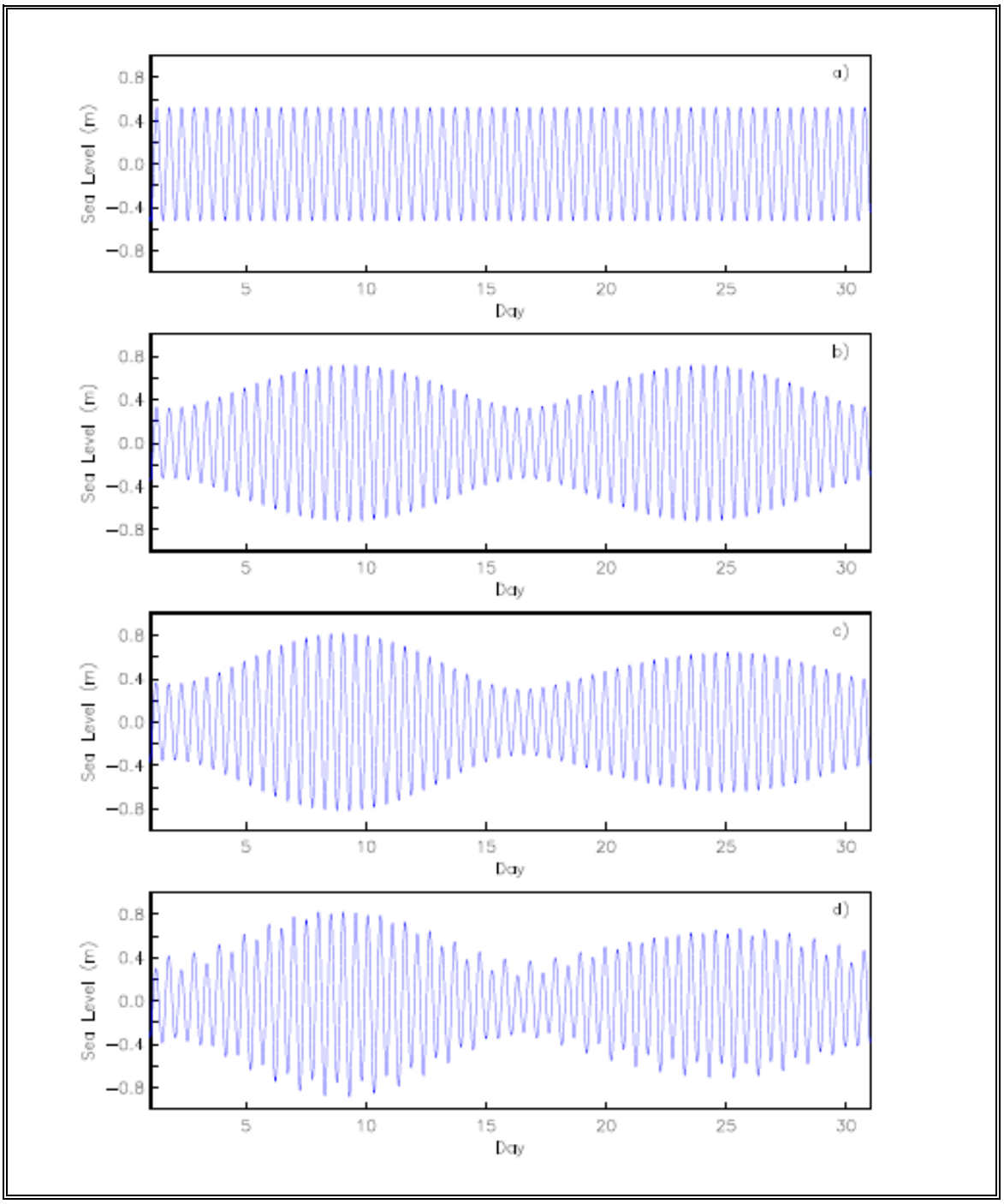

Figure 2-4: Tides at Longyearbyen 1-31 October 2006. a) Only M2, b) M2+S2, c) M2+S2+N2, d) M2+S2+N2+K1. Full Moon 7 Oct., New Moon 22 Oct. Lunar perigee 6 Oct. and apogee 19 Oct. Day starts at midnight UT (GMT). (Gjevik, 2006).

2.1.4 The Dynamic Theory of Tides

Given that the Equilibrium Theory does not explain real tides on its own, due to the basic assumptions that characterize it, the Dynamic Theory of tides was developed by contributions made by Bernoulli (1740) and Laplace (1775) (Gjevik, 2006). In it, the basic assumption is that the two tidal bulges discussed before behave as waves, and because of their extensive wavelength (compared to water depth), they specifically are considered to behave as long waves or shallow-water waves. Therefore a long wave is associated to every tide-generating force contributor (Moon and Sun), and as they are always present the long wave is always being driven by it. These waves are called forced waves. The limited ocean depth, which restricts long wave velocity, and the fact that the ocean is not continuous, but separated into several deep basins, traduces in long waves effectively being broken up into smaller systems. These systems are called amphidromes, and they work in such a manner that long waves rotate around a central point where tidal variation is null. The amphidromic systems along the Earth are shown in Figure 2-5, and as can be noticed, the sense of rotation is clockwise in the Southern Hemisphere and anticlockwise in the Northern Hemisphere. This way, Earth rotation and Coriolis Effect produce a wave crest (and opposite trough) rotating around an ocean basin, in the senses mentioned for each Hemisphere, and these waves are called Kelvin waves (Pugh, 1987).

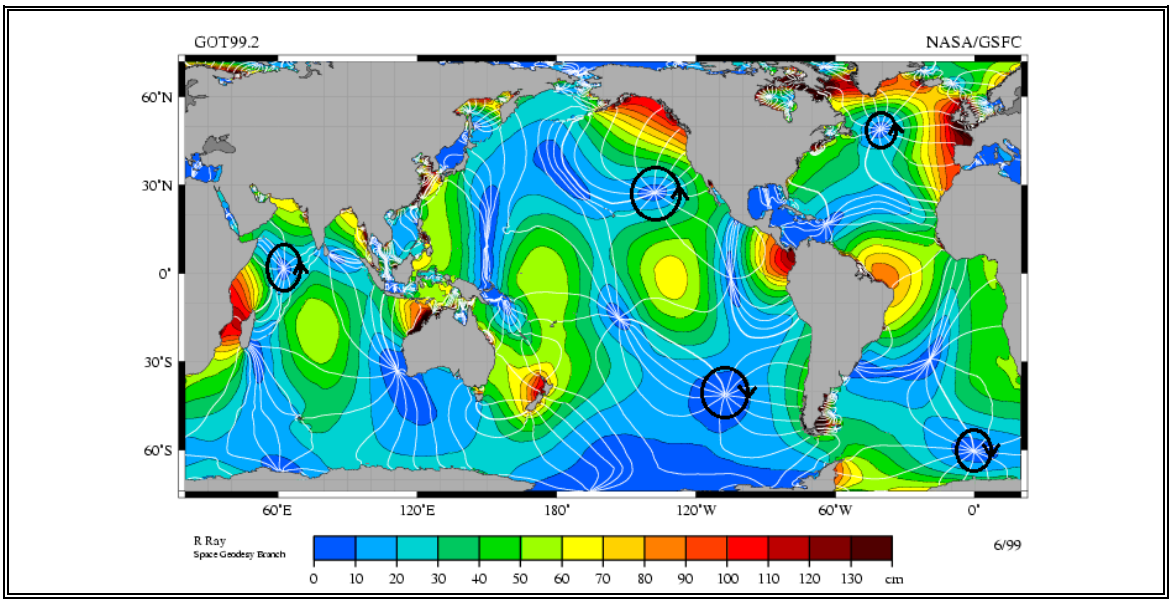

Figure 2-5: World tidal patterns and the amphidromic points.[3]

2.1.5 Tidal Level Prediction

As has been explained up until now, tides are consistent phenomena, which depend on astronomical cycles, and therefore are extremely predictable. In order to predict tides at a specific location there are several methodologies, yet the main one is called the Harmonic Analysis method. This is a method by which an observed tide can be modeled as a sum of a certain number of harmonic constituents or partial tides, which periods correspond to the periods of some relative astronomical movement between the Earth, Moon and Sun. The partial tides are harmonics the periodic motion of the water surface elevation at one location is expressed in terms of a cosine function that includes time. Equation (2.6) shows how the reconstruction of the observed tides is done (Masselink & Hughes, 2003).

$$\eta = \eta + \sum_{i=1}^{n} a_i \cos\left(2\pi f_i t - G_i\right) + \eta_r \quad t \tag{2.6}$$

Where η is the tidal water level, t is time, $\bar{\eta}$ is the mean sea level, and a_i, f_i and G_i are the amplitude, frequency and phase of the i-th partial tide, respectively. The last term

[3] Modified from R. Ray, "TOPEX/Poseidon: Revealing Hidden Tidal Energy", GSFC, NASA.

η_r is the residual water level, which is a correction term for differences between predicted and observed tidal records.

At different locations, each partial tide has a specific amplitude and phase, which depend on the geographical conditions of that place. Therefore, tidal prediction by the method of harmonic analysis typically involves a least-squares fitting of the principal partial tides to an existing tidal record for that location, in order to obtain their amplitudes and phases. Length of data series will determine the amount of constituents to be considered in the analysis, therefore longer series implies more constituents. This follows the Raleigh criterion for statistical analysis. Finally amplitudes, frequencies and phases obtained are then replaced in equation (2.6) to predict tides in the future (Masselink & Hughes, 2003).

2.1.6 Tidal Classification

Tides at different locations are rated depending on the local predominant tidal regime, which is defined using the criteria of the Courtier coefficient (SHOA, Glosario de Mareas y Corrientes (Publicación SHOA N° 3013), 1992). This coefficient is obtained from an amplitude relationship of the main semi diurnal and diurnal tidal harmonic constituents, calculated using equation (2.7).

$$F = \frac{(a_{K1}+a_{O1})}{(a_{M2}+a_{S2})} \tag{2.7}$$

Where the parameters are the amplitudes of each tidal constituent:

a_{K1} = Lunar-solar declination diurnal component.

a_{O1} = Lunar declination diurnal component.

a_{M2} = Main lunar semi diurnal component.

a_{K1} = Main solar semi diurnal component.

Finally, replacing these parameters in the equation, a value for the coefficient is obtained, which described the characteristic of tidal regime at that certain spot. The ranges for the values obtained are rated as follows:

F < 0.25	Semi diurnal tide regime.
0.25 < F < 1.50	Mixed regime, predominantly semi diurnal tide.
1.50 < F < 3.00	Mixed regime, predominantly diurnal tide.
F > 3.00	Diurnal tide regime.

2.2 Tidal Energetic Flow Models

As explained before, tidal waves are extremely predictable, due to the fact that they are driven by predictable astronomical motions. Therefore tidal models are a rather precise tool, and very useful to explain their local phenomena's in coastal regions. Many tidal models have already been developed, with different purposes of course: sediment transport, inter tidal biodiversity, energetic resource, among others.

Regarding the evaluation of tidal flow energetic resources in fjords or channels, estimations are based on the use of basic hydrodynamic equations, for one dimension, two dimensions or three dimensions: momentum balance and continuity. Basically studies developed up until now are separated into three main branches, depending on their scale:

- Tidal Energetic Resource (Large scale): Consists in models in which tidal flows and energetic potential are modeled, and the presence of turbines is incorporated to the basic equations, in order to determine their general effect as an extra drag coefficient.
- Tidal Farm Design (Medium Scale): Tidal flows are modeled with the presence of tidal farms, yet in this case flows are analyzed at smaller scale, in order to define distance between turbines in a row and between rows of turbines. This aims towards designing an optimal array of tidal turbines.
- Flow-Turbine Interaction (Small Scale): The interaction between turbine blades and flows are modeled and analyzed, in order to develop and define the adequate turbines to be used for a specific location.

All three branches are related, and must be incorporated into the large-scale tidal flow model, when one decides to design a definitive tidal farm. In these case studies related to the large and medium scale will be mentioned and analyzed, in order to introduce the actual status of research relating tidal models. Small-scale studies are beyond the scope of this particular thesis, given that the analysis of specific types of turbines is being tackled by other students in the framework of the Research & Development project.

2.2.1 Tidal Energetic Resource

a) Main Concepts

As has been studied for turbine array distributions in wind farms, the effect of a turbine over the fluid's natural flows must be considered in the modeling process, in order to ensure an optimal extraction of energy and therefore of farm design. At first, energetic potential in wind flows was estimated by the kinetic energy (KE) available in a certain transversal area of the flow, which is shown in equation (2.8) (Garret & Cummins, 2005).

$$KE = \frac{1}{2}\rho A u^3 \tag{2.8}$$

Where ρ is the fluid's density, A is the area spanned by the turbine, and u is the velocity of the flow.

In 1927, Betz discussed a simple model, in which he estimated that the maximum power attainable (MPA) was 16/27, or 59%, of the kinetic energy available in a flow, before it passes through the section of a turbine (given in equation (2.9)) (Betz, 1926). Although, Bergey (1980) argues it was earlier derived by Lanchester (1915). This limit to maximum power is called the Lanchester-Betz limit (Bergey, 1980). Some investigators believe this is unrealistic, due to the several assumptions Betz made to attain this value. As a matter a fact Gorban et al. (2001) obtained that, if curvature of streamlines were allowed, the efficiency factor drops down to 35% (Gorban, Gorlov, & Silantyev, 2001).

$$MPA = \frac{8}{27}\rho A u^3 \tag{2.9}$$

The large scale and small scale flow-device interaction has been widely studied for the case of wind farms, but not that much for tidal farms, yet the basic concepts of the first are applicable to the last. Some investigators have already begun to study the tidal flow energetic resource, and ways of incorporating the effect in a 1D, 2D or 3D model of a certain channel or fjord. Basically, the effect of turbines over hydrodynamic flows is incorporated into models as a sink of momentum, present as an additional drag coefficient in the basic flow equations (Blanchfield, Garrett, Wild, & Rowe, 2008). This way, Garrett and Cummins (2005) determined that kinetic energy overestimates the energetic potential of a channel, given that it does not take into account the influence turbines have over flows. A 1D model developed by them demonstrated how the incorporation of turbines into a channel, increased the total drag, therefore slowing down the hydrodynamic flows. This model considered flow through a channel of variable cross-section (as shown in Figure 2-6), and with dynamic equation (2.10) governing the flow's momentum budget (Garret & Cummins, 2005).

$$\frac{\partial u}{\partial t} + u\frac{\partial u}{\partial x} + g\frac{\partial \zeta}{\partial x} = -F \qquad (2.10)$$

Current speed $u(x,t)$ is assumed to vary with time *t* and position *x* along the channel. The slope of the surface elevation ζ provides the pressure gradient to drive the flow, and $F(x,t)$ represents an opposing force related to natural friction along the channel and the incorporation of turbines. Finally, if the channel is short compared to the tidal wavelength (which will usually be so, unless the channel is extremely long), volume conservation implies that the flux Au along the channel is independent of x and may be written as $Q(t)$.

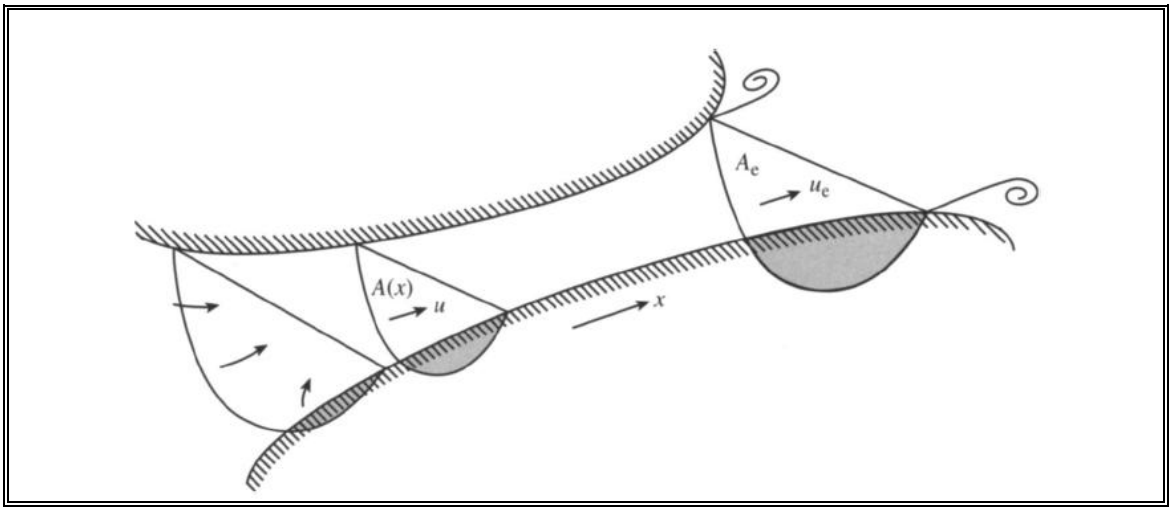

Figure 2-6: Channel of variable cross-section, which connects two basins with different tidal elevations. (Garret & Cummins, 2005).

By solving the basic equations, the authors managed to develop a model, which can give good preliminary estimates of power potential at different sites worldwide, obviously considering modifications for specific local characteristics. The main result obtained was that, to within 10%, the maximum average power available is approximately $0.22\rho g a Q_{\max}$, for a sinusoidal tidal head $a\cos\omega t$ and with $Q_{\max}$ denoting the peak volume flux in the undisturbed state (Garret & Cummins, 2005).

Another important result came from realizing that F (friction due to turbines) integrated along the channel, gives equation (2.11), in which Q is the flow and λ is related to the number of turbines and their position along the channel. This is extremely important, because it represents one possibility of representing small-scale turbine and farm effects into a large-scale model. Therefore, in farm design it is important to assess the overall effect of turbines by a single parametric coefficient (Garret & Cummins, 2005).

$$\int_0^L F dx = \lambda Q \tag{2.11}$$

Finally, an exponential turbine drag in the current speed ($\lambda|Q|^{n-1}Q$) is used to estimate the extractable power to a more realistic degree. Including this hypothesis in the basic hydrodynamic equations, non-dimensional equation (2.12) is obtained and then drawn

for different values of n in Figure 2-7. This way it is clearly observed how extracted power raises as more turbines are installed, until a certain point at which too many turbines choke the flow, and extraction efficiency is decreased (Garret & Cummins, 2005).

$$\frac{P}{P_0} = 4\lambda' \; Q' \; ^{n-1} Q'^2 \tag{2.12}$$

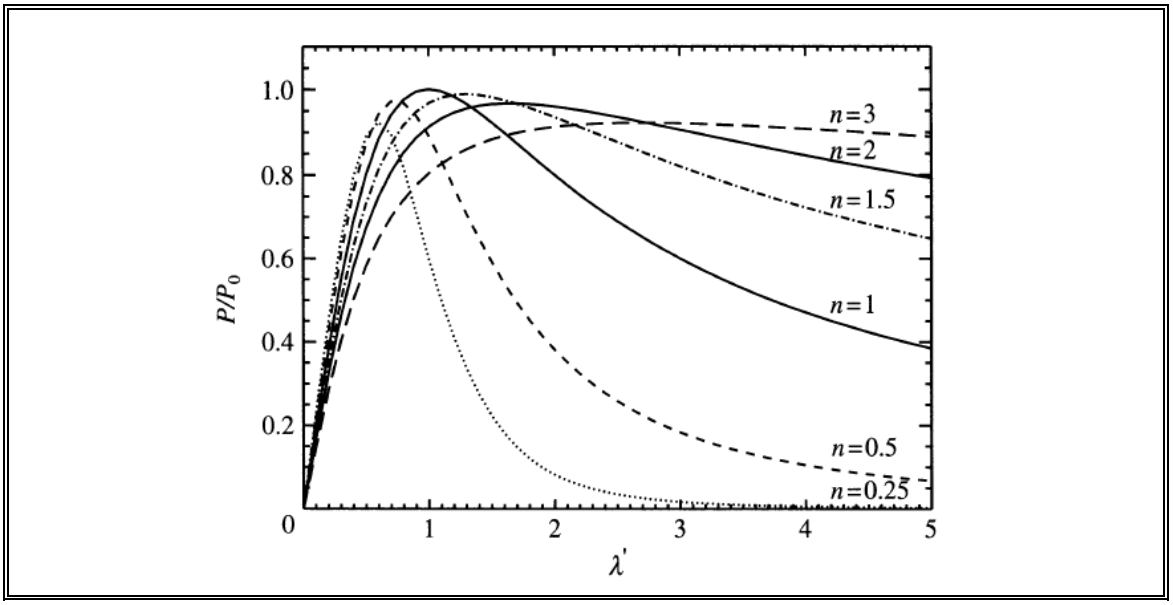

Figure 2-7: Power extraction as a function of the n_{th} exponential and non-dimensional turbine drag (λ). (Garrett & Cummins, 2007).

The study of Garrett and Cummins (2005) sets a base to a series of following studies, which is why it was important to explain in depth the procedures followed and the conclusions obtained. More advanced studies search to model flows in channels, applied to: specific locations (Defne, Haas, & Fritz, 2011; Rosenfeld, Shulman, Cook, Paduan, & Shulman, 2009); considering different topographical aspects and configurations (Blanchfield, Garrett, Wild, & Rowe, 2008); impacts on different hydrodynamic aspects (Polagye, Malte, Kawase, & Durran, 2008); and, varying turbine concentrations and distributions (Garrett & Cummins, 2008).

Important points to recall from these papers are methodologies followed and the results obtained, in order to use them understand the structure and concepts behind tidal models, and as a basis for this and future studies in Chacao Channel.

b) Real Applications

Not only is it important to revise the physical procedure used to model channels, but also think about the possible "products" which one searches to develop and the methodologies used. There are a series of studies relating hydrodynamic modeling (using ROMS, Mike 21, among others) at different spots around the world, and it was interesting to use their procedures as guides.

Rosenfeld et al (2009) and Defne et al (20010) modeled tides and currents with ROMS, and following a procedure very similar to the one proposed here. Investigations are based on 2D and 3D models, which are either fed with inputs from measurements or calibrated with them, which is done by comparing tidal components amplitudes at specific locations and other statistical parameters (Defne, Haas, & Fritz, 2011). Once having calibrated, results regarding tidal velocities at attractive locations, including tidal ellipse figures and maps with power density along the spots, as can be seen in Figure 2-8.

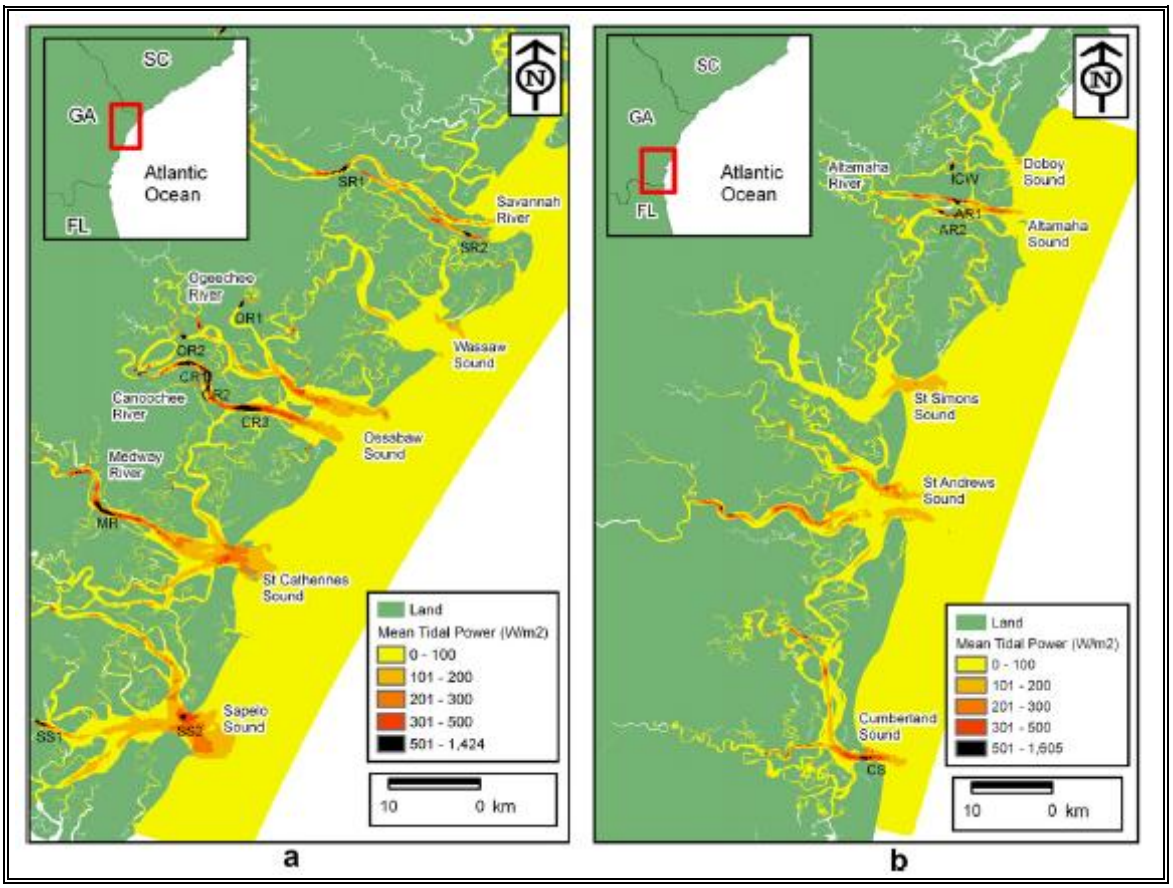

Figure 2-8: Mean power density maps along (a) the northern and (b) the southern coasts of Georgia with labeled high tidal streampower density (>500 W/m) areas. (Defne, Haas, & Fritz, 2011)

Finally, these studies help to guide the procedures and results to be presented in this study, in order to assure a proper "product" that can be used in future studies, and therefore is of value towards the design of a future tidal farm.

2.2.2 Tidal Farm Design

The past section detailed studies relating large scale models of a 1D flow in a channel and the effect that turbines induce over it, this section refers to a smaller scale, and revises studies regarding the optimal design of tidal farms and turbine spacing. Several investigators have addressed these issues and have explored them to a laboratory scale,

in order to understand turbine interactions and optimal spacing between devices, for future real scale tidal farm designs. This is a concept that began many years ago with wind farm research, when the first wind turbine arrangements had to be considered (Betz, 1926).

These issues started off with the Lanchester-Betz limit, also mentioned in the past section, given that it sets a maximum extractable energy from a certain available energy in a flowing fluid (Bergey, 1980). From there, Garrett and Cummins concluded in 2007, that optimal tidal farms involved occupying a complete transversal section of a channel. This conclusion came from the fact that gaps between turbines produced downstream mixing of enhanced flows through these gaps and slower flows passing through turbines, which bring energy dissipation (as seen in Figure 2-9). Therefore, tidal design must search to span the largest portion of the channel's section as possible (Garrett & Cummins, 2007).

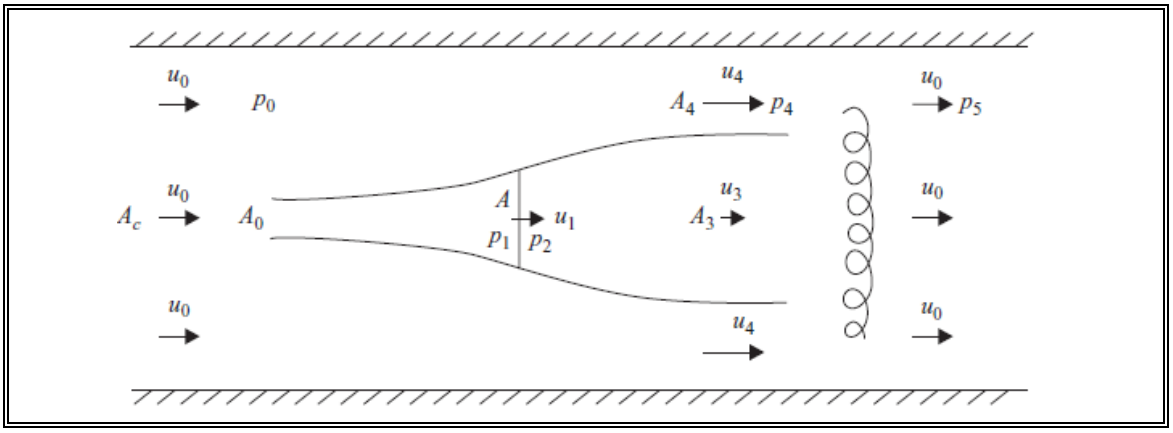

Figure 2-9: Definition sketch for a single turbine in a channel (Garrett & Cummins, 2007).

In the mentioned paper, the fraction u_3/u_0 is brought up as a tuning parameter to optimize energy extraction from hydrodynamic flows, being its ideal value 1/3. Therefore, it is concluded that maximum energy produced by the turbines is a fraction of the potential of a complete tidal fence (row of turbines spanned perpendicular to the flow direction), with the fraction being 2/3 if they occupy a small fraction of the channel

cross-section and decreasing to 1/3 if occupying most of the section. Quantitatively, an optimal number N of partial fences is expected to be calculated with equation (2.13) (Garrett & Cummins, 2007).

$$N \times \frac{4\varepsilon(1+\varepsilon)}{9(1-\varepsilon)^2} A_C u_0^3 = P \tag{2.13}$$

Where each parameter is:

ε: Fraction of the cross-sectional area taken up by the turbines.

A_C : Cross-sectional area.

u_0 : Turbine upstream flow velocity.

P: Power generated by the turbines.

In 2010, Vennell also concluded that to maximize turbine efficiency with a minimum number of turbines, the configuration must be designed to occupy the largest cross-sectional area permitted by navigational and environmental constraints. Maximum energy production requires the turbine blades to be tuned for a particular channel and turbine density, which is influenced by its drag coefficient, length, width and depth, tidal frequency and amplitude. This leads to the need to tune blade pitch in real time along a tidal cycle to maintain the u_3 / u_0 parameter at a constant optimal value. Therefore farms should first add turbines to its rows, and then add new rows if necessary. This is shown in Figure 2-10, as power is remained when cross-sectional area is optimized over row number (Vennell, 2010).

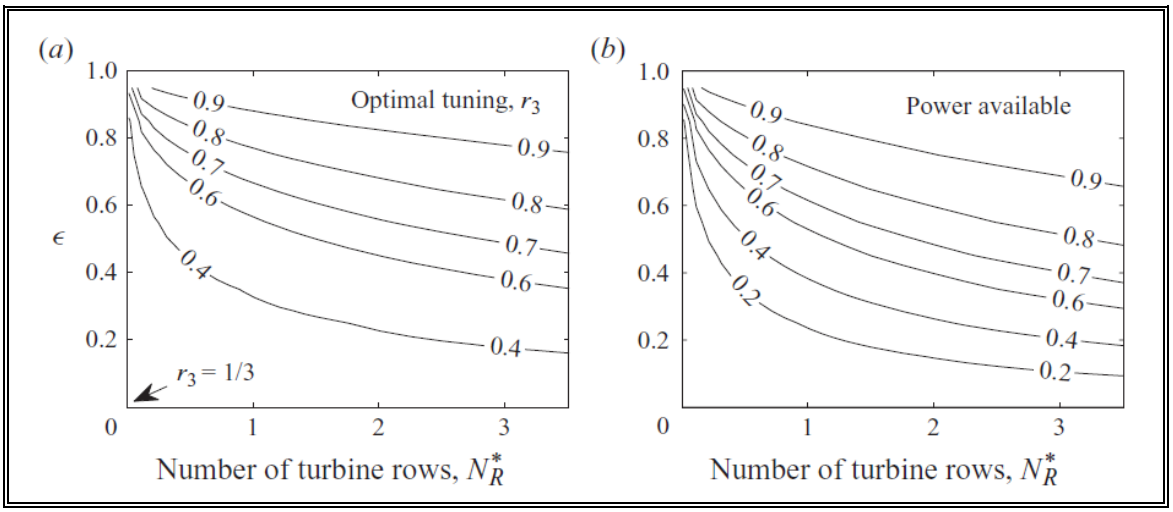

Figure 2-10: Tuning and power at optimal tuning for an inertial channel, $\lambda_0 = 0$. (a) Optimal tuning, $r_{3opt}(\varepsilon, N_R^*)$. (b) Fraction of a channel's potential available for production, $\overline{P}_{avail} / \overline{P}_{\max}$. (Vennell, 2010).

These results refer to the general rules one must consider when designing a tidal farm, yet several other studies enter in the detail of lateral and downstream distances between turbines which should be used for optimal turbine efficiency. In 2010, Lee et al modeled the tidal farm shown in Figure 2-11, where a lateral distance of two turbine diameters (D_S) was considered, in order to determine an optimal downstream distance between rows. Results presented in Figure 2-12, demonstrate that an optimal efficiency is obtained at a downstream distance of three diameters, and remains constant at larger values (Lee, Jang, Lee, & Hur, 2010).

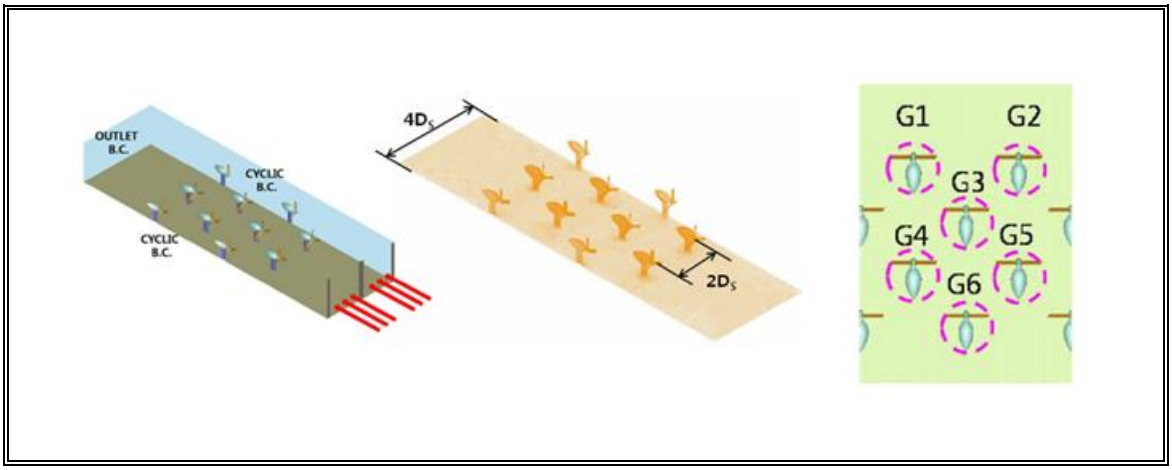

Figure 2-11: Tidal farm model. (Lee, Jang, Lee, & Hur, 2010).

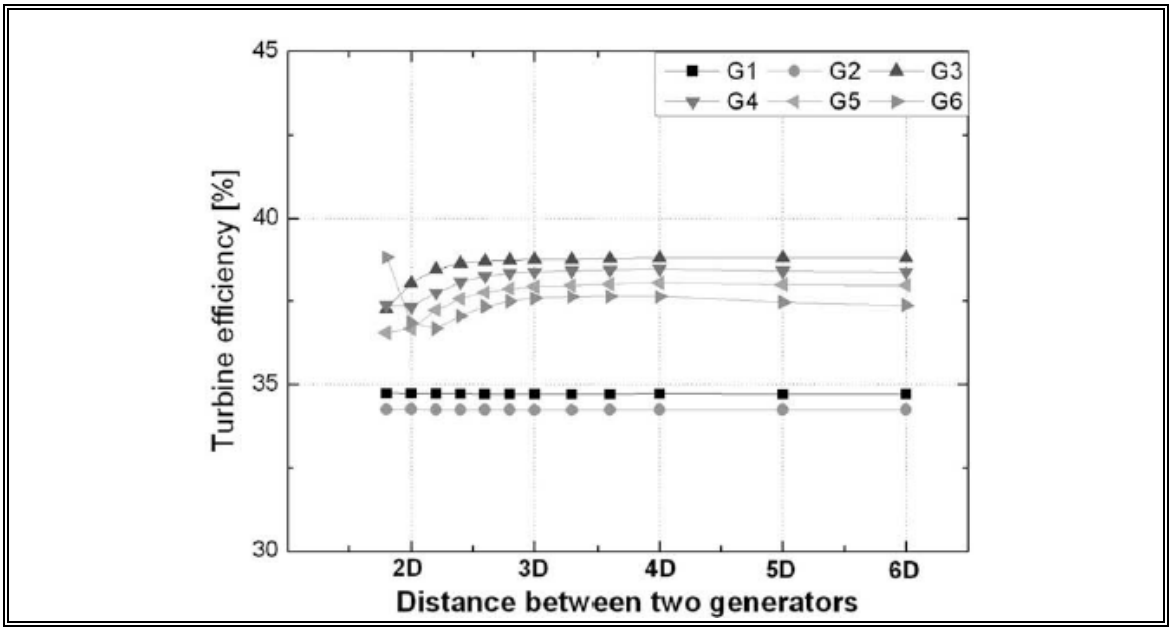

Figure 2-12: Results of tidal farm model, which show how at a downstream distance of 3D optimal turbine efficiency is obtained. (Lee, Jang, Lee, & Hur, 2010).

Another similar study by Myers & Bahaj this year (2012) modeled a farm of turbines and validated it with laboratory scale measurements. Porous disks were installed in a laboratory channel to reproduce tidal turbines in a real scale channel, and different

arrangements were evaluated in order to advance towards an optimal design. Figure 2-13 shows the dimensions of distances analyzed in the arrangements.

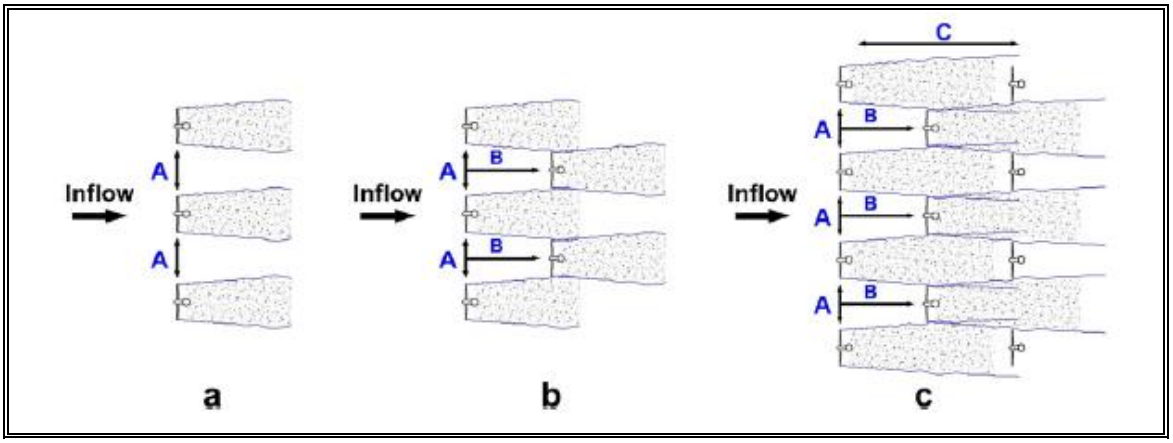

Figure 2-13: Arrangements of turbines in a channel and the dimensions studied to study their efficiency. (Myers & Bahaj, 2012).

Figure 2-14 shows the results for a dual single row arrangement of turbines, where one can observe how extremely close turbines produce a combined wake (a), that has further downstream velocity deficit (percentage loss of undisturbed velocity) effect than single wakes as turbines are separated by a larger distance (b and c) (Myers & Bahaj, 2012). Therefore, one conclusion was that when designing an array, one must determine a minimum lateral distance which avoids this effect.

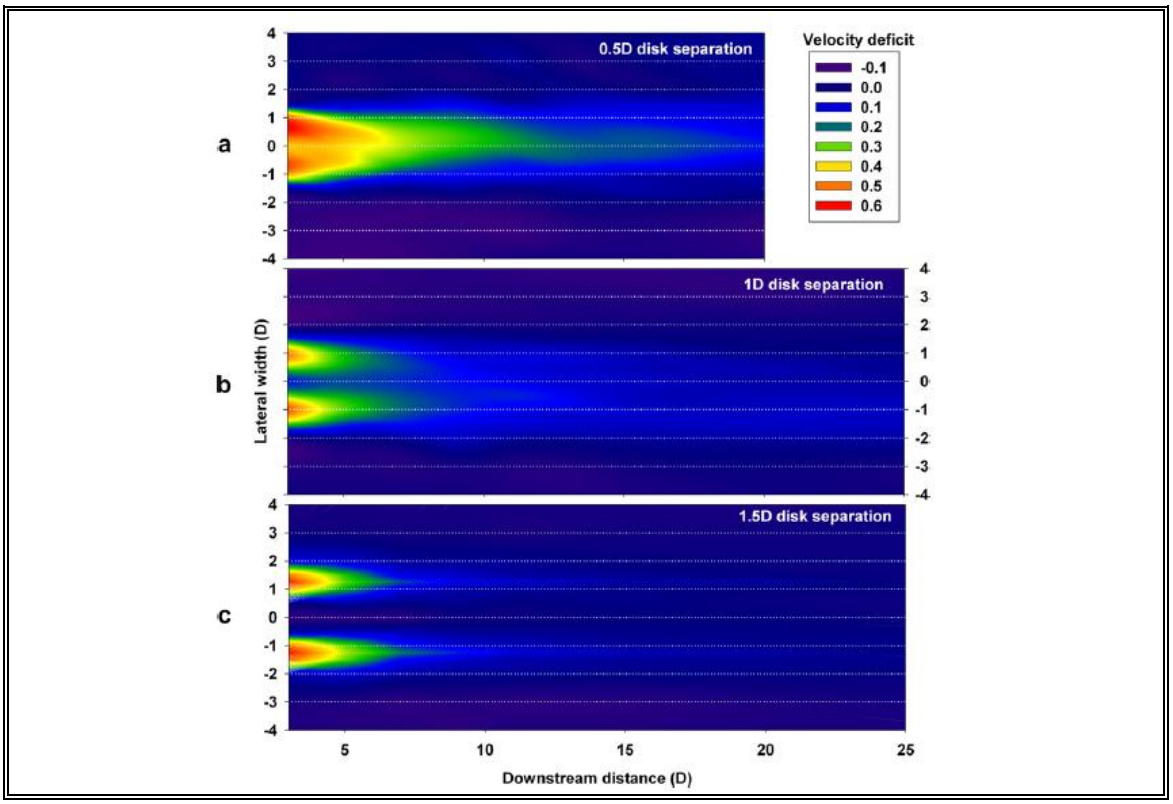

Figure 2-14: Model results of a dual single row arrangement of turbines over velocity deficit. (Myers & Bahaj, 2012).

Finally, Figure 2-15 sketches the velocity deficit effects of a two row arrangement, where an inferior level of velocity deficit is obtained at approximately 10 to 15 diameters, which is a larger result than that obtained by Lee et al. Another conclusion reached was that a third row of devices could be installed far downstream, but in a short-medium term wider 2-row arrays would offer a more favorable arrangement for a fixed number of devices within an array (Myers & Bahaj, 2012).

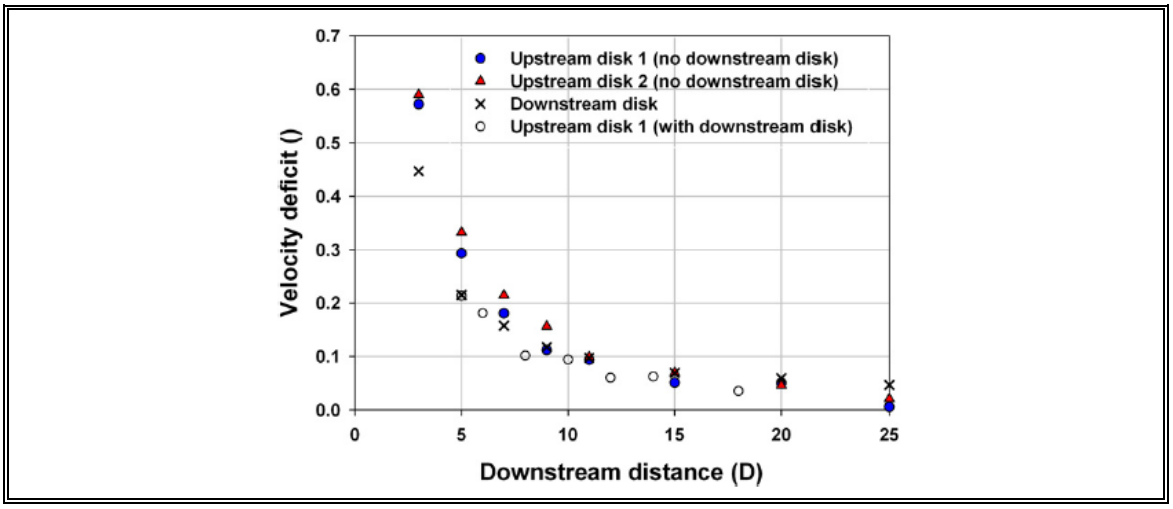

Figure 2-15: Longitudinal centerline velocity deficits for the two row turbine arrangement. (Myers & Bahaj, 2012).

All the results presented in this section allow understanding the stage at which tidal farm modeling and design are at present. This establishes the basic concepts and ideas that must be followed when a future tidal designing a farm that would be incorporated in the hydrodynamic model considered in this thesis. Once the proper procedure to incorporate their effect over tidal flows is defined, a tidal farm design must be thought of in terms of installed capacity, and therefore amount of turbines. Having a clear idea of how one must arrange them in a certain space, to extract as much energy as possible, will be extremely important for the incorporation in the tidal model.

2.3 Chacao Channel and the Southern Fjords

This section aims at establishing the basis of existent studies and data in the Chacao Channel and fjords region, so that results and conclusions obtained in this thesis improve those already suggested by previous studies. As well, knowledge of available data will allow deciding what data is useful and what data is missing for the models to be developed next.

2.3.1 Existent studies and papers

The southern coast of Chile, surrounding the great island of Chiloé, made up by a complex of channels and fjords, has caught the attention of fisherman, navigators, investigators, among other stakeholders, for a long time. Tides play an important role in several aspects of the region, including sediment transport, mixture and hydrodynamic current formations (García & Winckler, 2009; Salinas & Hormazábal, 2004; Silva, Calvete, & Sievers, 1997). This last point has brought to consider energy extraction from these currents for local, and even national, supply. In particular, Chacao Channel has been the main attraction, given its consistent fast flows, moderate depths and proximity to the Central Interconnected System (main Chilean electric grid). An international consulting company has identified Chacao Channel as one of the best spots in the world for the installation of tidal energy extraction devices, with a raw energy estimated between 600 and 800 MW, of which approximately 20 - 60% should be technically extractable, depending on spatial variation of the flow, bathymetry, and navigation requirements (Garrad-Hassan, 2009). Figure 2-16 shows three major channels with energy extraction potential, from which Chacao Channel is by far the most attractive.

Zone	Water depth [m]	O&M base	Average distance to nearest substation - cable routing [km]	Closest Electrical Grid (SIC)	Local Tidal Resource[23] [kW/m^2]	Estimate of the energy yield for a 30 MW tidal farm [GWh/annum]
Chacao	30-100	Cabo Froward or Puerto Montt	0-10 ~60	110kV 220kV	3.8 - 5.2	101-152
Corcovado Gulf	20-100	Cabo Froward or Puerto Montt	~30 ~95	66kV 110kV	0.72	19
Straits of Magallanes (Primera Angostura)	50 -70	Austral	none		3.6	99-126

Figure 2-16: Characteristics of three top energetic tidal channels in Chile, where Chacao Channel is by far the most attractive alternative. (Garrad-Hassan, 2009).

This region, also known as the Chilean Inland Sea (CIS), is divided in two main areas: the northern and southern CIS, as seen in Figure 2-17. Both have their own geographical characteristics, and therefore behave different with tidal wave propagation, yet are correlated between each other (Aiken, 2008). The main ocean water entrance, called Guafo Mouth, is the boundary between both areas, and allows an interaction. The northern (nCIS) side is made up by Chiloé Island, Chacao Channel, the Gulfs of Ancud and Corcovado, and has a larger area of water for tidal waves to travel. Instead, the southern side (sCIS) is rather different, in the sense that it is composed by several small channels, fjords and islands, which give tidal propagation (therefore hydrodynamic models) a harder job, although it is more exposed to open ocean. This side begins at Guafo Mouth, is composed by its main Moraleda Channel, and ends at Elefantes Estuary.

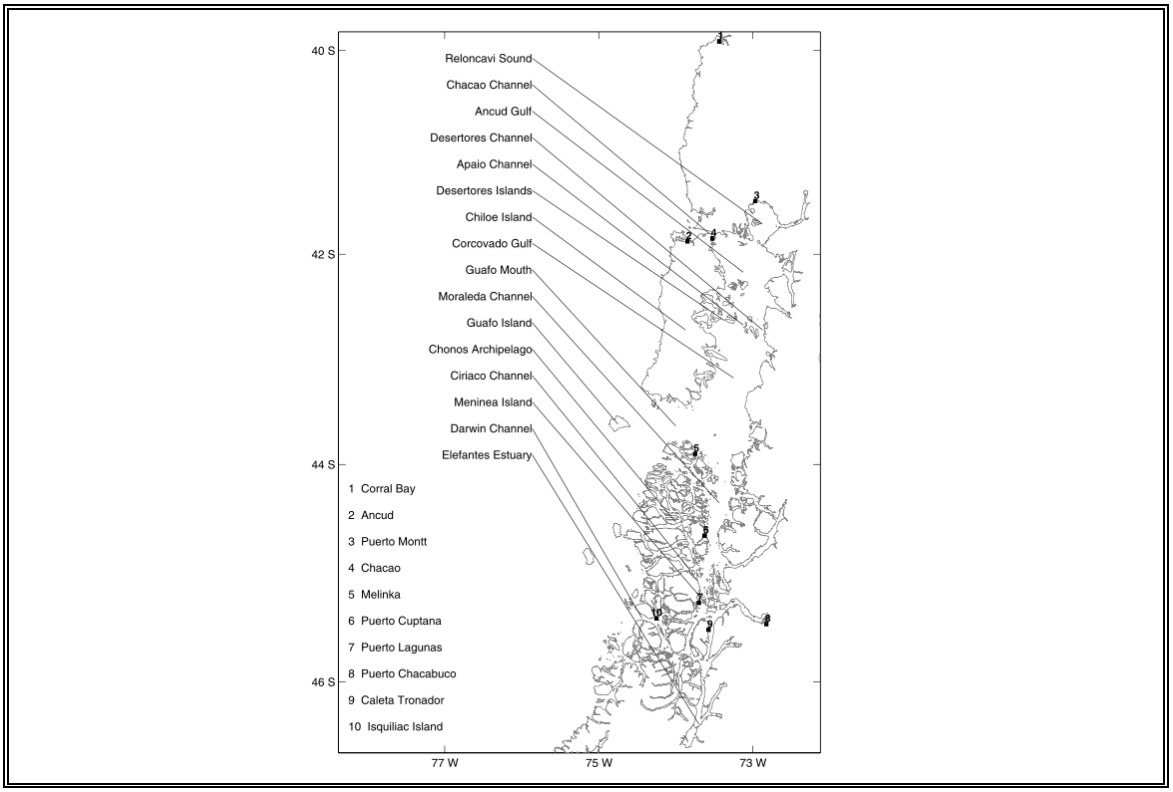

Figure 2-17: Detailed map of the CIS, including a description of main channels and gulfs. (Aiken, 2008).

Main scientific studies began to appear 10 to 15 years ago, and aimed at explaining the tidal wave propagation and related phenomena in the whole southern fjords region. In 2003, Cáceres et al studied tidal phenomena in the region, and analyzed the amplitude differences at certain points around the CIS, concluding that resonant conditions in the nCIS might exist (Cáceres, Valle-Levinson, & Atkinson, 2003). The existence of tidal variations of around 6 m at the Gulf of Ancud (Channel's east side) and 2 m at Coronados Gulf (Channel's west side), produce a head difference at either side of the it, which is traduced in flow velocities from 3 to 4.5 m/s in the Chacao Channel (Cáceres, Valle-Levinson, & Atkinson, 2003). A diagram showing this effect is presented in Figure 2-18, where it is seen how sea level difference causes a flow of water masses.

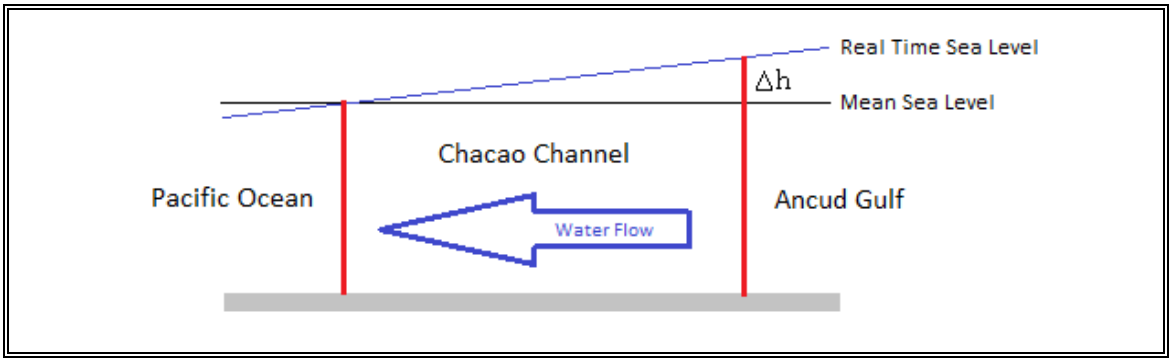

Figure 2-18: Diagram of tide level differences between both sides of Chacao Channel.

A later study done by Aiken in 2008, further emphasized the existence of tidal resonance of waves propagating northward along the Gulfs of Corcovado and Ancud, and actually proved it analyzing several variables. Figure 2-19 sketches tidal wave amplitude from Guafo Mouth to Reloncavi Sound, showing how the tidal wave length resonates along the Northern CIS, increasing its amplitude and also changing its phase. The resonant frequency is a bit larger than semi diurnal components, being close to $10h^{-1}$ ((Aiken, 2008).

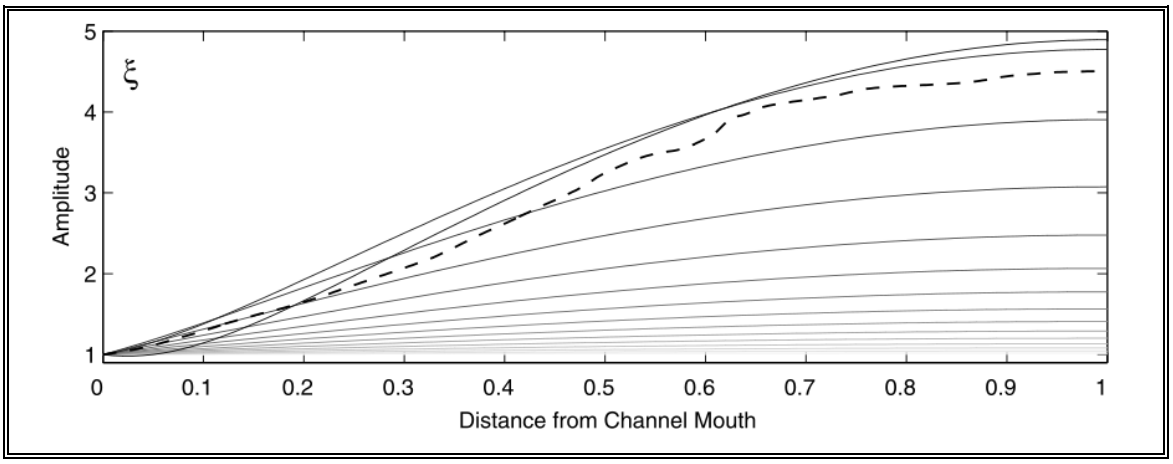

Figure 2-19: Amplitude (upper) and phase (lower) of a damped channel harmonically forced at its open end. The dashed curves indicate the modeled amplitude of M2 in the nCIS. For the solid curves, $r/\omega = 0.3$. (Aiken, 2008).

Another interesting conclusion that was reached by Cáceres et al. (2003), was the flow pattern of the transect where Remolinos Rock is located, where the influence of lateral variations of bathymetry produce recirculation around the pinnacle and over the slopes of the Channel. There, mean flow is flood dominated at all depths in shallow areas, and ebb dominated in the deeper areas of the same cross section. This way, recirculation reflects strong divergences and lateral shears that translate into a relevant contribution of nonlinear terms (advection, horizontal and vertical friction) to the momentum balance (Cáceres, Valle-Levinson, & Atkinson, 2003). This can be observed in Figure 2-20, as the arrows show in and out flow in different areas of the same cross section, and can be an important aspect to analyze at different sections of the Channel, in order to identify precisely the flow patterns for farm design.

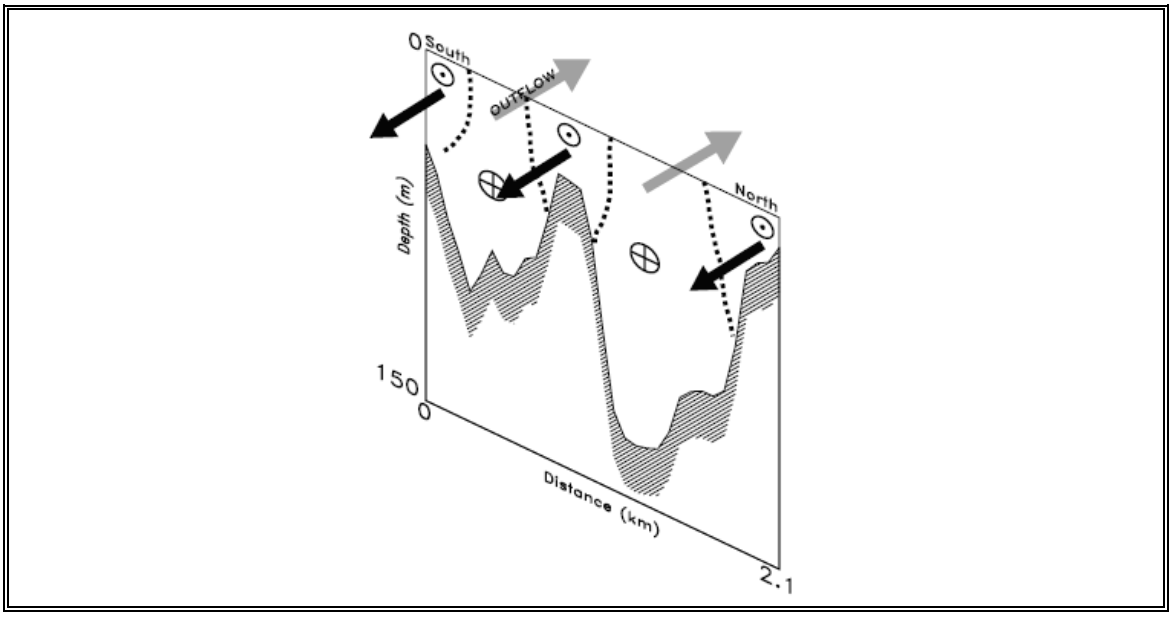

Figure 2-20: Schematic representation of the along-channel mean flow at Remolinos Rock transect. Outflow (gray arrows) and inflow (black arrows) regions are separated by strong convergences or lateral shears represented by the dashed lines. (Cáceres, Valle-Levinson, & Atkinson, 2003).

The conclusions and results obtained by these studies set the base for this particular thesis, which is in line with other investigations carried out at other tidal channels, aims at characterizing important aspects and conclusions related to tidal phenomena and energy resource assessment in the CIS, and especially in the Chacao Channel. A few other public studies and thesis relating the same area have been released in the past years, yet their results add no new information which is relevant to this thesis.

2.3.2 Available Data in the Channel

Last section was a brief compilation of main public studies that have been done in Chacao Channel and the fjords region. Additionally, a cadastre of available data in the region and Channel is also extremely important, in order to use those which are of proper quality and characteristics for the model built in this thesis, and further propose data collection locations for inputs in future models.

Data required for models in this case are basically three: bathymetry, sea surface levels (tides), and flow velocities.

a) Bathymetry

Bathymetry in these two models is taken from digital versions of Nautical Charts, given by SHOA. Figure 2-21 shows the Nautical Chart 7210, which is for the Chacao Channel, and also points out the locations of available tides (red) and flow velocities (blue) data. There are also nautical charts of a larger scale for the whole fjords region.

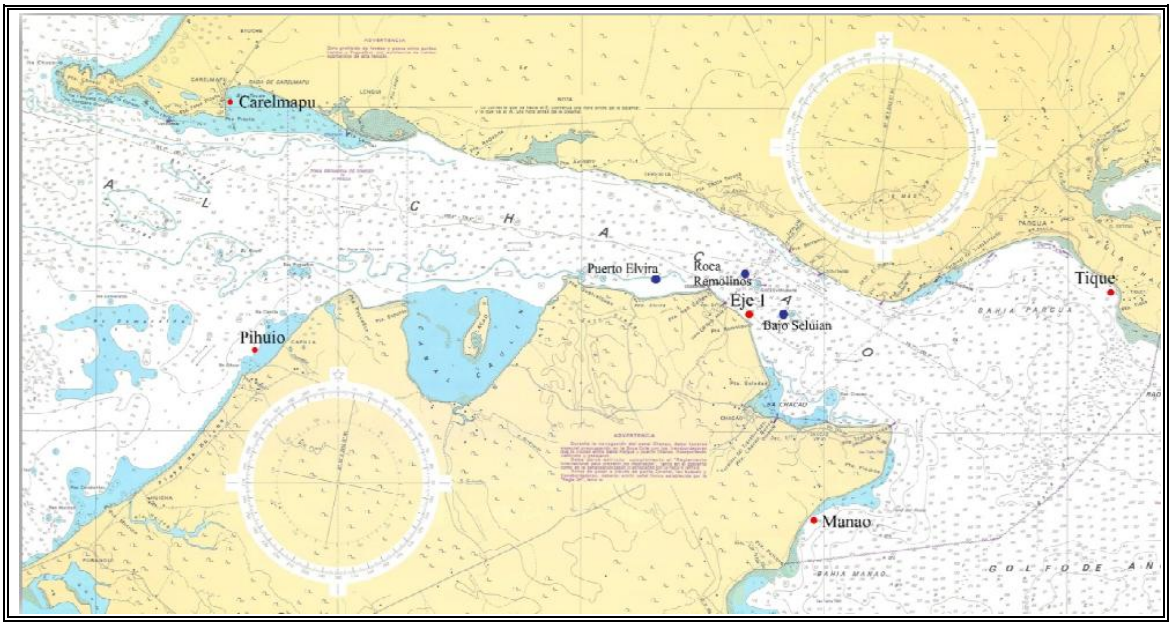

Figure 2-21: Available current and tide measurements in Chacao Channel. (Herrera, 2010).

b) Tides

Regarding tide measurements (or sea surface levels), there is available data at five points, which are detailed in Table 2-1, and their location specified in Figure 2-21. This data is a combination of SHOA measurements, and some measurements contracted by the Chilean Ministry of Public Works for a preliminary evaluation of a bridge that crosses the Chacao Channel (ICUATRO-COWI, 2000). These were not taken thought

for model inputs, therefore there quality is not the ideal for the purposes required in this study, yet they are good enough for an initial modeling approach.

Table 2-1: Summary of available tidal height measurements in modeled area. (Herrera, 2010).

Station	Latitud	Longitud	Measurement	Period Considered
Manao	41° 51' S	073° 30' W	41 days	03/12/1999 - 12/01/2000
Tique	41° 48' S	073° 24' W	106 days	30/11/1999 - 14/01/2000
			05 days	04/07/2000 - 08/07/2000
			46 days	23/07/2000 - 06/09/2000
Eje - 1	41° 48' S	073° 32' W	Permanent	03/12/1999 - 24/01/2001
Carelmapu	41° 45' S	073° 43' W	Permanent	15/01/2000 - 22/01/2001
Pihuio	41° 49' S	073° 41' W	36 days	26/05/2000 - 30/06/2000

c) Flow Velocities

Finally, flow velocities in the Channel are available at three specific points, which are detailed in Table 2-2, and once again their location specified in Figure 2-21.

Table 2-2: Summary of available velocity measurements in modeled area. (Herrera, 2010).

Station	Latitude	Longitude	Measurement	Period
Roca Remolinos	41° 47' S	072° 32' W	57 days	11/07/2000 - 05/09/2000
Puerto Elvira	41° 47' S	073° 35' W	56 days - 1 hour	12/07/2000 - 05/09/2000
Bajo Seluian	41° 48' S	073° 31' W	57 days - 1 hour	11/07/2000 - 05/09/2000

At Roca Remolinos, the ADCP was installed at 28 meters depth, using nine sampling layers of 2 meters thickness each. Measurements were done between depths 3.21 to 21.21 meters from the bottom, estimating velocity and direction of the current at each layer. On the other hand, at Puerto Elvira and Bajo Seluian the depths of installation were 30 meters, and measurements done above 3 meters from the bottom.

3. ROMS HYDRODYNAMIC MODEL

In order to implement a modeling tool that would accurately describe the tidal phenomenon in the south Chilean fjords and of the flow patterns in the Chacao Channel, a robust and flexible hydrodynamic model had to be chosen. For this, several commercial and open source models are currently available, where the Regional Ocean Modeling System (ROMS) appears to be one of the most extensively used. Its flexibility and its open source features, which allow modifying or adding routines for specific requirements, explain the popularity of ROMS among oceanographers and modelers (Haidvogel, Arango, Budgell, Cornuelle, Curchitser, & Di Lorenzo, 2008).

ROMS is a three-dimensional, free-surface, terrain-following, numerical model, which uses hydrostatic and Boussinesq approximations to solve the Reynolds-averaged Navier-Stokes equations. It has been used for various purposes in marine modeling systems, across a variety of space and time scales, including several tidal (Haidvogel, Arango, Budgell, Cornuelle, Curchitser, & Di Lorenzo, 2008).

The main stages for ROMS implementation include the following: a pre-process, in which model inputs are created and prepared; a process or model stage, in which the model runs and performs the computation of hydrodynamic variables; and a post-process, where the results obtained are worked and presented in graphic manners, that allows a proper analysis and interpretation. These and the basic equations ROMS uses to solve the problems will be further detailed in this chapter.

3.1 Basic Flow Equations

Solution routines of physical processes in the ROMS model are governed by the two basic hydrodynamic flow equations: mass conservation or continuity and momentum balance. As an option, equations related to chemical and biological processes are also available, although for this specific application we will focus on the hydrodynamics. The primitive equations, in Cartesian coordinates and two dimensions, used by ROMS where

obtained from its main website[4] and are presented below. As mentioned before, the first two are relevant for this specific model, the following three are simply presented for understanding of the model resolution procedure and structure.

Momentum balance in x and y directions:

$$\frac{\partial u}{\partial t} + \vec{v} \cdot \nabla u - fv = -\frac{\partial \phi}{\partial x} - \frac{\partial}{\partial z}\left(\overline{u'w'} - \nu \frac{\partial u}{\partial z}\right) + \mathcal{F}_u + \mathcal{D}_u \tag{3.1}$$

$$\frac{\partial v}{\partial t} + \vec{v} \cdot \nabla v + fu = -\frac{\partial \phi}{\partial y} - \frac{\partial}{\partial z}\left(\overline{v'w'} - \nu \frac{\partial v}{\partial z}\right) + \mathcal{F}_v + \mathcal{D}_v \tag{3.2}$$

Continuity equation for an incompressible fluid:

$$\frac{\partial u}{\partial x} + \frac{\partial v}{\partial y} + \frac{\partial w}{\partial z} = 0 \tag{3.3}$$

Advective-diffusive equation, for time evolution of scalar concentration field $C(x, y, z, t)$:

$$\frac{\partial C}{\partial t} + \vec{v} \cdot \nabla C = -\frac{\partial}{\partial z}\left(\overline{C'w'} - \nu_\theta \frac{\partial C}{\partial z}\right) + \mathcal{F}_C + \mathcal{D}_C \tag{3.4}$$

Equation of state:

$$\rho = \rho(T, S, P) \tag{3.5}$$

Under hydrostatic approximation, it is further assumed that the vertical pressure gradient balances the buoyancy force:

$$\frac{\partial \phi}{\partial z} = -\frac{\rho g}{\rho_o} \tag{3.6}$$

The variables used in the mentioned equations are the following:

$\mathcal{D}_u, \mathcal{D}_v, \mathcal{D}_C$	diffusive terms
$\mathcal{F}_u, \mathcal{F}_v, \mathcal{F}_C$	forcing terms
$f(x, y)$	Coriolis parameter
g	acceleration of gravity

[4] https://www.myroms.org/wiki/index.php/Documentation_Portal.

ν, ν_θ	molecular viscosity and diffusivity
P	total pressure $P \approx -\rho_o g z$
$\phi(x, y, z, t)$	dynamic pressure $\phi = (P/\rho_o)$
$\rho_o + \rho(x, y, z, t)$	total *in situ* density
$S(x, y, z, t)$	salinity
t	time
$T(x, y, z, t)$	potential temperature
u, v, w	the (x, y, z) components of vector velocity $\vec{v}$
x, y	horizontal coordinates
z	vertical coordinate
$\zeta(x, y, t)$	the surface elevation

3.2 Pre-Process

Once having decided to use ROMS as the model to reproduce tidal wave propagation and currents in the southern fjord region of Chile, there was a long learning process related to the use and structure of the model itself. Being an open source model, ROMS is quite complicated to understand (especially if one lacks experience in hydrodynamic modeling), yet the Forum[5] and WikiRoms[6] are extremely useful tools to overcome every kind of problems or unawareness.

As a part of this thesis, a simple and clear manual was written, and is included in Annex A. It explains how ROMS must be incorporated, built, compiled, run and post processed, as well as the programs and software that must be installed in the computer for correct operation. This way, next users of this model have an easy way through the ROMS

[5]https://www.myroms.org/forum/index.php.
[6]https://www.myroms.org/wiki/index.php/Documentation_Portal.

basics, manage to use the specific model developed and can incorporate possible improvements or changes.

3.2.1 Model Compilation

Next step was to build the specific model, which was going to make the calculations for the space control area and time period considered. As mentioned before, ROMS files include many different routines and sub routines to calculate and replicate different physical, chemical and biological phenomena; therefore one must build the model using the set of specific routines according to the specific application needs. In this case, where tidal propagation and currents had to be modeled, a certain mix of routines was manipulated and prepared, in order to perform the hydrodynamic modeling at a Regional and local scales (in the Chacao Channel). The list of routines used for these applications are shown in Annex B.

3.2.2 Open and Closed Boundaries

First step in the modeling process is to build the coastline of the area in study. For ROMS this is done in a package called Seagrid[7], which is a Matlab program available for all users and is also used to manage bathymetric characteristics and grid generation. In it one loads a coastline ".mat" file, which can be created from local nautical charts or extracted from online coastline databases for the area required, like the NOAA Coastline Extractor[8].

The open and closed boundaries define the domain or horizontal limits of the area to be modeled. The open boundaries are the limits of the modeling area which are made up of water, and therefore receive (and give) information to propagate along all the water cells of the grid. On the other hand, the closed boundaries are the limits that separate water from land, and therefore do not allow propagation of information, but do work as a region that may get wet and dry with the periodic movement of the sea over it.

---

[7] http://woodshole.er.usgs.gov/operations/modeling/seagrid/seagrid.html.
[8] http://www.ngdc.noaa.gov/mgg/coast/.

The condition at closed boundaries, or land limits, is one of velocity which consists in setting its gradient as zero at the edge. A ghost cell approach consisting in setting the flow velocity in the dry cell just outside of the wet domain equal to the closest interior value is adopted. A "wet-dry" routine is incorporated, which deals with varying extension of the area occupied by the sea (Aiken, 2008).

At open boundaries, a different condition is set for ocean currents (velocities) and sea surface elevation (tidal wave) (Aiken, 2008).

- Ocean currents: the Flather condition is set, which for the normal component of the barotropic velocity radiates out deviations from exterior values at the speed of the external gravity waves, with equation (3.7). The exterior values are often used to provide tidal boundary conditions to the barotropic mode (Flather, 1976).

$$\bar{u} = \overline{u}^{ext} - \sqrt{\frac{g}{D}}(\varsigma - \varsigma^{ext}) \tag{3.7}$$

  Where D is the depth at a certain point on the boundary, and ς is the sea surface level.

- Sea surface elevation: the Chapman condition is set, which assumes all outgoing signals leave at the shallow-water wave speed of $\sqrt{gD}$. Therefore surface elevation is calculated using equation (3.8). Time derivatives can be handled either explicitly or implicitly. The model uses an implicit time step, with the term $\frac{\partial \varsigma}{\partial \xi}$ being evaluated at the new time step (Chapman, 1985).

$$\frac{\partial \varsigma}{\partial t} = \pm\sqrt{gD}\,\frac{\partial \varsigma}{\partial \xi} \tag{3.8}$$

3.2.3 Bathymetry

The bathymetry refers to the geometry of the Channel seabed, which of course defines the vertical limits of the area being modeled. This is done through the Matlab based Seagrid package, referred to earlier. After loading the coastline file, one must load a

“.mat” bathymetric file, which returns a depth at defined points (called Probes) all over the modeling area. The density of bathymetric information must be defined previously depending on the availability of the information and the resolution of the required results. In this case, information was obtained from Nautical Charts published by the Chilean Navy Hydrographic and Oceanographic Service (SHOA), which do not have the ideal modeling density, given their navigational use, yet still are useful to build a large scale model and provide a relatively dense span of data.

It is important to consider the planimetry (horizontal) and altimetry (vertical) reference systems, in order to make sure that the information being used is coincident and coherent between each other. Otherwise, this could bring important errors in the model results.

- Altimetry reference system:

Usually bathymetric information is referred to the Probe Reduction Level (PRL), yet ROMS is referred to the Mean Sea Level (MSL). Therefore all the data obtained from Nautical Charts had to be adapted to the MSL, which is a procedure that must be done carefully, given that not all Charts are referred to the same PRL. This procedure is explained in detail later on in the text, at section 4.2.2.

- Planimetry reference system:

The information incorporated also must be carefully adapted to a unique horizontal reference, in X and Y axes. There are two main reference systems or “datums” used worldwide, which are the Universe Transverse Mercator (UTM) and the World Geodetic System (WGS84). Both are equally adequate, yet in this case ROMS and the Charts provide information in WGS84, therefore this system was the chosen one. This system gives the planimetric position of the points in the modeling area in degrees, minutes and seconds, and allows referencing any point on the Earth without the need of another as reference.

3.2.4 Grid Generation

Once the model boundaries and bathymetric characteristics are defined, one must specify the region or area of interest and the location of nodes where model outputs will

be given. This, once again, is done in Seagrid, which is an interactive application to generate boundary-fitted, orthogonal curvilinear grids, with four corners defined by the user. The space between nodes in the area defined can also be specified, in order to obtain a grid with information at a distance that allows proper analysis for established objectives. Given that ROMS resolves the basic equations by the finite differences method, grids and cells are square, with a certain defined number of nodes per axe (X and Y), although the grid can be adjusted at certain points for its adaptation to coastline characteristics. Figure 3-1 shows ROMS grid structure and location of information in cells, from 0 to L in the X axis and from 0 to M in the Y axis. Rho and psi points are the names of nodes where certain information is given; and u and v points, are those where the velocity in X and Y direction are given, respectively.

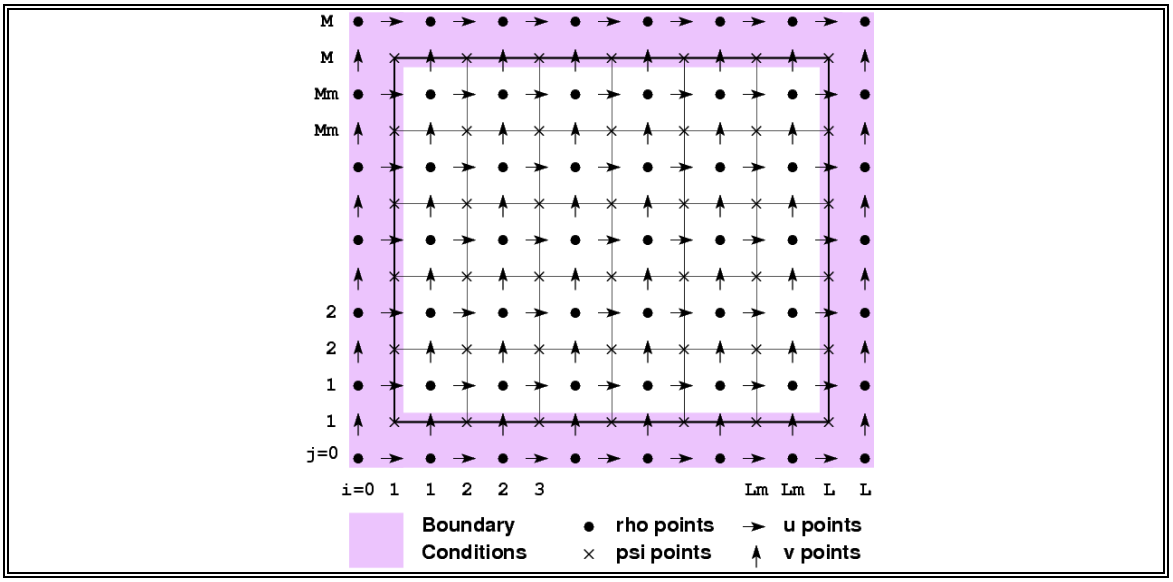

Figure 3-1: Diagram of ROMS grid structure.[9]

Once the specific modeling area in the zone of study is defined, a so-called land masking procedure must be performed in order to identify land and water areas for the

[9] https://www.myroms.org/wiki/index.php/Documentation_Portal.

information to be propagated along the proper cells. This way all the boundaries of the model are defined, and the input grid file is created.

3.2.5 Time-step

For computational economy, the hydrostatic primitive equations for momentum are solved using an explicit time-stepping scheme[10]. This way time-step is chosen based on the width of the grid cells, in a way that the Courant number is not larger than 1, but not much smaller either so as not to unnecessarily increase the computing time needed. This coefficient enforces model stability and a correct registration of results along the modeling period, so that gravity waves do not travel further than one grid cell between one time step and the next. Equation (3.9) shows the relationship that allows calculating this coefficient in order to determine your time-step.

$$\frac{\Delta t}{\Delta x_{i-j}} v_{as} \leq CFL \tag{3.9}$$

Where:

CFL: Courant-Friedrichs-Levy coefficient.

Δt: Time-step used for the modeling process.

Δx_{i-j}: Length of the cell that joins nodes i and j.

V_{as}: Tidal wave velocity of propagation in shallow waters, which is calculated as square root of the product of depth and gravity acceleration.

3.2.6 Tides

Of course one of the main steps in the pre-process is the creation of the input tidal file, which is the main forcing element of this particular model. The tidal information is extracted from an online global model of ocean tides called TPXO[11] (version 7.1), which best-fits, in a least-squares sense, the Laplace Tidal Equations and along track averaged data from TOPEX/Poseidon obtained with OSU Tidal Inversion Software. This model

[10] https://www.myroms.org/main.php?.
[11] http://volkov.oce.orst.edu/tides/global.html.

was created by Egbert and Erofeeva in 2002, and the methods used to compute the model are described in their papers (Egbert & Erofeeva, 2002).

Tides are given as complex amplitudes of earth-relative sea-surface elevation for the eight primary harmonic constituents (M2, S2, N2, K2, K1, O1, P1, Q1). The models simulations run in this thesis only consider these eight constituents of tide, given that they are the most significant ones in forcing tides in the CIS (Aiken, 2008). Finally a Matlab routine is used to obtain the output of this global tidal model, and interpolate it to the defined grid as initial conditions, which force the model at its boundaries. This is done for the regional nCIS model, yet this one provides the boundary conditions for the nested model, therefore the global model is not used for the local Chacao Channel model.

3.2.7 Model Period

A different time window is considered for the regional and nested models. The regional nCIS model required a minimal 6 month period, in order to satisfy the Raleigh criterion, which determines the minimum time-series length needed to properly resolve all the eight main tidal components. By doing so, all the tidal components were accurately reproduced throughout the area of interest, so open boundary conditions provided to the Chacao Channel model were appropriate.

For the case of the Chacao Channel model, it is net tidal currents which were of primary interest, rather than individual harmonics; therefore the simulation of a complete lunar period was sufficient to obtain the proper results. A complete lunar cycle consists of nearly 30 days (29.53 days to be more specific). Therefore once having nested the child grid in the regional model, and created the boundary conditions for it, a 30 day period run was considered.

It is important to note that one must consider a 2 to 3 day model warm-up period before it reaches a physically sound regime. Therefore this additional time period was considered in both, regional and nested models.

3.2.8 Other Parameters

Several other parameters can be modified as a model input, if this is necessary for a specific purpose, like: bottom drag coefficients; wetting and drying parameters; horizontal and vertical viscosity coefficients for momentum and active tracers; turbulent closure parameters; generic length-scale turbulence closure parameters; mean density and background Brunt-Vaisala frequency; Eigen problem parameters; linear equation of state parameters; slipperiness parameter; stochastic optimal parameters; among other input and output parameters to make the model as precise and specific as required. These parameters and values are very useful as calibration tools, in order to fit model results with measurements.

For the ROMS model implemented here, default parameters values were used, but once more precise field information is available, sensitivity analysis and model calibration should be performed in order to improve numerical results. For this particular case, if calibration was to be done, bottom drag, wetting and drying, and viscosity parameters are the most sensitive ones, and therefore should be the first options to vary.

3.3 Process

With all the required inputs created, the regional model is run in order to capture the main features of the tidal wave propagation in the nCIS. Then, boundary conditions for the child nested Chacao Channel model are provided in order to compute the flow hydrodynamics at a smaller scale.

The regional model aims at propagating the tidal components from deep waters (hundreds of kilometers offshore), into the northern fjords region surrounding Chiloe Island, and to capture the resonant dynamics described in section 2.3, which is responsible for the amplification of tidal amplitudes at Reloncaví Sound and tidal currents at the Chacao Channel. The boundary conditions for the nested model are provided in the form of tidal ellipses, wave amplitude components and phases.

The local nested model of the Chacao Channel aims at describing the spatio-temporal evolution of tidal currents over one lunar cycle, in order to identify hot spots for energy extraction and assessment of device production.

3.4 Post-Process

This stage deals with the process, analysis and presentation of the numerical data generated by the model. The modeling approach implemented here produces a large series of data in space and time, which must be classified, treated and statistically analyzed in order to assess the tidal energetic resource of the Chacao Channel. The regional and nested models have different purposes, and consequently their results require specific treatments.

Regional nCIS model:

- A sensitivity analysis of grid size and modeled time period will be performed, to understand the effects these could have over results.
- Amplitude and phase of all eight major tidal constituents will be compared to available measurements at four different locations along the Chacao Channel, in order to test the relevance of the model.
- Tidal resonance along the gulfs of Corcovado and Ancud until Reloncaví Sound will be studied, and compared to Aiken's (2008) results, by sketching the variation of tidal amplitude with the distance traveled from the mouth.

Chacao Channel model:

- Detailed characterization of the Chacao Channel's hydrodynamic behavior, combined with a description of its topographical aspects.
- Tidal currents variations will be analyzed along the channel, in order to further understand potential tidal resource availability in space and time
- Averaged flows over transects along the Channel will be computed in order to identify the most attractive sections in terms of kinetic energy.
- Power maps of tidal currents will be presented along the Channel, in order to

assess power availability at specific locations for future energy extraction with Marine Current Energy Converters (MCEC).

- Recommendations of locations for future measuring equipments (tide gauges and ADCP's) will be given, so that proper model calibration is done in the future.

4. CHILEAN INLAND SEA AND CHACAO CHANNEL HYDRODYNAMICS

This section details how the nested 2D ROMS models were built, and the inputs they used to reproduce the tidal phenomena occurring in the CIS and Chacao Channel, respectively. After detailing the modeling process, the main results obtained will be presented and analyzed.

4.1 2D ROMS Regional Model

A first model of the whole northern region of the Chilean Inland Sea was built and run, in order to propagate tidal waves along it and therefore provide boundary conditions for the Chacao Channel model. The inputs and steps followed are detailed in the following sections.

4.1.1 Bathymetry

The bathymetric information for the regional model was obtained from the SHOA nautical charts numbers 7000 and 8000, which are at a scale of 1:500.000. This resolution is good enough for the scale of modeling being done here; therefore it was not necessary to include more detailed charts. All the charts of the area involved are shown in Figure 4-1 (SHOA, Cartas y Publicaciones Náuticas (Publicación SHOA N° 3000), 2010).

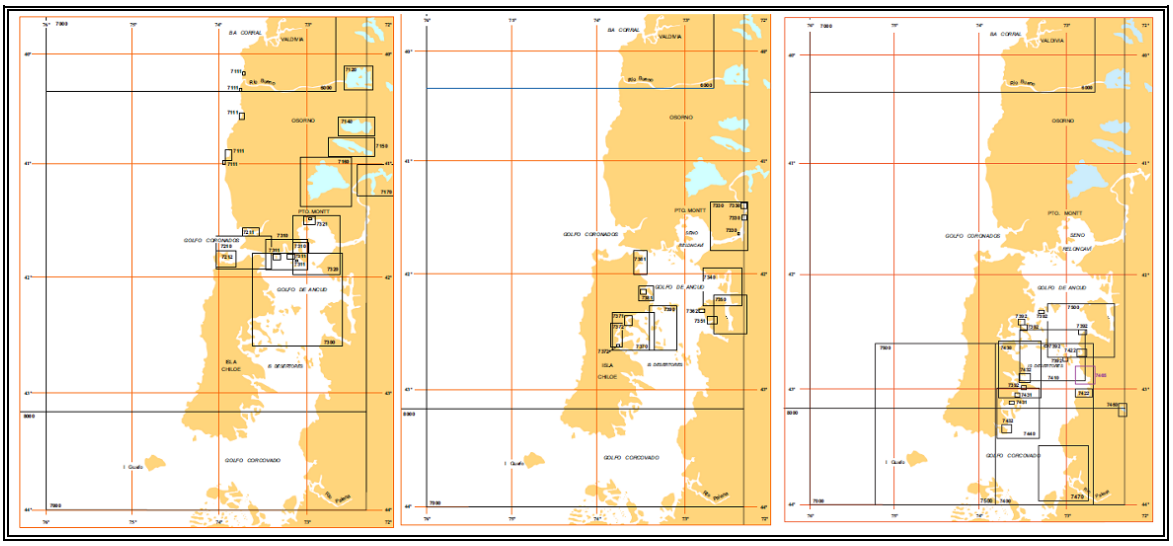

Figure 4-1: Detail of SHOA nautical charts available in the region. (SHOA, Cartas y Publicaciones Náuticas (Publicación SHOA N° 3000), 2010).

Although values in nautical charts are referenced to the Probe Reduction Level and ROMS to the Mean Sea Level, it was not necessary to apply corrections to the bathymetry because of large depths found at these scales. Therefore depths were incorporated without corrections (Aiken, 2008).

4.1.2 Limits

For the regional model, limits where defined as shown in Figure 4-2, where the red square represents the complete modeled area, the orange line represents the open boundaries, and the yellow arrows represent the points of tidal wave entrance towards the CIS from the Pacific Ocean. This makes up an area of approximately 430 km long and 360 km wide region, which is equivalent to an area of 154,800 km².

Figure 4-2: Sketch of model limits, open boundaries and tidal wave entrance.

As can be seen from the figure, the western limit goes far offshore, in order to force the model with tidal information produced with the TPXO model, which is accurate in open seas. Eastern limit of course is completely closed, as it is on top of the continent. Southern and northern limits are partially closed, given that they have land sections and water sections respectively, where tidal variation information is received at open boundaries and passed on along the grid cells in the modeled area.

4.1.3 Sensitivity Analysis

Having defined the limits of the area involved in the model, a choice of grid size, time step and modeling period had to be done. In order to define these, a sensitivity analysis was done in order to test the response of the model to variations in these variables.

a) Model Grid Size

A first sensitivity analysis was done with grid size, in order to determine how a variation in grid size influenced the numerical results produced by the model, keep all other parameters constant. Three models of different grid sizes were run, for the single M2 tidal constituent, and for a time window of 10 days with a sampling rate of 20 minutes, yet decreasing time step so that the Courant number was not larger than 1. This is presented in Table 4-1.

Table 4-1: Toy models characteristics for varying grid size.

	Model 1	**Model 2**	**Model 3**
Length	10 days		
Register Frequency	20 min		
Tidal Constituents	M2		
Grid Size	10 km	5 km	2,5 km
Nodes in X	36	72	144
Nodes in Y	43	86	172
Time-step	12 s	10 s	4 s

The amplitude of the M2 tide along the axis of the nCIS was chosen as the metric with which to compare the models. By analyzing how the M2 semidiurnal constituent was amplified by resonance along the gulfs of Corcovado and Ancud, until Reloncaví Sound, differences could be compared to see the grid's influence (Aiken, 2008). The results are presented in Figure 4-3.

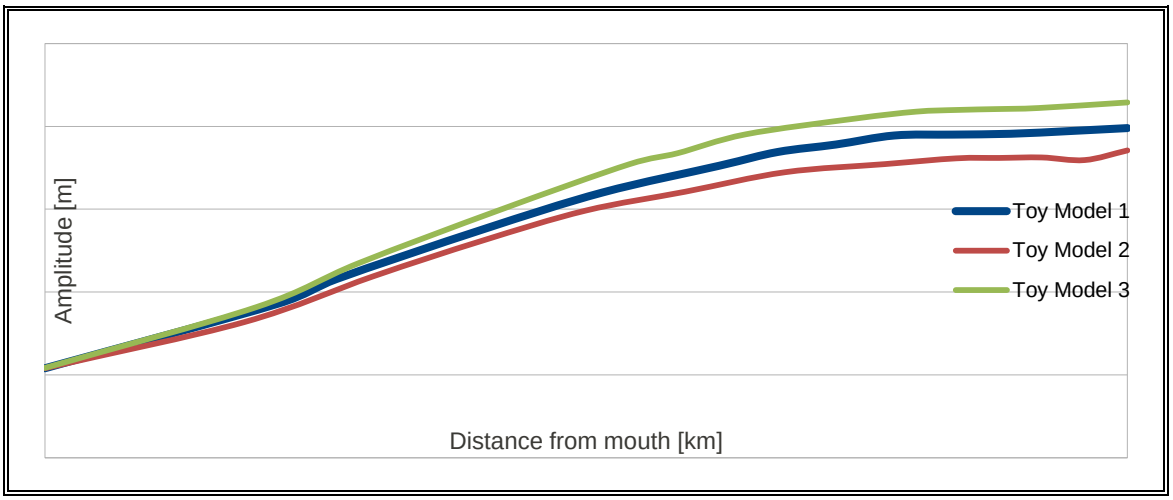

Figure 4-3: Comparison of tidal resonance effect over varying grid sizes, for M2 tidal component.

Figure 4-3 shows how tidal wave propagation varies for each three models, therefore demonstrating model sensitivity to grid size. This is explained by the close proximity of tidal waves to resonance in the area, making it extremely sensitive to geographical variations and model resolution. It can be concluded that grid size actually does have an effect over tidal wave propagation in the models. In this case, models 1 and 3 seem to over amplify the tidal wave as it propagates through the area, therefore leading to choose model 2 as the best fit. This way a grid size of 5 km is chosen to reproduce tidal waves in the regional model, and as a boundary input for the high resolution Chacao Channel model.

Since grid size and time-step together set Courant number values, choosing a value for one of them and setting Courant at a maximum value equal to 1, gives the value for the other. In this case, grid size was the main parameter, therefore time-step was chosen based on its value.

b) Model Period

Next, a test between two models considering all eight major tidal constituents (M2, N2, S2, K2, K1, O1, P1, and Q1) was run, but this time grid size was fixed and it was length

of modeling period that varied. Table 4-2 shows the characteristics of each of these models.

Table 4-2: Model characteristics for varying modeling length.

	Modelo 3a	**Modelo 3b**
Grid size	2,5 km	
Register Frequency	1 hour	
Tidal Constituents	M2, N2, S2, K2, K1, O1, P1, Q1	
ΔX	144	
ΔY	172	
Time-step	6 s	
Length	30 days	7 months

The results between both models were then compared with component amplitude values at two main points in the Ancud Gulf (Manao and Tique, shown in Figure 4-4), where measurements were done in 2000 by an engineering company as a part of a study for a bridge connecting the island of Chiloé with the continent (Sutherland, Foreman, & Garrett, 2006). This way, results obtained with the models can be compared for a proper definition of model length, given that certain components develop different than others along the gulfs, and an ideal length is chosen to properly reproduce tidal propagation.

Figure 4-4: Location of tidal measurements in Ancud Gulf.

Table 4-3 shows the results obtained from each model, where it is clear that a 30 day modeling period is not sufficient to resolve all 8 tidal components. Given that the model has a resolution of 5 km, it will not properly reproduce tides inside the Chacao Channel, where Carelmapu and Pihuio are located. Therefore only Manao and Tique are chosen because they are in a more exposed area, and less sensitive to bathymetric errors. At both points, 30 day models did not achieve a value for N2, K2, P1 and Q1 components, whilst 7 month models did. This shows that a 7 month model period must be attained for the regional model, in order to allow the generation of a time series long enough to accurately extract the 8 tidal harmonics. This is a characteristic of all tidal models, given by the Raleigh criterion.

Table 4-3: Sensitivity results for tidal components at Manao and Tique.

Constituent	Period	Manao			Tique		
		Amplitud [m]					
	[hr]	Model 2a	Model 2b	Measured	Model 2a	Model 2b	Measured
M2	**12.42060**	1.8666	1.8633	1.801	1.8635	1.8557	1.763
S2	**12.00000**	0.7014	0.8598	0.577	0.6991	0.8555	0.741
N2	**12.65835**	0.4331	0.4445	0.498	0.4315	0.4423	0.439
K2	**11.96723**	-	0.1924	-		0.1915	0.201
K1	**23.93447**	0.2731	0.2196	0.270	0.2726	0.2191	0.212
O1	**25.81934**	0.1484	0.1441	0.146	0.1483	0.1438	0.146
P1	**24.06589**	-	0.0745	-		0.0744	0.072
Q1	**26.86836**	0.0277	0.0291	0.030	0.0277	0.0291	0.030

Finally, it is clear that the regional model is doing a good job in reproducing tides inside Corcovado and Ancud Gulfs. Table 4-3 shows that differences between modeled and measured amplitudes of tides at Manao and Tique, are at average around 1 or 2 centimeters, although S2 component was not reproduced as well as the others. Analyzing the time period effect, one can actually notice that there is a slight difference between the 30 day model and the 7 month model. The shorter model did not allow the creation of enough data to estimate K2 and P1, and it can be observed that some components are improved when expanding the modeling period. This leads us to conclude, that as long as computational capacity allows it, a longer modeling period is necessary for the generation of time series long enough for reproduction of all time series.

4.1.4 Model Grid

As was defined in the past section, a 5 km sized grid was chosen to span the whole area, which means it has 86 rows and 72 columns, meaning a total of 6,192 nodes. Figure 4-5 shows the grid used in the Seagrid platform, which was then incorporated to the model run.

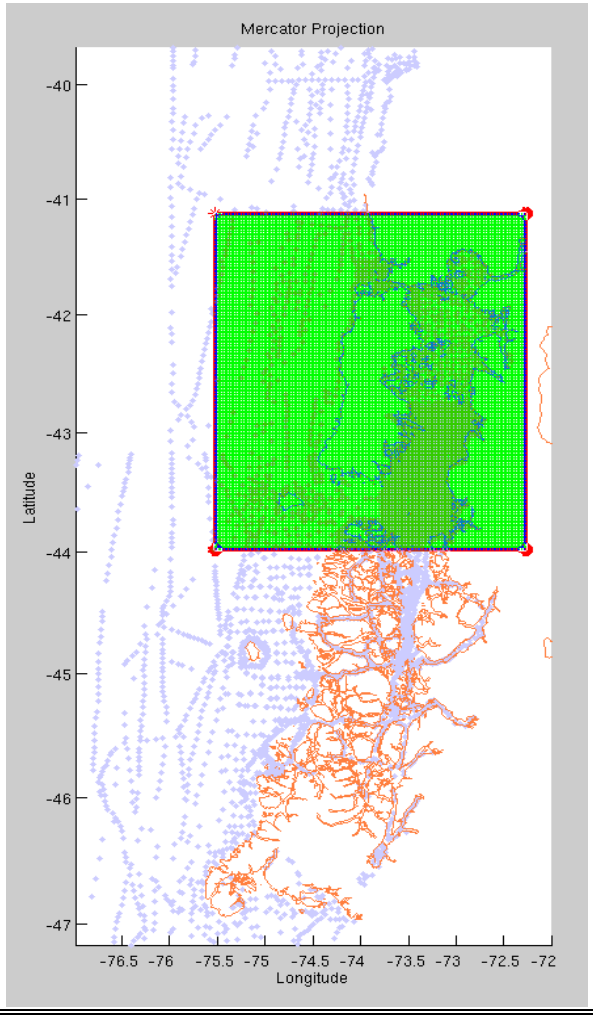

Figure 4-5: Regional model grid of 86 rows and 72 columns.

4.1.5 Period

As well as the grid size, the sensitivity analysis allowed to determine a proper modeling period, in order to obtain results as real as possible. From the analysis done, a modeling period of one month was not enough to reproduce all main tidal constituents; therefore a modeling period of 7 months was a satisfying value to obtain adequate results of tidal propagation. Although it is actually the Raleigh criterion, included in T-Tide's least squares analysis of data series, which sets this period. Therefore it's the amount of time you need to be able to resolve the contributions from the 8 harmonics.

4.1.6 Model Calibration

Model calibration is a necessary step in the modeling process, especially for the regional model, given that it works as an input for the nested Chacao Channel model. In this case, results can be compared with tidal measurements available at some specific points along the modeled area. A few are permanent measurements which do give out good statistical values, yet some other measurements available were made at certain periods which are not statistically strong enough to give proper results. Table 2-1 (page 35) shows a summary of sea surface height measurements at different points, which were used in the calibration process.

This way, these measurements are not trust worthy enough to use as a calibration reference, and in the future this model should be properly calibrated, using proper measured data, to obtain as near to real results. Anyway, results obtained in this model have proved to be good, but could eventually be improve significantly. As mentioned before, parameters relating bottom drag, fluid characteristics, mixing and advection can be used as calibration adjustment "dials". While improving the performance of the regional model is an important goal for studying tidal energy in the Chacao Channel, the results obtained are sufficiently accurate to provide realistic boundary conditions for the high resolution Chacao Channel model.

4.2 2D ROMS Chacao Channel Model

Once having obtained the results from the regional model, boundary conditions for the nested model could be derived, and the local Chacao Channel model was ready to be built and run. The following section details the building process and inputs incorporated to it.

4.2.1 Limits

For this particular model limits had to be defined in a way that all the Chacao Channel was incorporated, but as well considering a larger area to take into account a stabilization area at both ends of the channel, where results could be affected by

boundary conditions. As shown for the past model, Figure 4-6 shows the model limits, where the red line shows the complete area incorporated in the model, and orange lines represent the open boundaries where model is forced by outputs of the regional model. This makes up an area of approximately 53 km wide and 30 km high, which is equivalent to an area of 1,590 km².

Figure 4-6: Limits of the Chacao Channel model.

Limits and boundaries of the model show how, clearly the model is forced at both Channel ends, at the northwest (Pacific Ocean) and southeast (Ancud Gulf) corners, respectively. This information is then passed on to neighbor cells, until the whole area is spanned, for the complete modeling period.

4.2.2 Bathymetry

Bathymetric information for this model was taken from the SHOA Nautical Chart N°7210 of Chacao Channel, which is shown in Figure 4-7, yet modified by Herrera (2010) due to discordance in reference planes.

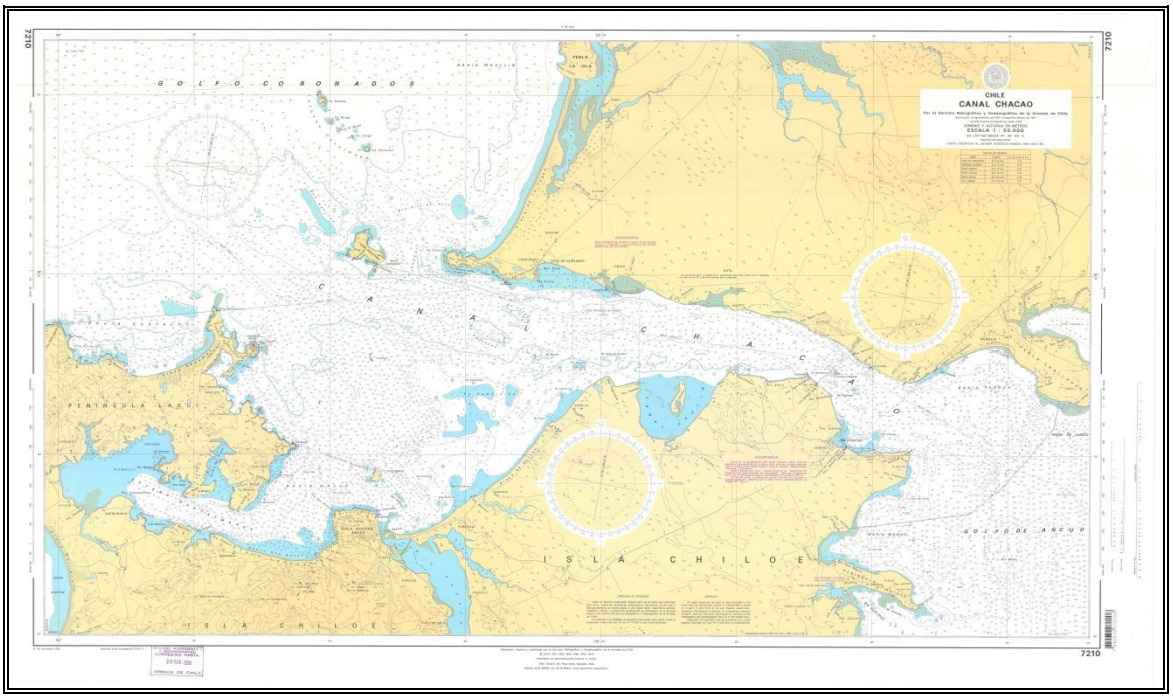

Figure 4-7: Nautical Chart N°7210 of Chacao Channel. (SHOA, Cartas y Publicaciones Náuticas (Publicación SHOA N° 3000), 2010).

This slight discordance between nautical chart information and ROMS modeling inputs, where the first uses PRL as a reference and the second uses MSL, meant data had to be adjusted so that inputs were correctly prepared. In particular, the nautical chart 7210 was elaborated using minimal astronomical tides at Chacao, Pargua, Carelmapu and Ancud, which makes it difficult to set a single reference for the whole data in the modeling area. Yet all boundary conditions must be referenced to a same plane, making it necessary to adjust all the data.

The data utilized as an input for this model was modified to correct this discordance, using the methodology given by publication SHOA N°3105, "Instrucciones Hidrográficas N°5". This consisted in estimating the Probe Reduction Level (PRL) along the whole modeled area, which was established considering the sum of all main individual tidal constituents N_2, S_2, M_2, K_1 y O_1, as seen in equation (4.1).

$$NRS = Z_0 - (H_{M2} + H_{S2} + H_{N2} + H_{K1} + H_{O1}) \quad (4.1)$$

Where:

Z_0 = Mean Sea Level.

$H_{M2}, H_{S2}, H_{N2}, H_{K1}, H_{O1}$ = Semi amplitude of the respective constituents.

It must be considered that the PRL calculated at all 5 measuring stations are not comparable between each other, given that they are a function of the tidal sensor or the difference between the fixed tidal level and the instrumental zero of each station. Finally, it was concluded that there was not a common datum to establish the model bathymetry; therefore the mean sea level was defined as the horizontal plane reference. This criterion was used for all data along the model area.

Final bathymetric data used as input is shown in Figure 4-8, in a 3D view, which is visualized from Ancud Gulf channel mouth towards the Pacific Ocean. There the variation in sea bottom can be seen along the Channel, and a preliminary idea of hydrodynamic flow hot spots and directions can be thought of.

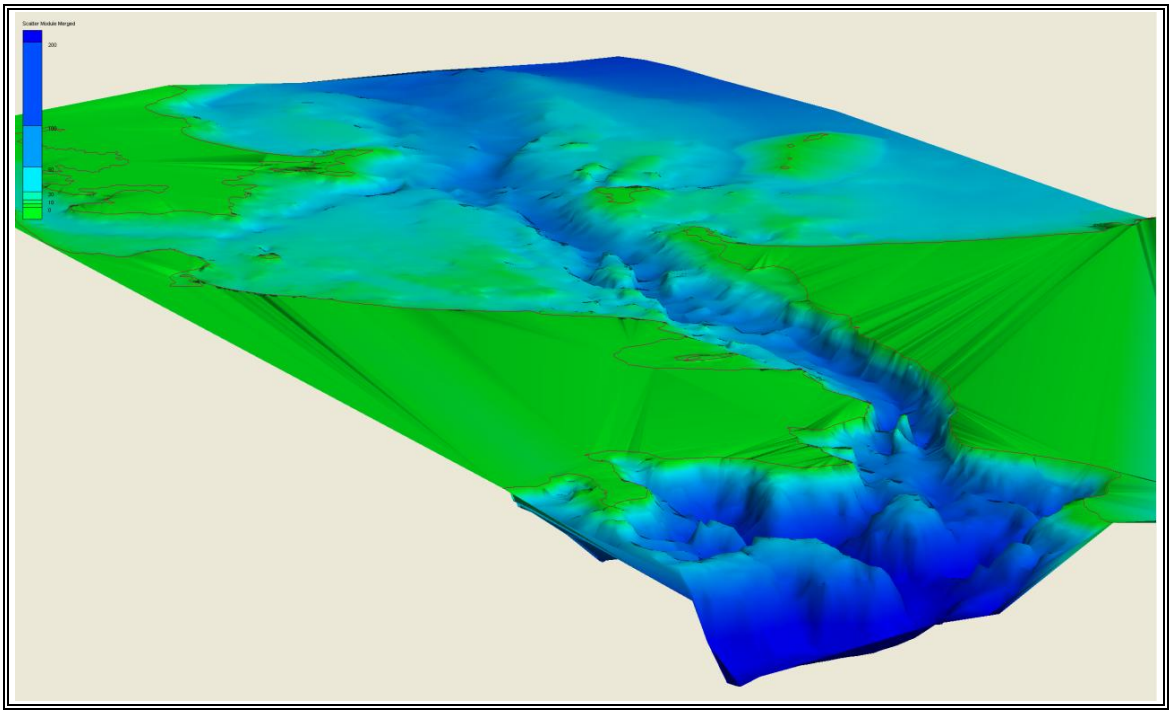

Figure 4-8: 3D view of Chacao Channel bathymetry. (Herrera, 2010).

4.2.3 Model Grid

The grid size chosen for this model was basically limited by computational availability, because although ideally a 10 to 50 m grid should be incorporated, this requires an extremely high computational capacity. The grid chosen for this particular model was one with cells of 370 m side length (see Figure 4-9). This is equivalent to a grid with 143 nodes in the X direction (columns) and 82 nodes in the Y direction (rows), which means a total of 11,726 nodes.

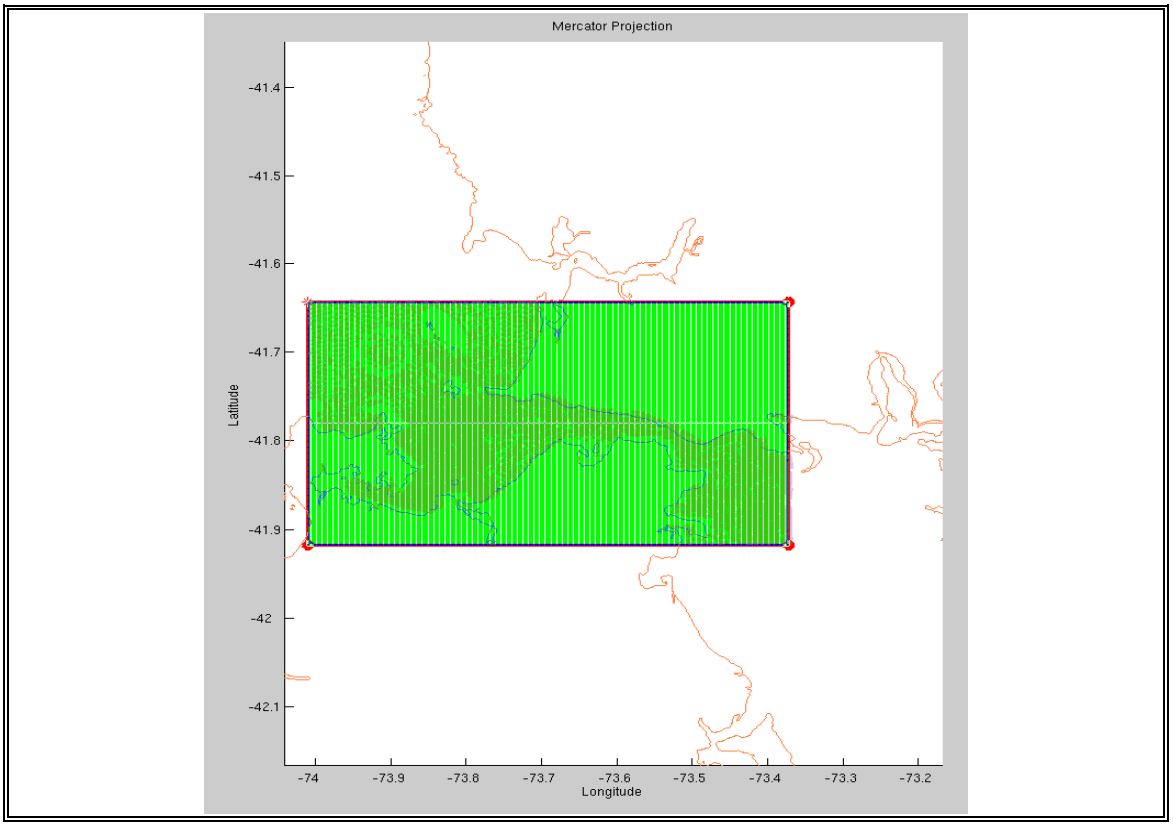

Figure 4-9: Chacao Channel Seagrid model grid of 82 rows and 143 columns.

4.2.4 Nesting Process

The nesting process basically consists in a Matlab routine that does the following steps to create an input forcing file for the nested model:

- Read in time series from the regional model domain.
- Calculate the tidal harmonics at each point in the large domain using T-TIDE package (Pawlowicz, Beardsley, & Lentz, 2002).
- Convert velocity harmonics (amplitude and phase lag) to the tidal ellipse format.
- Interpolate each required harmonic to the small domain grid.
- Add the tidal constituent data to the ROMS forcing file.

4.2.5 Model Calibration

The last step in the modeling process is to calibrate the model results with real data, in order to insure that information given by the model is realistic. For this particular model there are sea level surface data from the five stations mentioned before (Table 2-1), and there are also velocity data from three stations, which are specified in Table 2-2.

With this data one can proceed to adjust model parameters, in order to make results fit with measurements and eventually have a model as close to reality as possible. In this case, boundary conditions were given by another model; therefore it was important to make sure that results from that large model were certain before adjusting the nested model. Once again, data available at the moment were not strong enough to calibrate the model as precisely as should be done, yet it was useful as a benchmark. In the future, longer period coordinated measurements along the Chacao Channel should and will be done, and these will have to be used to calibrate this model properly. As well, from the experience obtained in this study, recommendations regarding tide gauges and ADCP's locations will be given, so that this process is done correctly for future model building.

5. RESULTS AND DISCUSION

5.1 Regional Model

Firstly, the regional model was run for two main reasons: understand and study the behavior of tidal waves through the geographically complex region of Chiloé and the southern fjords of Chile; and, generate boundary conditions to a local medium scale model of Chacao Channel. The results presented below point towards accomplishing those two main objectives.

5.1.1 Tidal Components Comparison

First of all, it was extremely important to compare model results with real measurements, to make sure that the model was properly reproducing the tidal propagation in the region. This was done by comparing values of the main tidal constituents, at specific points where these measurements were available. As was explained before, some sea surface level measurements have been done in Chacao Channel, for diverse studies and investigations, and this information was used as a benchmark to qualify how well the model was doing. One must add that these measurements are not located at the ideal locations to compare with the model, nor are they of the appropriate extension for tidal constituent reconstruction, therefore they are not an ideal comparison. Eventually, proper measurements will be done, at locations thought for model calibration and of the proper time length. Table 5-1 shows the results obtained.

Table 5-1: Measured and modeled comparison of main tidal components.

Constituent	Amplitud [m]							
	Manao		Tique		Carelmapu		Pihuio	
	Model	Measured	Model	Measured	Model	Measured	Model	Measured
M2	1.8633	1.801	1.8557	1.763	0.7991	0.916	0.7085	0.889
S2	0.8598	0.577	0.8555	0.741	0.3122	0.354	0.2727	0.251
N2	0.4445	0.498	0.4423	0.439	0.1764	0.214	0.1568	0.237
K2	0.1924	-	0.1915	0.201	0.0711	0.102	0.0632	-
K1	0.2196	0.270	0.2191	0.212	0.1756	0.185	0.1704	0.234
O1	0.1441	0.146	0.1438	0.146	0.118	0.124	0.1161	0.117
P1	0.0745	-	0.0744	0.072	0.0581	0.062	0.0565	-
Q1	0.0291	0.030	0.0291	0.030	0.0237	0.025	0.0229	0.030

As can be observed, tidal constituents N2, K2, K1, O1, P1 and Q1 are well reproduced by the model at all four spots, presenting mean errors under 10 centimeters (and in some cases less). Constituents M2 and S2 are over estimated at all four spots, at average by a difference of around 50 centimeters. These differences either can mean a need to adjust certain model parameters, or to improve the quality of measurements. Even so, differences obtained are in an acceptable range and there is a clear correct proportion between constituents, therefore the model is reproducing tides correctly in order to generate boundary conditions for the Chacao Channel model. At Manao and Pihuio, measurement lengths were not long enough to reproduce constituents K2 and P1, which is why these values are not given. Finally, it is important to mention that all the amplitudes obtained here were done so with T_TIDE model, which is a Matlab based model that uses harmonic analysis method, based on time series data (Pawlowicz, Beardsley, & Lentz, 2002).

5.1.2 Tidal Resonance

The CIS is an extremely complex region in geographic terms, which makes it very difficult to model and obtain adequate results, but this does not mean it cannot be done. One of the main objectives of this regional model was to study and understand tidal propagation in the region, which included tidal resonance effects. This resonant effect

was proposed by Cáceres (2003), reaffirmed by Aiken (2008), and is the main forcing factor for currents in Chacao Channel. This is why it was extremely important for the model to properly reproduce this effect, which would also prove its proper functioning. Figure 5-1 shows a sketch of the tidal amplitude augmentation as the wave travels from Guafo Mouth to Reloncavi Sound. This figure shows a clear resemblance to the one built by Aiken (2008), and shows a very similar result, confirming the proper work of this model.

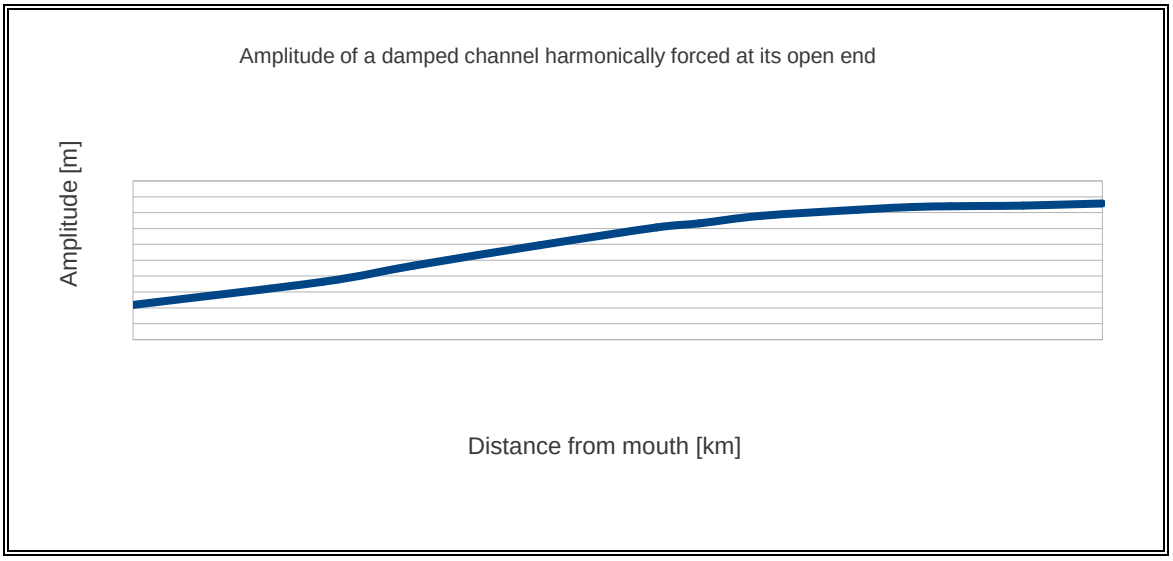

Figure 5-1: Tidal wave amplitude resonance from Guafo mouth to Reloncaví Sound.

Together, with augmentation of tidal amplitude to over 4.5 meters at Ancud Gulf, there is a phase lag between tidal peaks at each side of Chacao Channel, which produces even larger height differences and therefore explains the high tidal flows. This phase lag occurs because tidal waves that enter through Guafo mouth and travel northwards through the Gulfs of Corcovado and Ancud, begin to slow as depths become smaller, and therefore reach the eastern side of the Channel with a certain lag with respect to the same wave reaching the open ocean western side. This way, from model results it was

determined that waves reach the eastern side of Chacao Channel with a one hour lag approximately, with respect to the wave reaching western side.

Understanding the existence of a resonant tidal wave in the nCIS (and the lag between each side), gives a good idea of how tides work in the region and explains the existence of large tidal flows in Chacao Channel. Not much detail is necessary for this particular model, especially for the objective it has. Aiken (2008) goes into a major detail of the complete CIS, and discusses the sensitivity of tidal propagation to changes in its geographical characteristics, which helps to get an even better idea of the complete tidal propagation phenomena.

5.2 Chacao Channel Model

Output results from the regional model were used as forcing inputs to this Chacao Channel model. After having run this model several conclusions and results were obtained, which are presented and discussed in the following section.

5.2.1 Hydrodynamics in the Chacao Channel

In order to visualize and understand velocity distributions within the Chacao Channel, it was important to begin presenting figures with velocities along the channel in extreme situations over the whole modeling period. In this case, Figure 5-2 and Figure 5-3 show velocities in Syzygy along the Channel at flood and ebb tide respectively; similarly, Figure 5-4 and Figure 5-5 show velocities in Quadrature along the Channel at flood and ebb tide respectively. These figures allow to visualize the distributions and variations as flows flood (enter the Channel from open ocean) or ebb (exit the Channel towards open ocean). It is also interesting to visualize the shape of the plume that is formed as flows enter and exit, which is clearly related to the shape of the Channel bed.

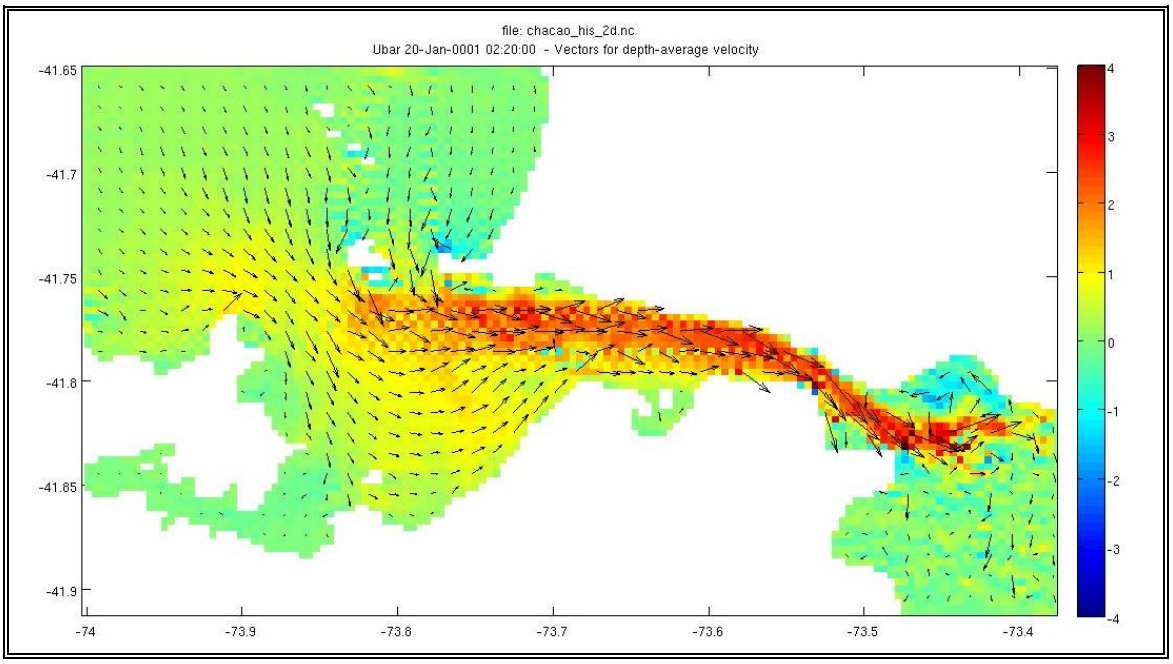

Figure 5-2: Modeled flood flow velocities (m/s) at Syzygy.

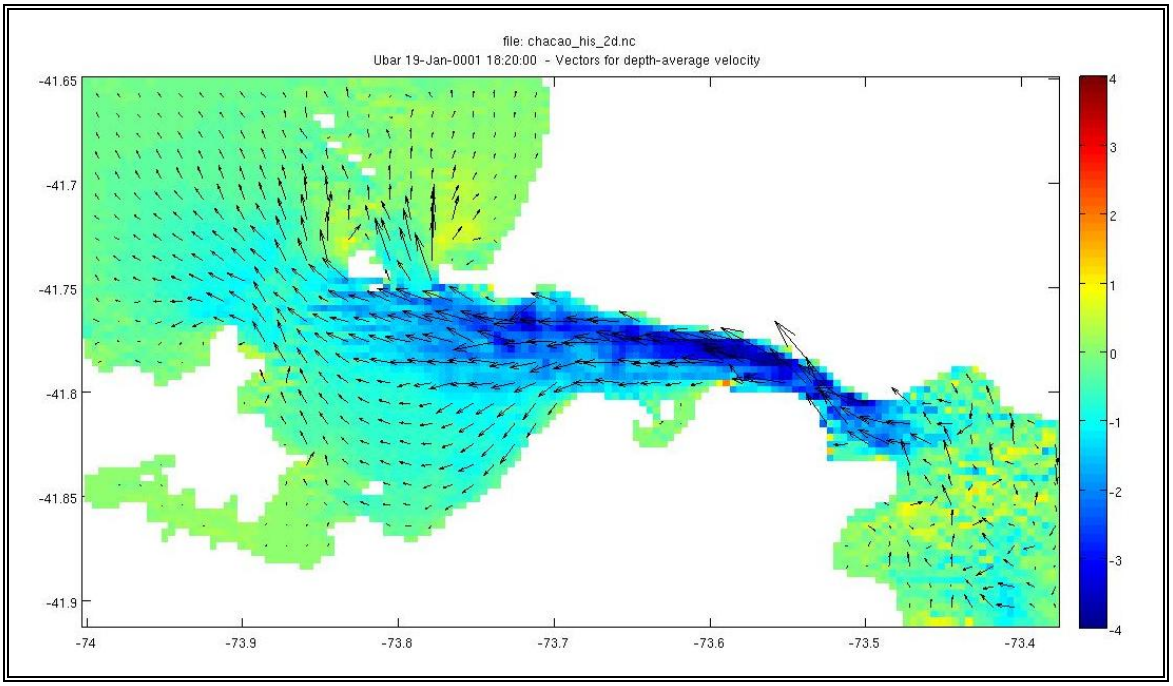

Figure 5-3: Modeled ebb flow velocities (m/s) at Syzygy.

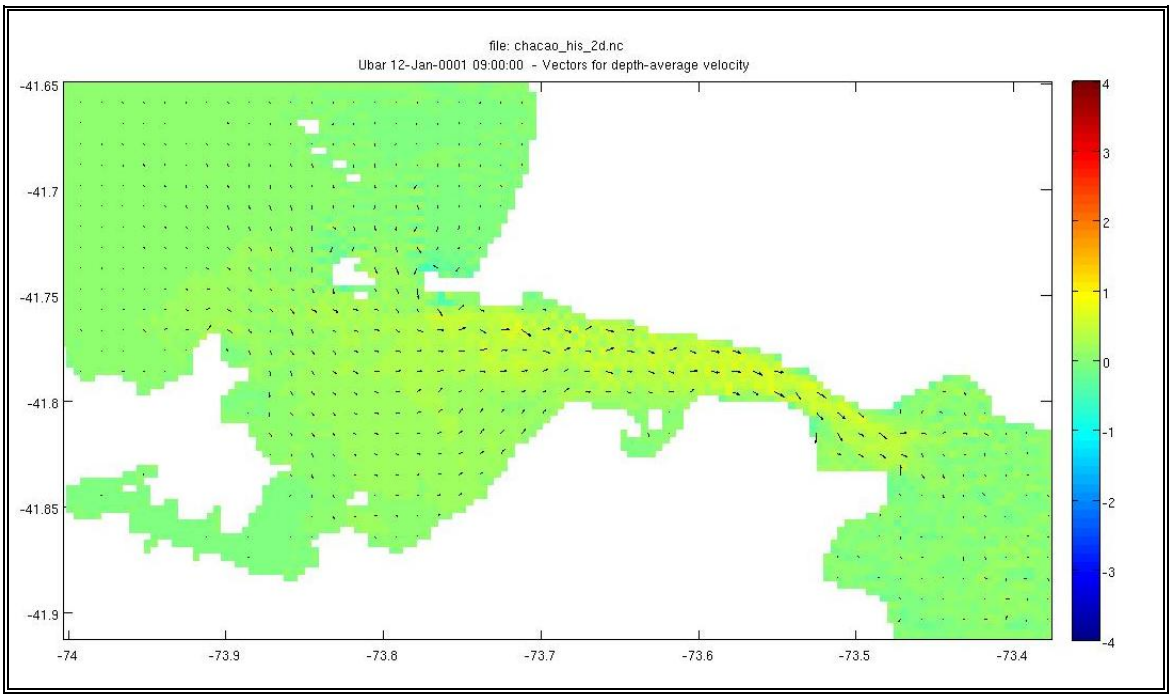

Figure 5-4: Modeled flood flow velocities (m/s) at Quadrature.

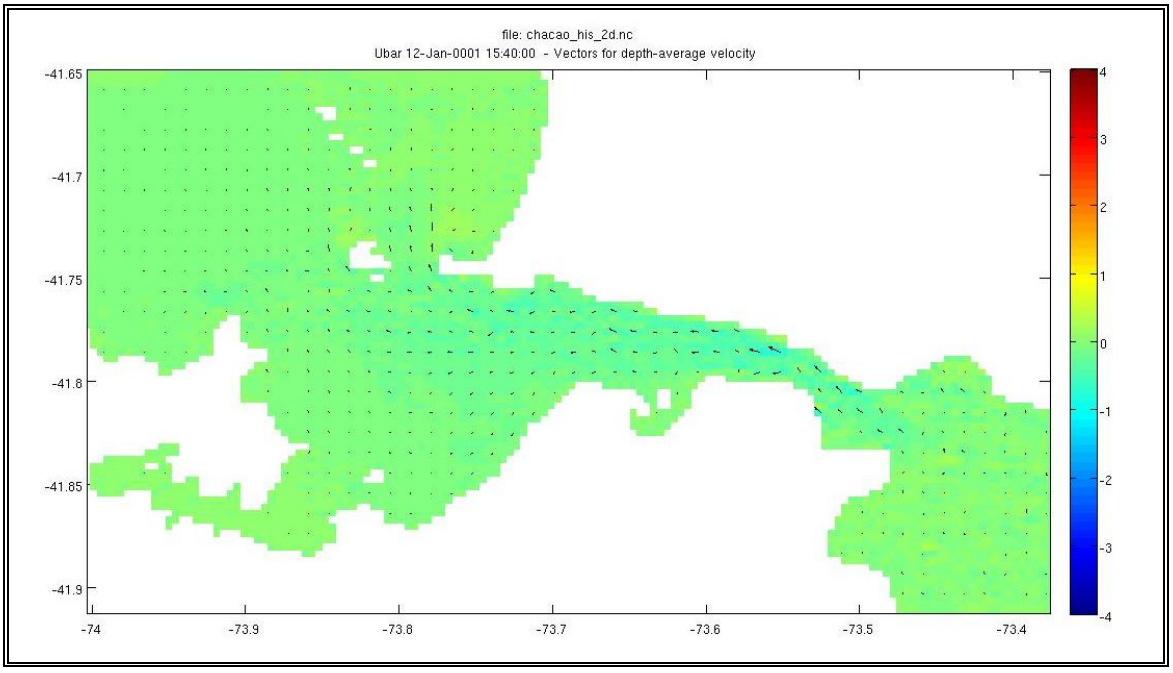

Figure 5-5: Modeled flow velocities (m/s) at Syzygy.

From these figures, it can be seen how velocity distribution changes with ebb and flood tide, and also how maximum velocities change at Syzygy and Quadrature. It is important to notice how velocities change in both these situations, where flows at ebb are larger than those at flood, even though one would believe it's the other way round, given the larger volume of mass pressuring Channel water at its open ocean end. Basically, by observing areas of darkest colors in the region of modeling, one can identify spots with the highest flows along the Channel. The spots of largest currents in these maps coincide with hot spots identified by past modeling studies done in the Channel, using Mike21 (Herrera, 2010). The spot with largest currents along the Channel is Remolinos Rock, which is clearly explained by it being the narrowest section of it. This way a funnel effect produces extremely strong currents, but as well extremely turbulent and harder to predict. Tidal turbines require constant, quasi-steady flows, which is why this spot is not considered a good place for turbine deployment.

Two spots with different flow patterns are chosen to perform an analysis of velocity time series over the whole modeling period. Figure 5-6 shows variations of velocity at Remolinos Rock (blue) and Carelmapu (green), together with a curve representing the sea surface level difference between both ends of Chacao Channel (red). This figure is useful to see how velocities vary at these two spots, where values range between 1 m/s at Quadrature and 3.5 m/s at Syzygy. In parallel, sea surface height differences range between 0.5 m at Quadrature and 2.5 m at Syzygy.

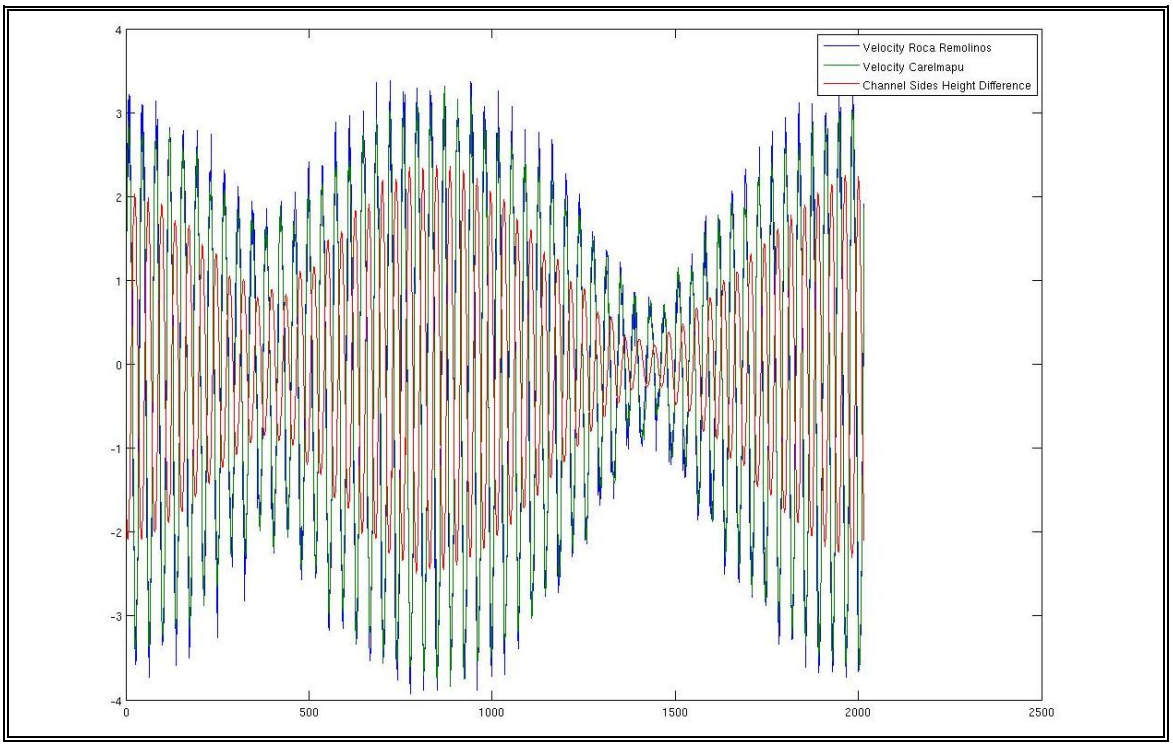

Figure 5-6: Tidal velocities at Carelmapu (green) and Remolinos Rock (blue), compared with tidal differential between both sides (red).

Zooming in to peak values at Syzygy in Figure 5-7, one can observe the lag existent between peak tidal height differences and peak velocities, which also help to understand how long it takes flows to respond to its forcing element (tidal height difference between the Channel ends).

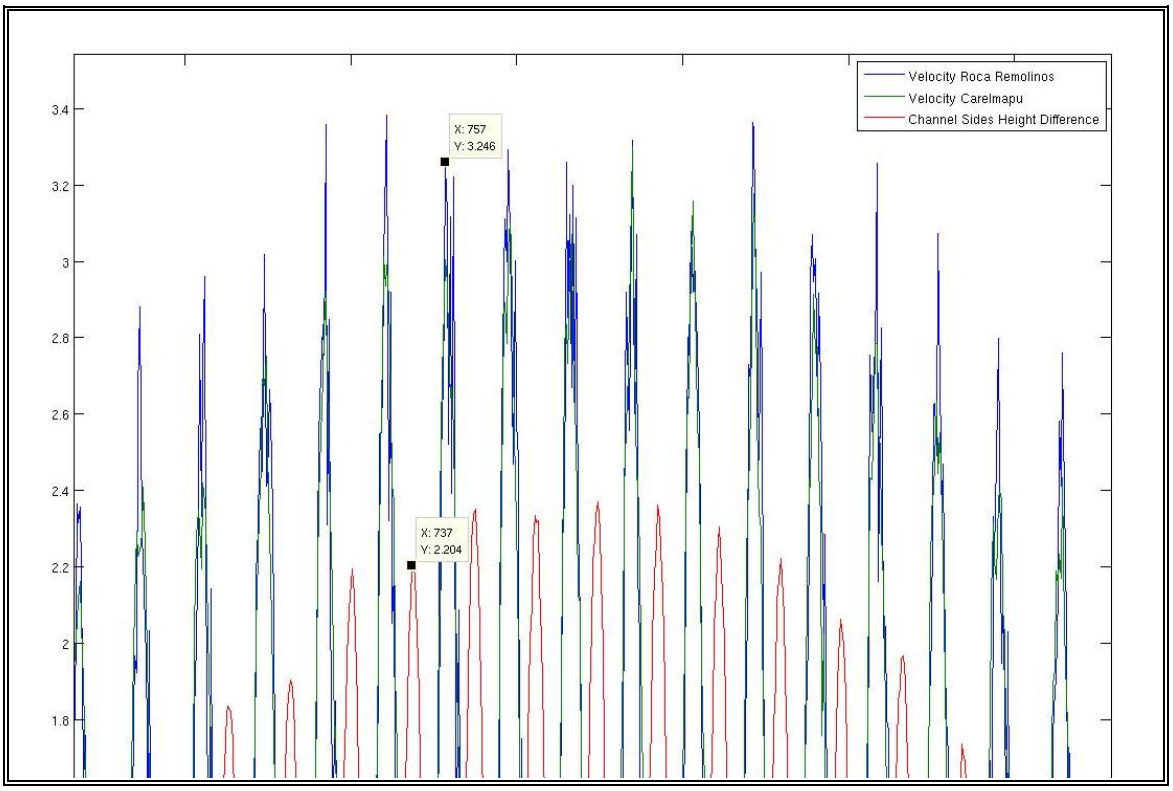

Figure 5-7: Zoom in to lag between peak tidal differential and peak velocities, in order to calculate response time due to drag.

At that particular moment, a lag of approximately 1 hour occurs, meaning the roughness of the Channel delays the maximum velocities by this amount with respect to its forcing driver. This analysis allows defining the lags that will exist between peak tidal differences, which can be predicted with high precision, and peak tidal velocities, which one searches to estimate in order to estimate available and extractable power. This characteristic is extremely important to correctly design a tidal power plant in the future, and define its hourly energy production.

5.2.2 Chacao Channel Characteristics

An analysis of specific bathymetric (or geographical) characteristics of the Chacao Channel must be done, in order to support the comprehension of tidal characteristics and profile analysis detailed later on. In Figure 5-8, one can observe the specific portion of

the whole modeled area that was taken to estimate power available in the Channel. By reducing the area, the calculations are less, and one moves away from boundaries where certain errors could be incorporated due to instability. Figure 5-9 (a) and (b) describe mean channel width and depth from open ocean end to Ancud Gulf end.

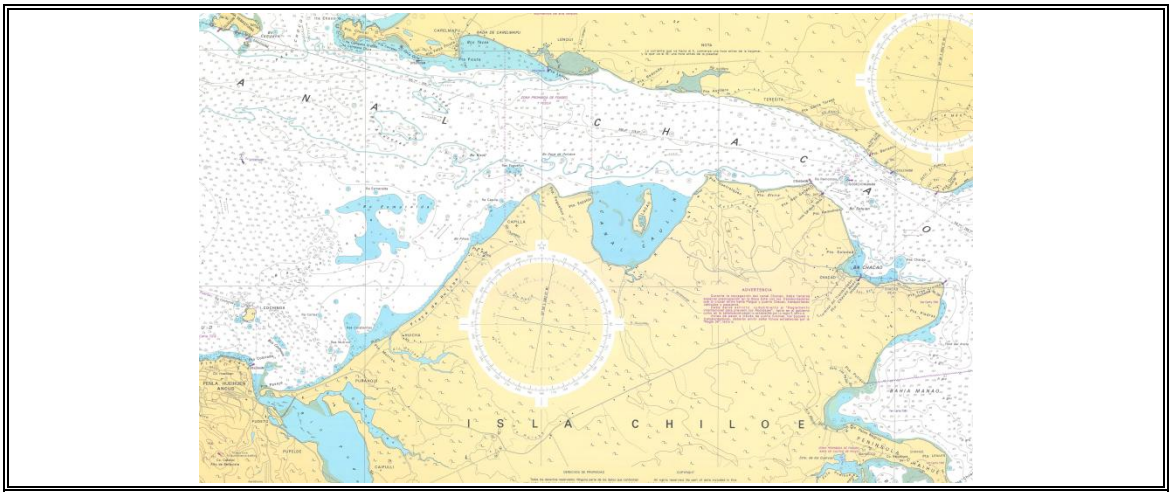

Figure 5-8: Portion of modeled area defined for profile analysis. (SHOA, Cartas y Publicaciones Náuticas (Publicación SHOA N° 3000), 2010).

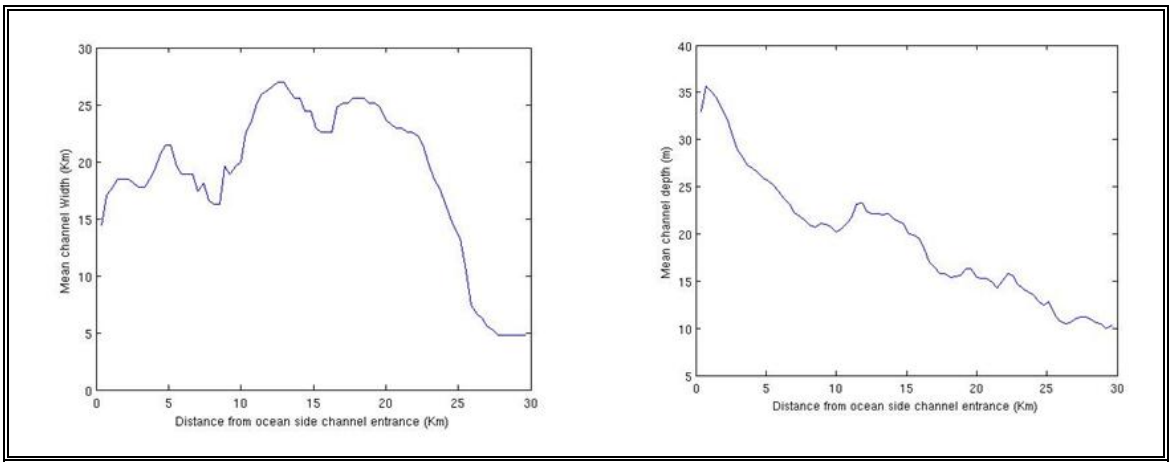

Figure 5-9: Mean depth (a) and width (b) along transversal profiles of the Chacao Channel.

5.2.3 Profile Analysis

Once velocities during the whole modeling period, and for every node in the grid, were obtained, a post process of calculating available power along the Channel transects was done. First all velocities had to be interpolated to the same nodes in the grid, as can be seen in Figure 3-1 (page 44). This way, all data was interpolated to psi points which are located in the middle of each square, both in x and y directions. Having all data at a same point it was possible to begin calculating volumetric flows and power, both extremely important parameters when searching to design a tidal turbine or farm, given that they allow generating energy.

First step was to calculate flows along the Channel transects (transversal area), to further estimate available power in a month time along the Chacao Channel. This was done by using equation (5.1), and the application of it can be understood by following the detail given in Figure 5-10.

$$Power = \iint_S \rho \frac{v^2}{2} \bar{v} \cdot \hat{n} ds = \sum \rho \frac{u^3(t)}{2} [(z + zeta)_{i-\frac{1}{2}} + (z + zeta)_{1+\frac{1}{2}}] \Delta y \quad (5.1)$$

Where u is the velocity in the X direction, and z, zeta and Δy are as seen in Figure 5-10.

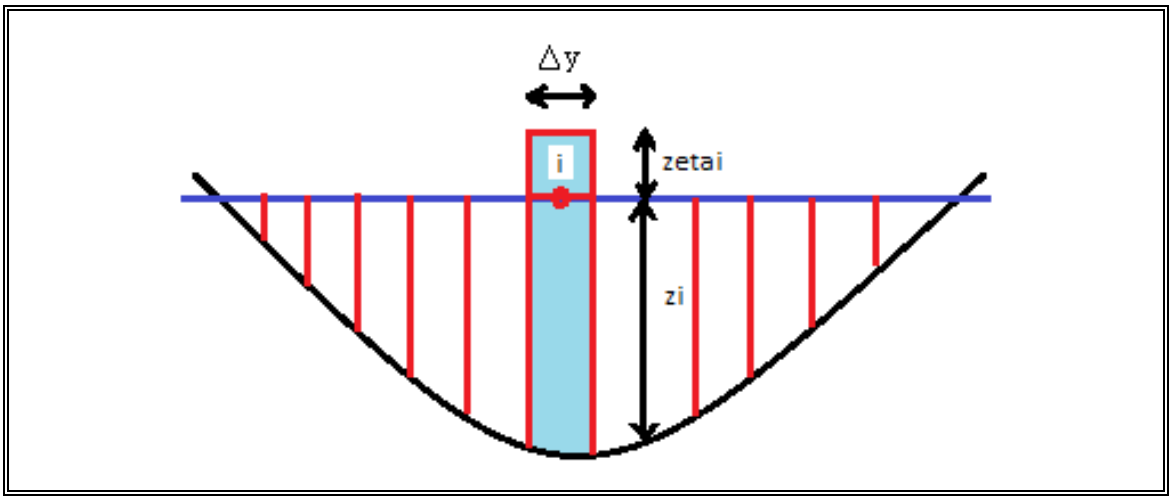

Figure 5-10: Transect detail to calculate flows and power along the Channel.

After having calculated the available power along transects in the Chacao Channel, one could identify specific areas along it that offered more power or energy than others. This way Figure 5-11 and Figure 5-12, show a velocity and power profile along the Channel for ebb and flood tides, which helps to explain how energy is distributed along it and why, according to its physical characteristics.

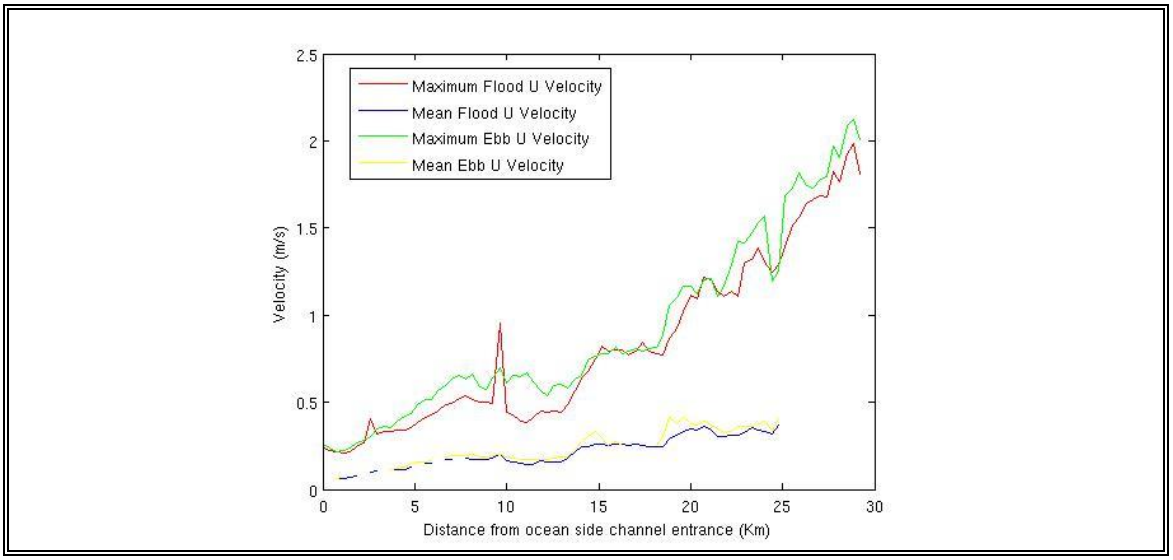

Figure 5-11: Velocity profile analysis along the Chacao Channel.

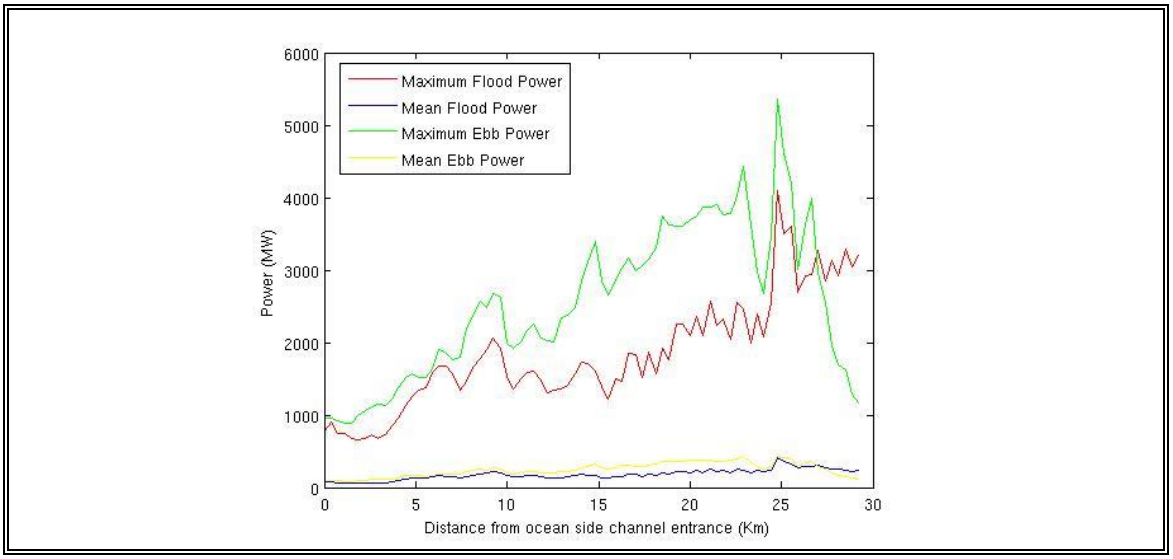

Figure 5-12: Power profile analysis along the Chacao Channel.

It is extremely clear how velocity and power raise as one moves from the open ocean end of the Channel to the Ancud Gulf end. The mean transect velocity obviously raises because of the decrease in mean channel width and depth from one end to another, which causes the same volume of water go through a smaller section, meaning a higher velocity. Therefore there is a clear "funnel effect", as the flows advance from one end to another. As can be seen as well, both mean and maximum velocity and power are larger along the Channel at ebb tide than at flood tide, meaning flows from the ocean to the Gulfs are lighter than those following the opposite direction. Once again, these results allow to better understand the dynamics of tide in the Channel in space and time, information that should be extremely useful when designing a tidal farm, and estimating daily and hourly extracted energy. This does not necessarily mean that one must extract energy from the section with largest power available, but does help to identify possible hot spots and have an idea of the energy available.

Both spots mentioned in section 5.2.1 can be identified in the figures, where Carelmapu represents the peak around 15 km distance, and Roca Remolinos the peak around 25 km distance. These spots are the only ones mentioned here, because they have already been analyzed in past studies and they represent two well-known places in the area, where measurements are available. This does not mean that they are the best spots for tidal turbines deployment, as a matter a fact it will not be feasible to test pilot devices under such extreme conditions.

Finally, Figure 5-13 shows mean velocities in the y direction. This detail allows identifying spots along the Channel that present cleaner flows in a single direction, which makes it easier to establish turbine direction. Of course sections with a more constant velocity direction are best, because this means turbines can be installed facing a certain direction, therefore making energy extraction more efficient. In general, both mean and maximum V velocities remain constant along the Channel, with the exception of a few peaks, where probably a specific shape in the Channel causes more movement of the flows in the lateral direction.

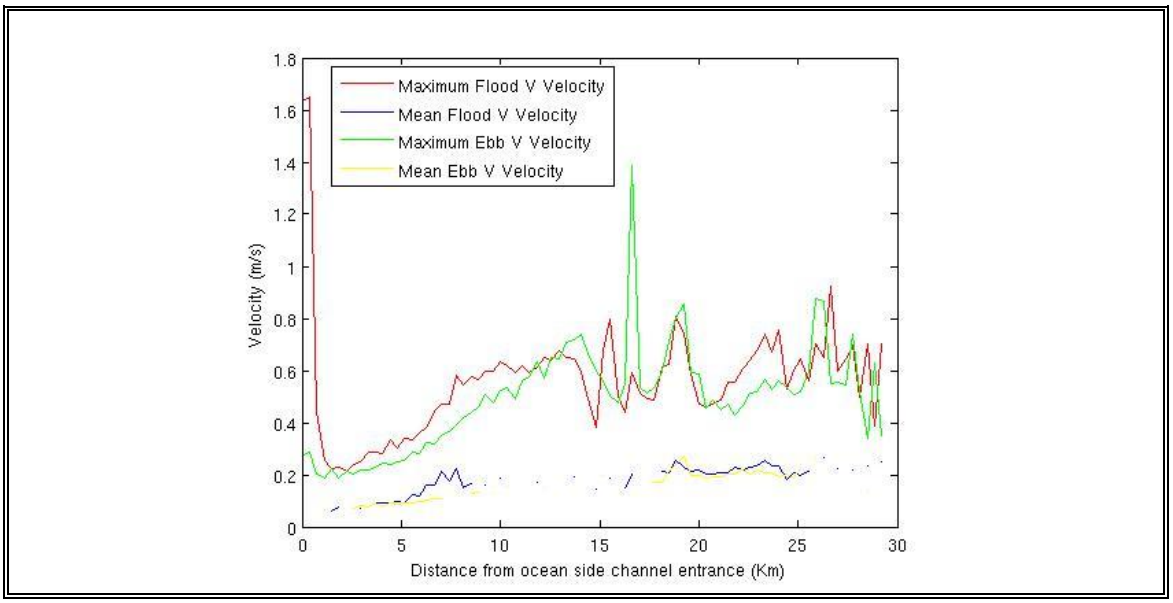

Figure 5-13: Velocity in Y direction (perpendicular to flow direction) profile analysis along the Chacao Channel.

5.2.4 Potential Estimation

Last, comes an estimation of mean and maximum power available at flood and ebb tides, all along the Channel, not averaged along the transect. These results are given in Figures 5-14 and 5-15 respectively, in the form of power maps.

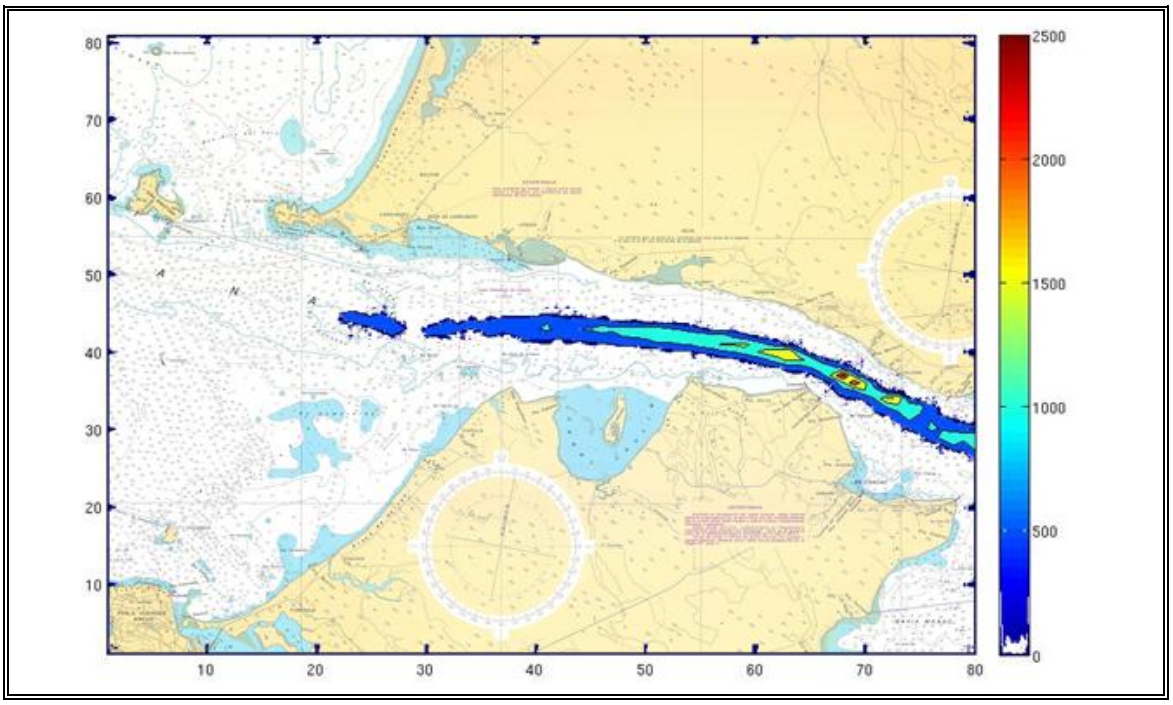

Figure 5-14: Maximum tide power (MW) in the Chacao Channel.

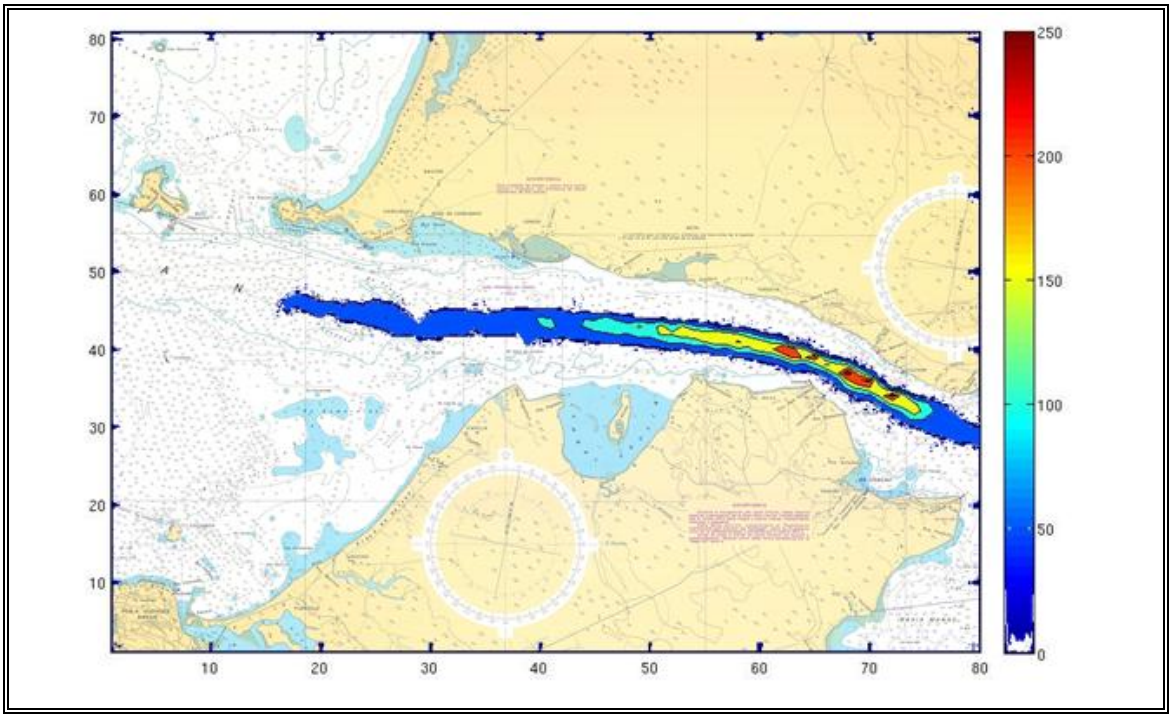

Figure 5-15: Mean tide power (MW) in the Chacao Channel.

From these figures power distribution can be analyzed, given that this shows a map of power along the Channel, where largest maximum and mean power is located at narrowest sections of the channel. Therefore “funnel effect” mentioned before, can also be seen in these figures as power rises along the Channel, obviously with some specific areas that are more attractive than others. Zones close to the Channel sides are not included in these figures because their power values are not far from zero. This is explained by low velocities in these areas, caused by a poor resolution of bathymetric information in shallow waters. This emphasizes the need to improve bathymetric resolution along the Channel. Finally, both figures show extremely high flows at Roca Remolinos, moderate high flows at Carelmapu, and variability between ebb and flood tides, with ebb tides showing a larger potential for tidal flows than flood tide.

5.3 Recommendations for Future Instrumental Installation

Finally, a set of location recommendations for future instrumental deployment, to create good input information for model improvements, is done. Equipment considered is ADCP’s (for current velocities and sea surface level) and tide gauges (for sea surface level). Therefore the recommendations made will refer to characteristics needed for proper deployment and measurement, as well as those needed to generate useful data for model calibration.

First, in order to calibrate a model in the Channel properly, measurements along it and at both sides would be necessary. Obviously more installed instruments are better, yet too many might be unpractical and expensive, therefore at least one must consider measurements at each mouth and both sides, and in the middle also at both sides. This involves dividing the Channel in three areas as can be seen in Figure 5-16.

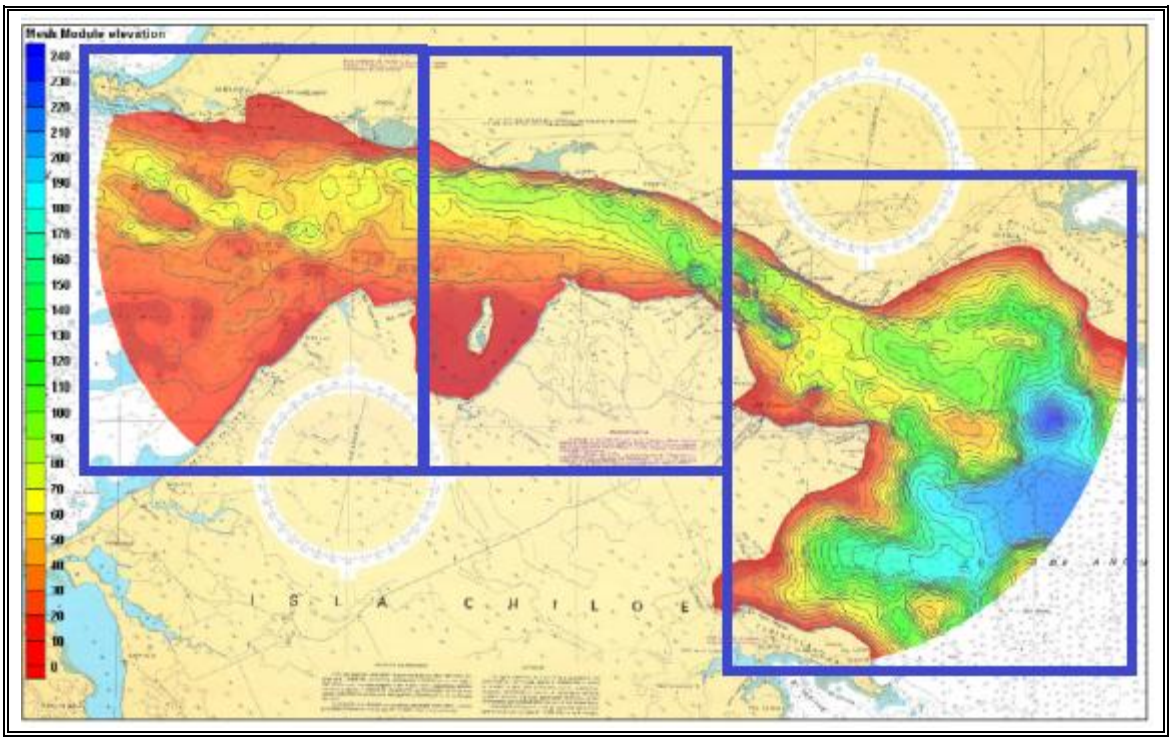

Figure 5-16: Chacao Channel bathymetry and equipment distribution division. (Winckler & Contreras, 2009).

Once having made this division, the criteria used to define exact location of ADCP's and tide gauges in each area along the Channel are:

- Distribution:

  Properly distribute them in order to obtain calibration parameters for models, along the complete channel, with at least one at each mouth and one in the middle, for both sides.

- Depth (Figure 5-16 shows bathymetric map of the Channel):

  For ADCP's, define their location at spots where depth is not larger than 50 meters (orange to red colored regions in Figure 5-16), given that beyond those depths deployment is not feasible.

For tide gauges, define their location at spots on the coast where a deep pool of water is formed, so that instrument is not left dry at extreme low tides. This will actually imply visiting site conditions, because maps are not fine enough.

- Other activities:

Finally, when deciding on the location of instruments for measurements, possible interruption or clashes with other activities must be considered, because of possible theft or damage (with a consequent data loss). Fortunately, strong currents in the Chacao Channel do not allow the performance of many other activities. Figure 5-17 shows areas of benthonic resources extraction, and Figure 5-18 areas of aqua farming activities. Ideally, areas shown in both areas should be avoided to insure equipment security.

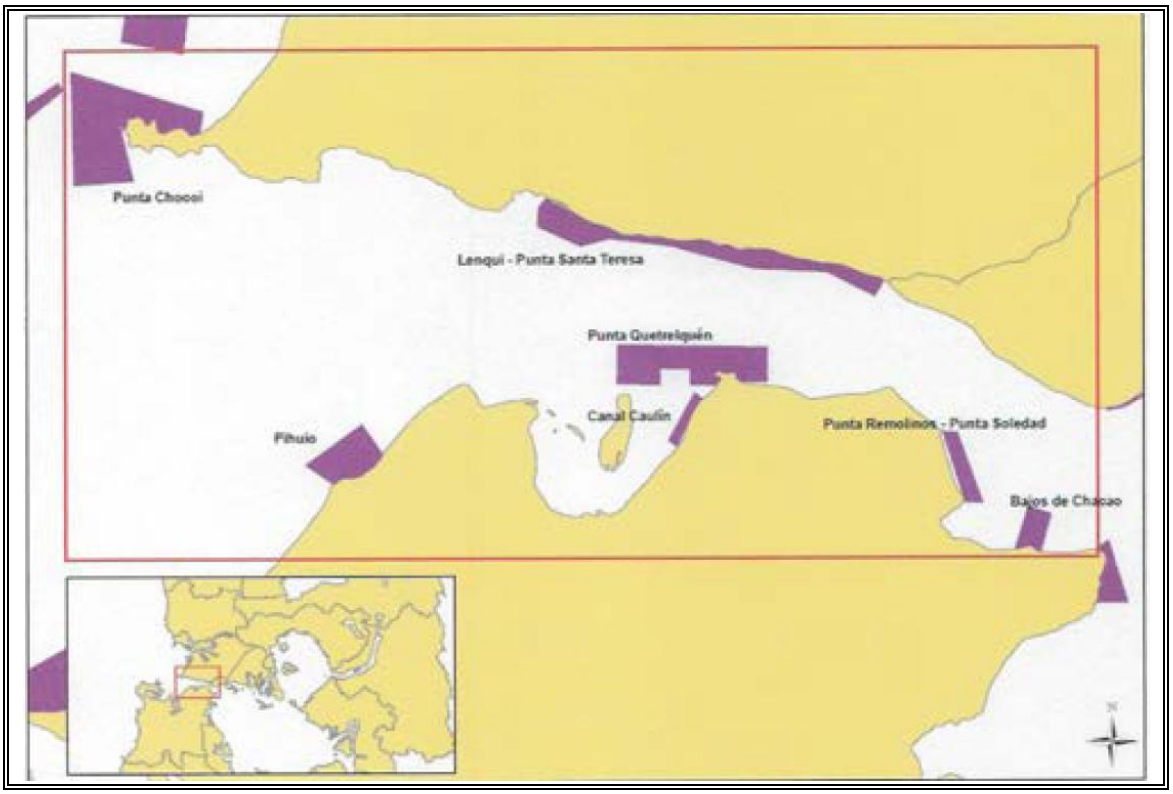

Figure 5-17: Areas of benthonic resources extraction. (Kosiel, 2012).

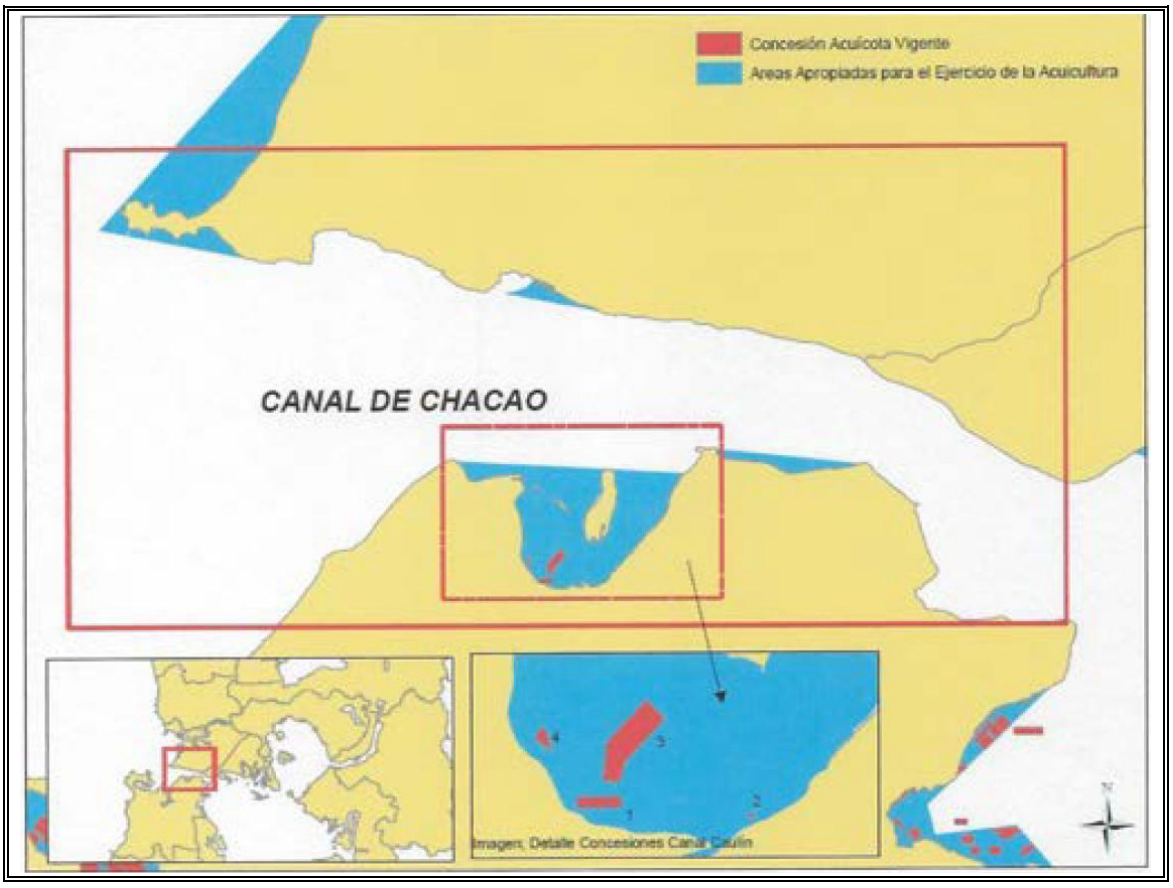

Figure 5-18: Areas of aqua farming activities. (Kosiel, 2012).

By taking into account all the issues mentioned in this section, one comes down to a distribution of areas in which ADCP's and tide gauges can be located to obtain high quality data for future model input. It is important to also consider the location of former measurement equipment (Figure 2-21), which generated the existent data, given that some of their locations could be adequate for a new deployment. Finally these recommendations for future instrument deployment will directly benefit the research project in which this thesis is involved, given that it will help definition of locations for proper data generation. This way next models generated in this project, will be able to start from the basis established by this study.

6. CONCLUSIONS

After having analyzed tidal behavior along the CIS and the Chacao Channel in detail, several conclusions can be brought up, and also future considerations for modeling improvements in the area. To follow the structure presented up until now, these will be given for each model in particular.

6.1 Regional Model

Regional model tidal surface estimations results, were properly reproduced and made a good boundary forcer for the local Chacao model. Even so, eventually the model should be calibrated with proper local measurements data, in order to assure a realistic model.

The model for this case had a width of 5 km, yet in the future a finer grid should be created, and this will depend on the computational capacity that one has. This will require a large computational capacity.

An unusual inconsistent relationship of resolution and amplification is observed, which can be explained by the proximity of tidal waves to resonance in the region. In the future, a closer analysis of this effect must be done, in order to determine the real sensitivity of the model to these characteristics.

A clear phenomenon of resonance in the northern CIS is present, and is the reason to the large tidal variations at Ancud Gulf, which forms a surface difference with the opposite end of the Channel, producing large velocities in it. The phase lag between tidal waves at each end also magnifies this effect.

Computational power or capacity is a necessary tool to allow generation of high resolution. If this is not possible, results and objectives will be very hard to accomplish, and resolution will have to be enlarged. This was an limiting issue for this study.

6.2 Chacao Channel Model

The model gives good results for flows in the Chacao Channel, managing to identify distribution of velocity and power along it, and therefore corroborating certain spots identified by past studies. Still it can be adjusted and perfected to obtain even better

results. For this, a finer resolution grid should be implemented, yet this will require finer bathymetric data and better quality currents and tides measurements. As well, a better computational capacity must be included.

A “funnel effect” was identified in the Channel, given the geographic characteristics of it. This causes velocities at narrowest transects to be extremely high, yet also extremely turbulent which is not the ideal conditions for turbine deployment.

There is also a phase lag between peak tidal difference between the Channel ends, and peak velocities at selected spots, which is probably caused by the Channel drag. This is a useful detail when planning and estimating daily and hourly energy production. As turbines will eventually introduce a new source of drag, this could delay even more the peak velocities, therefore it will be important to further define this effect and how much it will lag energetic production.

It is important to mention that zones with largest currents are not necessarily the ideal ones for pilot or array deployment. First devices should be tested under milder conditions, for further translation to larger currents. Anyway, one must take into account that narrower sections are generally accompanied by larger turbulence, which is not a good environment for efficient turbine operation.

6.3 Future Considerations

Prepare finer sensitivity analysis of model resolution and tidal reproduction in the regional model, in order to properly understand the unusual results obtained in this case. This will obviously require a much larger computational capacity than that occupied here.

On site measurements of tides, currents and fine bathymetry will have to be done, yet this time considering ideal locations and characteristics for future model inputs. Criteria for future measuring equipment location were analyzed, and recommendations were given.

Incorporate a third dimension, in order to further understand local tide phenomena, and also study the existence of stratification effect, which would have influence over turbine energy production.

Determine a procedure to incorporate turbine presence in the model, in order to improve the results of flows in the Channel. This should be done by adding an input file in which one could specify a certain amount of momentum extraction, depending on the turbine, and this way be able to estimate the effect these would have over natural flows.

After having estimated effect of turbines over flows, a biochemical model should be run and calibrated with on-site data, in order to study the effect the turbines could have over local sea flora and fauna. This is a very important item, because once tidal farms are ready for installation, impacts must be understood and studied in detail.

A few models of the Chacao Channel have already been built and run, yet non in 3D or using proper on-site data. All of them give similar results regarding available power and energy, and location of hot spots. Still no model that incorporates a third dimension or the presence of tidal extracting turbines has been developed. This thesis searched to set the base for a former 3D model that incorporates these parameters and advances towards the design of an optimum tidal farm.

REFERENCES

Aiken, C. M. (2008). Barotopic tides of the Chilean Inland Sea and their sensitivity to basin geometry. *Journal of Geophysical Research*, 113, 1-13.

Bergey, K. H. (1980). The Lanchester-Betz Limit. *J. Energy*, 382-384.

Betz, A. (1926). Wind-Energie und ihre Ausnutzung durch Windmühlen. *Vandenhock and Ruprecht.* Göttingen, Germany.

Blanchfield, J., Garrett, C., Wild, P., & Rowe, A. (2008). The extractable power from a channel linking a bay to the open ocean. *Power and Energy*, 222(A3), 289-297.

Blanchfield, J., Garrett, C., Wild, P., & Rowe, A. (2008). Tidal stream power resource assessment for Maset Sound, Haida Gwaii. *Power and Energy*, 222(A3), 485-492.

Borgel, R. (1970). Geomorfología de las regiones australes de Chile. *Geografía de Chile "Tierra Australis"*, 20, 135-140.

Cáceres, M., Valle-Levinson, A., & Atkinson, L. (2003). Observations of cross-channel structure of flow in an energetic tidal channel. *J. Geophys. Res.*, 108(C4), 3114.

Chapman, D. (1985). Numerical treatment of cross-shelf open boundaries in a barotropic coastal ocean model. *J. Phys. Oceanogr.*, 15, 1060-1075.

Defne, Z., Haas, K. A., & Fritz, H. M. (2011). Numerical modeling of tidal currents and the effects of power extraction on estuarine hydrodynamics along the Georgia coast, USA. *Renewable Energy*, 36, 3461-71.

Egbert, G., & Erofeeva, S. (2002). Eficient inverse modeling of barotropic ocean tides. *Journal of Atmospheric and Oceanic Technology*, 19, 183-204.

Flather, R. A. (1976). A tidal model of the northwest European continental shelf. *Memoires de la Societe Royale de Sciences de Liege*, 6, 141-164.

García, R. G., & Winckler, P. G. (2009). Generación de Energía por Corrientes de Marea en Chile. Una aplicación al caso de Melinka. *Anales del Instituto de Ingenieros de Chile*, 121, 87-102.

Garrad-Hassan. (2009). *Preliminary Site Selection - Chilean Marine Energy Resources.* Santiago, Chile: Comisión Nacional de Energía.

Garret, C., & Cummins, P. (2005). The power potential of tidal currents in channels. *Proc. R. Soc.*, 461, 2563-2572.

Garrett, C., & Cummins, P. (2007). The efficiency of a turbine in a tidal channel. *J. Fluid Mech.*, 588, 243-251.

Garrett, C., & Cummins, P. (2008). Limits to tidal current power. *Renewable Energy*, 33, 2485-2490.

Gjevik, B. (2006). *Lectures on Tides.* University of Oslo.

Gorban, A. N., Gorlov, A. M., & Silantyev, V. M. (2001). Limits of the turbine efficiency for free fluid flow. *Journal Energy Resource Technology,* 123, 311-317.

Haidvogel, D. B., Arango, H., Budgell, W. P., Cornuelle, B. D., Curchitser, E., & Di Lorenzo, E. (2008). Ocean forecasting in terrain-following coordinates: Formulation and skill assessment of the Regional Ocean Modeling System. *Journal of Computational Physics*, 227, 3595-624.

Herrera, R. A. (2010). *Análisis de Factibilidad Técnico-Económico del Recurso Energético asociado a las corrientes de Marea en el Canal de Chacao.* Santiago, Chile: Departamento de Ingeniería Civil, Universidad de Chile.

ICUATRO-COWI. (2000). *Estudio de Ingeniería Concesión Puente sobre el Canal de Chacao, Volúmen 5C: Estudios Marítimos.* Santiago, Chile.

Kosiel, K. (2012). *Informe de Respuesta - Solicitud de Información en el Marco de la Ley N°20.285.* Puerto Montt.

Lee, S. H., Jang, K., Lee, J., & Hur, N. (2010). A numerical study for the optimal arrangement of ocean current turbine generators in the ocean current power parks. *Current Applied Physics*, 10, 137-141.

Masselink, G., & Hughes, M. (2003). *Introduction to Coastal Processes & Geomorphology*. London, England: Hodder Education.

Morthorst, P. E. (2004). *Wind Energy - The Facts, Volume 2.* Coppenhagen, Denmark.

Myers, L. E., & Bahaj, A. S. (2012). An experimental investigation simulating flow effects in first generation marine current converter arrays. *Renewable Energy*, 37, 28-36.

Pawlowicz, R., Beardsley, B., & Lentz, S. (2002). Classic tidal harmonic analysis including error estimates in MATLAB using T_TIDE. *Computers and Geosciences*, 28, 929-937.

Polagye, B., Malte, P., Kawase, M., & Durran, D. (2008). Effect of large-scale kinetic power extraction in time-dependent estuaries. *Power and Energy*, 222(A3), 471-484.

Pugh, D. (1987). *Tides, Surges and Mean Sea-Level.* Natural Environment Research Council.

RenewableUK. (2011). *Wave and Tidal Energy in the UK.*

Rosenfeld, L., Shulman, I., Cook, M., Paduan, J., & Shulman, L. (2009). Methodology for a regional tidal model evaluation, with application to central California. *Deep-Sea Research II*, 56, 199-218.

Salinas, S., & Hormazábal, S. (2004). Capacidad de transporte de la constricción de Meninea para un flujo de dos capas y el efecto de la corriente de marea. *Cienc. Technol. Mar*, 27(1), 5-15.

Schepetkin, A. F., & McWilliams, J. C. (2005). The regional oceanic modeling system (ROMS): a split-explicit, free-surface, topography-following-coordinate oceanic model. *Ocean Modelling*, 9, 347-404.

Sepúlveda, I. (2011). *Simulación de Turbinas Hidráulicas para extracción de energía de mareas en modelos Hidrodinámicos y aplicación en el Canal de Chacao.* Santiago, Chile: Departamento de Ingeniería Civil, Universidad Técnica Federico Santa María.

Serway, R. A., & Jewett, J. W. (2010). *Physics for Scientists and Engineers, Vol 1.*

SHOA. (1992). *Glosario de Mareas y Corrientes (Publicación SHOA N° 3013).* Valparaíso, Chile: Imprenta de la Armada de Chile.

SHOA. (1999). *Instrucciones Oceanográficas N° 2, Método Oficial para el Cálculo de los Valores No Armónicos de la Marea (Publicación SHOA N° 3202).* Valparaíso, Chile: Imprenta de la Armada de Chile.

SHOA. (2010). *Cartas y Publicaciones Náuticas (Publicación SHOA N° 3000).* Valparaíso, Chile: Imprenta de la Armada de Chile.

Silva, N., Calvete, C., & Sievers, H. A. (1997). Características oceanográficas físicas y químicas de canales australes Chilenos entre Puerto Montt y Laguna San Rafael (Crucero Cimar-Fiordo 1). *Cienc. Technol. Mar.*, 20, 23-106.

Sutherland, G., Foreman, M., & Garrett, C. (2006). Tidal current energy assessment for Johnstone Strait, Vancouver Island. *Power and Energy*, 221, 147-157.

Vennell, R. (2010). Tuning turbines in a tidal channel. *Journal of Fluid Mechanics*, 663, 253-267.

Vennell, R. (2011). Estimating the power potential of tidal currents and the impact of power extraction on flow speeds. *Renewable Energy*, 1-8.

Winckler, P., & Contreras, M. (2009). *Estudios de Evaluación del Potencial de Energía de Corrientes de Marea y Oleaje entre las IV y X Regiones, Chile.* Santiago, Chile: Universidad de Valparaíso.

APPENDICES

APPENDIX A: ROMS MANUAL

This is a basic and short manual for ROMS use, in the Chacao Channel model, and which can be used for other applications. It includes the download, installation, input file creation, compilation, run, nest and post-process. All this considers using a Linux Ubuntu Operating System as a platform, which is highly recommended in order to simplify ROMS use, and Matlab 7.10 (R2010a). For more information or help, enter:

WikiROMS: https://www.myroms.org/wiki/index.php/Documentation_Portal
ROMS Forum: https://www.myroms.org/forum/index.php
Linux Commands: http://www.oscarbernal.net/index.php?/content/view/34/20/

1. Download

- You must begin by entering the ROMS website (www.myroms.org) and registering. For this a series of personal and technical questions will have to be answered, regarding your research centre, it's purposes, and the use you will give the model. After that you will receive an answer by email.
- Now you have a username and password, with which you will be able to download the model code.
- Enter the Unix terminal and create a src folder where you will keep the ROMS source code. You can place this wherever you wish in your directory tree (here we assume under your home directory "~") and name it whatever you like.

  ex. cd ~
  mkdir src
- Check out the latest ROMS source code replacing *nils* with the ROMS user name you registered with.

  ex. svn checkout --username nils https://www.myroms.org/svn/src/trunk src
- Now the ROMS code has been downloaded into your computer, with the following folders: Atmosphere, Build, Compilers, Data, Lib, Master, Output,

ROMS, User, and Waves. The only folder which matters is the ROMS folder, and maybe at some moment the Build folder.

2. Installation

Programs: SCNTOOLS, MexCDF, RPSStuff, Seagrid.

Once the ROMS code has been installed, a few programs, which may not come included in the Unix memory, will have to be installed and incorporated to the Matlab path.

- *SCNTOOLS (http://code.google.com/p/jsonnetcdf/downloads/detail?name=netcdfAll-4.1.jar&can=2&q=):*

Download "netcdfAll-4.1.jar".

On Matlab, add to path, write: "javaaddpath('/location/of/the/file/netcdfAll-4.1.jar');".

Next on Matlab, set preference: "setpref('SCNTOOLS', 'USE_JAVA', true);".

- *MexCDF(http://mexcdf.sourceforge.net/):*

Two files must be downloaded: a general MexCDF and a specific one for the Matlab version (in this case R2010a).

Add to Matlab path: "mexcdf/mexnc" and "mexcdf/scntools".

- *RPSStuff (http://woodshole.er.usgs.gov/operations/sea-mat/rpsstuff-html/index.html):*

Add this file to Matlab path.

*Seagrid (*http://woodshole.er.usgs.gov/operations/modeling/seagrid/seagrid.html*):*

Download Seagrid as indicated in the above website, and follow instructions.

Once downloaded, add to path: "Seagrid", "Seagrid/presto" and

"Seagrid/mex_matlab74_linux32" (or the one according to Matlab version). Follow use instructions from the website mentioned above.

*- OTPS (*http://volkov.oce.orst.edu/tides/*):*

Tidal forcing model. Download and use through Matlab.

3. Input files

a. Grid:

- Open Matlab.
- Type "seagrid" and the Seagrid platform will open up.
- Load a bathymetry and coastline file.
- Load grid corner points file, or manually select them. Square them using the seagrid file matrix on Matlab platform, and update file on Seagrid.
- Compute land mask, and correct manually if necesary.
- Next, compute depths.
- Save seagrid file, and exit seagrid.
- On Matlab use "seagrid2roms_v2" routine to create NetCDF file of the grid.

b. Tides:

- In Matlab, enter the OTPS file, and in it the Data file, where the "Model_PO" (Pacific Ocean) must be.
- Use the "otps2frc_v3" routine to create the tidal forcing NetCDF file.
- Before you must call the grid file, and the specific date you want the components to be modeled (in this case June 2000).

c. Input Files adjustments and Tips:

- All points in the grid must have values over zero, therefore all land points (h=0)

are changed to h=1. Load the grid file, find the zero value points, change the zero values for ones and replace in original grid NetCDF file.

```
ex.   var=nc_varget('nils_grd_1.nc', 'h');
      ind=find(var==0);
      var(ind)=1;
      nc_varput('nils_grd_1.nc', 'h', var);
```

- To avoid model blow-up, all points in the grid must be over 10 m depth, therefore all depth points under 10 must be assigned h=10.

```
ex.   var=nc_varget('nils_grd_1.nc', 'h');
      h(var<10)=10;
      nc_varput('nils_grd_1.nc', 'h', var);
```

4. Compile

- Edit the “makefile” for the specific project or model which will be run (ex. Chacao, Nils, etc), by entering the name of the Roms_Application in line 62 of that file.
- In MyDir/ROMS/Include create a “.h” file which incoporates the ROMS routines for the specific model you will work with. In this specific case it is the “chacao.h” for the Chacao Channel model and “nils.h” for the Regional Chiloé model. This file will be used during the compiling process.
- Open the Unix terminal and cd (enter) “MyDir” folder, where the whole ROMS model is based in the computer.
- Once in that folder type “make clean” to clean up the past compiling files.
- Now, type “make” and wait for the executable oceanG, oceanS or oceanM.
- If your build was successful it will not have reported any errors, and there will be an executable file in your Projects/upwelling directory called oceanG. The "G" in the file name indicates build.bash activated the USE_DEBUG option.

- If USE_DEBUG were not selected, the executable would be oceanS, where the "S" indicates "serial" or "single-processor" because we deactivated MPI.
- If you had activated MPI with the USE_MPI option the executable would be named oceanM.

5. Run

- Having the executable created, you must create a ".in" file in the same folder where the executable is located. This file has the specific modelling details: input/output files, time spacing and recording, etc.
- Once your ".in" file is ready, you may run the model by entering (cd) the folder where both files are located and writing "./oceanS < nils.in (or the name of your .in file)".

APPENDIX B: ROMS MODEL COMPILATION ROUTINES

Hernan G. Arango

The following is short description of all available CPP options.

OPTIONS associated with momentum equations:

The default horizontal advection is 3rd-order upstream bias for
3D momentum and 4th-order centered for 2D momentum. The default
vertical advection is 4th-order centered for 3D momentum. If this
is the case, no flags for momentum advection need to be activated.

The 3rd-order upstream split advection (UV_U3ADV_SPLIT) can be used
to correct for the spurious mixing of the advection operator in
terrain-following coordinates. If this is the case, the advection
operator is split in advective and viscosity components and several
internal flags are activated in "globaldefs.h". Notice that
horizontal and vertical advection of momentum is 4th-order centered
plus biharmonic viscosity to correct for spurious mixing. The total
time-dependent horizontal mixing coefficient are computed in
"hmixing.F".

WARNING: Use the splines vertical advection option (UV_SADVECTION)
only in shallow, high vertical resolution applications.

UV_ADV use to turn ON or OFF advection terms
UV_COR use to turn ON or OFF Coriolis term
UV_U3ADV_SPLIT use if 3rd-order upstream split momentum advection
UV_C2ADVECTION use to turn ON or OFF 2nd-order centered advection
UV_C4ADVECTION use to turn ON or OFF 4th-order centered advection
UV_SADVECTION use to turn ON or OFF splines vertical advection
UV_VIS2 use to turn ON or OFF harmonic horizontal mixing
UV_VIS4 use to turn ON or OFF biharmonic horizontal mixing
UV_SMAGORINSKY use to turn ON or OFF Smagorinsky-like viscosity
UV_LOGDRAG use to turn ON or OFF logarithmic bottom friction
UV_LDRAG use to turn ON or OFF linear bottom friction
UV_QDRAG use to turn ON or OFF quadratic bottom friction
UV_PSOURCE use to turn ON or OFF point Sources/Sinks
Q_PSOURCE use to turn ON or OFF mass point Sources

OPTIONS associated with tracers equations:

The default horizontal and vertical advection is 4th-order centered.

The 3rd-order upstream split advection (TS_U3ADV_SPLIT) can be used to correct for the spurious diapycnal diffusion of the advection operator in terrain-following coordinates. If this is the case, the advection operator is split in advective and diffusive components and several internal flags are activated in "globaldefs.h". Notice that horizontal and vertical advection of tracer is 4th-order centered plus biharmonic diffusion to correct for spurious diapycnal mixing. The total time-dependent horizontal mixing coefficient are computed in "hmixing.F". It is also recommended to use the rotated mixing tensor along geopotentials (MIX_GEO_TS) for the biharmonic operator.

WARNING: Use the splines vertical advection option (TS_SVADVECTION) only in shallow, high vertical resolution applications.

TS_U3ADV_SPLIT use if 3rd-order upstream split tracer advection
TS_A4HADVECTION use if 4th-order Akima horizontal advection
TS_C2HADVECTION use if 2nd-order centered horizontal advection
TS_C4HADVECTION use if 4th-order centered horizontal advection
TS_MPDATA use if recursive MPDATA 3D advection
TS_U3HADVECTION use if 3rd-order upstream horiz. advection
TS_A4VADVECTION use if 4th-order Akima vertical advection
TS_C2VADVECTION use if 2nd-order centered vertical advection
TS_C4VADVECTION use if 4th-order centered vertical advection
TS_SVADVECTION use if splines vertical advection
TS_DIF2 use to turn ON or OFF harmonic horizontal mixing
TS_DIF4 use to turn ON or OFF biharmonic horizontal mixing
TS_SMAGORINSKY use to turn ON or OFF Smagorinsky-like diffusion
TS_FIXED use if diagnostic run, no evolution of tracers
T_PASSIVE use if inert passive tracers (dyes, etc)
SALINITY use if having salinity
NONLIN_EOS use if using nonlinear equation of state
QCORRECTION use if net heat flux correction
SCORRECTION use if freshwater flux correction
SOLAR_SOURCE use if solar radiation source term
SRELAXATION use if salinity relaxation as a freshwater flux
TS_PSOURCE use to turn ON or OFF point Sources/Sinks

Tracer advection OPTIONS for adjoint-based algorithms:

Some of the tracer advection algorithms are highly nonlinear and may become unstable when running the tangent linear, representer, and adjoint models. This may affect the convergence of the 4DVar data assimilation algorithms. Therefore, it is possible to choose a simpler (less nonlinear) horizontal and vertical tracer advection scheme, if so desired, for the tangent linear, representer and adjoint models. Notice that this strategy still allows us to use highly nonlinear tracer advection schemes in the basic state upon which the tangent linear and adjoint models are linearized. Also, it allows us to use those schemes that have not been adjointed yet, for example, TS_MPDATA. Recall that basic state trajectory is computed by running the nonlinear model.

The flags below are optional. By default, the same options chosen for the nonlinear model are selected for the tangent linear, representer, and adjoint models.

TS_A4HADVECTION_TL use if 4th-order Akima horizontal advection
TS_C2HADVECTION_TL use if 2nd-order centered horizontal advection
TS_C4HADVECTION_TL use if 4th-order centered horizontal advection
TS_U3HADVECTION_TL use if 3rd-order upstream horiz. advection

TS_A4VADVECTION_TL use if 4th-order Akima vertical advection
TS_C2VADVECTION_TL use if 2nd-order centered vertical advection
TS_C4VADVECTION_TL use if 4th-order centered vertical advection
TS_SVADVECTION_TL use if splines vertical advection

Pressure gradient algorithm OPTIONS:

If no option is selected, the pressure gradient term is computed using standard density Jacobian algorithm. Notice that there are two quartic pressure Jacobian options. They differ on how the WENO reconciliation step is done and in the monotonicity constraining algorithms.

DJ_GRADPS use if splines density Jacobian (Shchepetkin, 2000)
PJ_GRADP use if finite volume Pressure Jacobian (Lin,1997)
PJ_GRADPQ2 use if quartic 2 Pressure Jacobian (Shchepetkin,2000)
PJ_GRADPQ4 use if quartic 4 Pressure Jacobian (Shchepetkin,2000)
WJ_GRADP use if weighted density Jacobian (Song,1998)

ATM_PRESS use to impose atmospheric pressure onto sea surface

OPTIONS for surface fluxes formulation using atmospheric boundary layer

(Fairall et al, 1996):

There are three ways to provide longwave radiation in the atmospheric boundary layer: (1) Compute the net longwave radiation internally using the Berliand (1952) equation (LONGWAVE) as function of air temperature, sea surface temperature, relative humidity, and cloud fraction;

(2) provide (read) longwave downwelling radiation only and then add outgoing longwave radiation (LONGWAVE_OUT) as a function of the model sea surface temperature; (3) provide net longwave radiation (default).

BULK_FLUXES use if bulk fluxes computation
NL_BULK_FLUXES use bulk fluxes computed by nonlinear model
COOL_SKIN use if cool skin correction

LONGWAVE use if computing net longwave radiation
LONGWAVE_OUT use if computing outgoing longwave radiation
EMINUSP use if computing E-P

OPTIONS for wave roughness formulation in bulk fluxes:

COARE_TAYLOR_YELLAND use Taylor and Yelland (2001) relation
COARE_OOST use Oost et al (2002) relation
DEEPWATER_WAVES use Deep water waves approximation

OPTIONS for shortwave radiation:

The shortwave radiation can be computed using the global albedo equation with a cloud correction. Alternatively, input shortwave radiation data computed from averaged data (with snapshots greater or equal than 24 hours) can be modulated by the local diurnal cycle which is a function longitude, latitude and day-of-year.

ALBEDO use if albedo equation for shortwave radiation
DIURNAL_SRFLUX use to impose shortwave radiation local diurnal cycle

Model configuration OPTIONS:

SOLVE3D use if solving 3D primitive equations
CURVGRID use if curvilinear coordinates grid
MASKING use if land/sea masking
BODYFORCE use if applying stresses as bodyforces
PROFILE use if time profiling
AVERAGES use if writing out time-averaged data

AVERAGES_DETIDE use if writing out time-averaged detided fields
DIAGNOSTICS_BIO use if writing out biological diagnostics
DIAGNOSTICS_UV use if writing out momentum diagnostics
DIAGNOSTICS_TS use if writing out tracer diagnostics
ICESHELF use if including ice shelf cavities
SPHERICAL use if analytical spherical grid
STATIONS use if writing out station data
STATIONS_CGRID use if extracting data at native C-grid

OPTIONS for Lagrangian drifters:

FLOATS use to activate simulated Lagrangian drifters
FLOAT_VWALK use if vertical random walk
VWALK_FORWARD use if forward time stepping vertical random walk

OPTION to activate conservative, parabolic spline reconstruction of
vertical derivatives. Notice that there also options (see above) for
vertical advection of momentum and tracers using splines.

SPLINES use to activate parabolic splines reconstruction

OPTIONS for analytical fields configuration:

Any of the analytical expressions are coded in "analytical.F".

ANA_BIOLOGY use if analytical biology initial conditions
ANA_BMFLUX use if analytical spatially varying bottom roughness
ANA_BPFLUX use if analytical bottom passive tracers fluxes
ANA_BSFLUX use if analytical bottom salinity flux

ANA_BTFLUX use if analytical bottom temperature flux
ANA_CLOUD use if analytical cloud fraction
ANA_DIAG use if customized diagnostics
ANA_FSOBC use if analytical free-surface boundary conditions
ANA_GRID use if analytical model grid set-up
ANA_HUMIDITY use if analytical surface air humidity
ANA_INITIAL use if analytical initial conditions
ANA_M2CLIMA use if analytical 2D momentum climatology
ANA_M2OBC use if analytical 2D momentum boundary conditions
ANA_M3CLIMA use if analytical 3D momentum climatology
ANA_M3OBC use if analytical 3D momentum boundary conditions
ANA_MASK use if analytical Land/Sea masking
ANA_PAIR use if analytical surface air pressure
ANA_PASSIVE use if analytical inert tracers initial conditions
ANA_PERTURB use if analytical perturbation of initial conditions
ANA_PSOURCE use if analytical point Sources/Sinks
ANA_RAIN use if analytical rain fall rate
ANA_SEDIMENT use if analytical sediment initial fields
ANA_SMFLUX use if analytical surface momentum stress
ANA_SPFLUX use if analytical surface passive tracers fluxes
ANA_SPINNING use if analytical time-varying rotation force
ANA_SRFLUX use if analytical surface shortwave radiation flux
ANA_SSFLUX use if analytical surface salinity flux
ANA_SSH use if analytical sea surface height
ANA_SSS use if analytical sea surface salinity
ANA_SST use if analytical SST and dQdSST
ANA_STFLUX use if analytical surface temperature flux
ANA_TAIR use if analytical surface air temperature
ANA_TCLIMA use if analytical tracers climatology

ANA_TOBC use if analytical tracers boundary conditions
ANA_VMIX use if analytical vertical mixing coefficients
ANA_WINDS use if analytical surface winds
ANA_WWAVE use if analytical wind induced waves

OPTIONS for horizontal mixing of momentum:

VISC_GRID use to scale viscosity coefficient by grid size
MIX_S_UV use if mixing along constant S-surfaces
MIX_GEO_UV use if mixing on geopotential (constant Z) surfaces

OPTIONS for horizontal mixing of tracers:

CLIMA_TS_MIX use if diffusion of tracer perturbation (t-tclm)
DIFF_GRID use to scale diffusion coefficients by grid size
MIX_S_TS use if mixing along constant S-surfaces
MIX_GEO_TS use if mixing on geopotential (constant Z) surfaces
MIX_ISO_TS use if mixing on epineutral (constant RHO) surfaces

OPTIONS for vertical turbulent mixing scheme of momentum and tracers (activate only one closure):

BVF_MIXING use if Brunt-Vaisala frequency mixing
GLS_MIXING use if Generic Length-Scale mixing
MY25_MIXING use if Mellor/Yamada Level-2.5 closure
LMD_MIXING use if Large et al. (1994) interior closure

OPTIONS for the Generic Length-Scale closure (Warner et al., 2005):

The default horizontal advection is third-order upstream bias. The default vertical advection is 4th-order centered advection.

CANUTO_A use if Canuto A-stability function formulation
CANUTO_B use if Canuto B-stability function formulation
CHARNOK use if Charnok surface roughness from wind stress
CRAIG_BANNER use if Craig and Banner wave breaking surface flux
KANTHA_CLAYSON use if Kantha and Clayson stability function
K_C2ADVECTION use if 2nd-order centered advection
K_C4ADVECTION use if 4th-order centered advection
N2S2_HORAVG use if horizontal smoothing of buoyancy/shear
ZOS_HSIG use if surface roughness from wave amplitude
TKE_WAVEDISS use if wave breaking surface flux from wave amplitude

OPTIONS for the Mellor/Yamada level 2.5 closure:

The default horizontal advection is third-order upstream bias. The default vertical advection is 4th-order centered advection.

N2S2_HORAVG use if horizontal smoothing of buoyancy/shear
KANTHA_CLAYSON use if Kantha and Clayson stability function
K_C2ADVECTION use if 2nd-order centered advection
K_C4ADVECTION use if 4th-order centered advection

OPTIONS for the Large et al. (1994) K-profile parameterization mixing:
mixing:

LMD_BKPP use if bottom boundary layer KPP mixing
LMD_CONVEC use to add convective mixing due to shear instability

LMD_DDMIX use to add double-diffusive mixing
LMD_NONLOCAL use if nonlocal transport
LMD_RIMIX use to add diffusivity due to shear instability
LMD_SHAPIRO use if Shapiro filtering boundary layer depth
LMD_SKPP use if surface boundary layer KPP mixing

OPTIONS to activate smoothing of Richardson number, if SPLINES is not activated:

RI_HORAVG use if horizontal Richardson number smoothing
RI_VERAVG use if vertical Richardson number smoothing

OPTIONS for Meinte Blass bottom boundary layer closure:

The Options MB_Z0BL and MB_Z0RIP should be activated concurrently.

MB_BBL use if Meinte Blaas BBL closure
MB_CALC_ZNOT use if computing bottom roughness internally
MB_CALC_UB use if computing bottom orbital velocity internally
MB_Z0BIO use if biogenic bedform roughness for ripples
MB_Z0BL use if bedload roughness for ripples
MB_Z0RIP use if bedform roughness for ripples

OPTIONS for Styles and Glenn (2000) bottom boundary layer closure:

SG_BBL use if Styles and Glenn (2000) BBL closure
SG_CALC_ZNOT use if computing bottom roughness internally
SG_CALC_UB use if computing bottom orbital velocity internally
SG_LOGINT use if logarithmic interpolation of (Ur,Vr)

OPTIONS for the Sherwood/Signell/Warner bottom boundary layer closure:

SSW_BBL use if Sherwood et al. BBL closure
SSW_CALC_ZNOT use if computing bottom roughness internally
SSW_LOGINT use if logarithmic interpolation of (Ur,Vr)
SSW_CALC_UB use if computing bottom orbital velocity internally
SSW_FORM_DRAG_COR use to activate form drag coefficient
SSW_ZOBIO use if biogenic bedform roughness from ripples
SSW_ZOBL use if bedload roughness for ripples
SSW_ZORIP use if bedform roughness from ripples

Lateral boundary conditions OPTIONS:

Select ONE option at each boundary edge for free-surface, 2D momentum, 3D momentum, and tracers. The turbulent kinetic energy (TKE) conditions are only activated for the Generic length scale or Mellor-Yamada 2.5 vertical mixing closures. If open boundary radiation conditions, an additional option can be activated at each boundary edge to include a passive (active) nudging term with weak (strong) values for outflow (inflow).

Option to impose a sponge layer near the lateral boundary:

SPONGE use if enhanced viscosity/diffusion areas

OPTIONS to impose mass conservation at the open boundary:

EAST_VOLCONS use if Eastern edge mass conservation enforcement

WEST_VOLCONS use if Western edge mass conservation enforcement
NORTH_VOLCONS use if Northern edge mass conservation enforcement
SOUTH_VOLCONS use if Southern edge mass conservation enforcement

OPTIONS for periodic boundary conditions:

EW_PERIODIC use if East-West periodic boundaries
NS_PERIODIC use if North-South periodic boundaries

OPTIONS for closed boundary conditions:

EASTERN_WALL use if Eastern edge, closed wall condition
WESTERN_WALL use if Western edge, closed wall condition
NORTHERN_WALL use if Northern edge, closed wall condition
SOUTHERN_WALL use if Southern edge, closed wall condition

Additional OPTION for radiation open boundary conditions:

RADIATION_2D use if tangential phase speed in radiation conditions

Eastern edge open boundary conditions OPTIONS:

EAST_FSCHAPMAN use if free-surface Chapman condition
EAST_FSGRADIENT use if free-surface gradient condition
EAST_FSRADIATION use if free-surface radiation condition
EAST_FSNUDGING use if free-surface passive/active nudging term
EAST_FSCLAMPED use if free-surface clamped condition
EAST_M2FLATHER use if 2D momentum Flather condition
EAST_M2GRADIENT use if 2D momentum gradient condition

EAST_M2RADIATION use if 2D momentum radiation condition
EAST_M2REDUCED use if 2D momentum reduced-physics
EAST_M2NUDGING use if 2D momentum passive/active nudging term
EAST_M2CLAMPED use if 2D momentum clamped condition
EAST_M3GRADIENT use if 3D momentum gradient condition
EAST_M3RADIATION use if 3D momentum radiation condition
EAST_M3NUDGING use if 3D momentum passive/active nudging term
EAST_M3CLAMPED use if 3D momentum clamped condition
EAST_KGRADIENT use if TKE fields gradient condition
EAST_KRADIATION use if TKE fields radiation condition
EAST_TGRADIENT use if tracers gradient condition
EAST_TRADIATION use if tracers radiation condition
EAST_TNUDGING use if tracers passive/active nudging term
EAST_TCLAMPED use if tracers clamped condition

Western edge open boundary conditions OPTIONS:

WEST_FSCHAPMAN use if free-surface Chapman ondition
WEST_FSGRADIENT use if free-surface gradient condition
WEST_FSRADIATION use if free-surface radiation condition
WEST_FSNUDGING use if free-surface passive/active nudging term
WEST_FSCLAMPED use if free-surface clamped condition
WEST_M2FLATHER use if 2D momentum Flather condition
WEST_M2GRADIENT use if 2D momentum gradient condition
WEST_M2RADIATION use if 2D momentum radiation condition
WEST_M2REDUCED use if 2D momentum reduced-physics
WEST_M2NUDGING use if 2D momentum passive/active nudging term
WEST_M2CLAMPED use if 2D momentum clamped condition
WEST_M3GRADIENT use if 3D momentum gradient condition

WEST_M3RADIATION use if 3D momentum radiation condition
WEST_M3NUDGING use if 3D momentum passive/active nudging term
WEST_M3CLAMPED use if 3D momentum clamped condition
WEST_KGRADIENT use if TKE fields gradient condition
WEST_KRADIATION use if TKE fields radiation condition
WEST_TGRADIENT use if tracers gradient condition
WEST_TRADIATION use if tracers radiation condition
WEST_TNUDGING use if tracers passive/active nudging term
WEST_TCLAMPED use if tracers clamped condition

Northern edge open boundary conditions OPTIONS:

NORTH_FSCHAPMAN use if free-surface Chapman condition
NORTH_FSGRADIENT use if free-surface gradient condition
NORTH_FSRADIATION use if free-surface radiation condition
NORTH_FSNUDGING use if free-surface passive/active nudging term
NORTH_FSCLAMPED use if free-surface clamped condition
NORTH_M2FLATHER use if 2D momentum Flather condition
NORTH_M2GRADIENT use if 2D momentum gradient condition
NORTH_M2RADIATION use if 2D momentum radiation condition
NORTH_M2REDUCED use if 2D momentum reduced-physics
NORTH_M2NUDGING use if 2D momentum passive/active nudging term
NORTH_M2CLAMPED use if 2D momentum clamped condition
NORTH_M3GRADIENT use if 3D momentum gradient condition
NORTH_M3RADIATION use if 3D momentum radiation condition
NORTH_M3NUDGING use if 3D momentum passive/active nudging term
NORTH_M3CLAMPED use if 3D momentum clamped condition
NORTH_KGRADIENT use if TKE fields gradient condition
NORTH_KRADIATION use if TKE fields radiation condition

NORTH_TGRADIENT use if tracers gradient condition
NORTH_TRADIATION use if tracers radiation condition
NORTH_TNUDGING use if tracers passive/active nudging term
NORTH_TCLAMPED use if tracers clamped condition

Southern edge open boundary conditions OPTIONS:

SOUTH_FSCHAPMAN use if free-surface Chapman condition
SOUTH_FSGRADIENT use if free-surface gradient condition
SOUTH_FSRADIATION use if free-surface radiation condition
SOUTH_FSNUDGING use if free-surface passive/active nudging term
SOUTH_FSCLAMPED use if free-surface clamped condition
SOUTH_M2FLATHER use if 2D momentum Flather condition
SOUTH_M2GRADIENT use if 2D momentum gradient condition
SOUTH_M2RADIATION use if 2D momentum radiation condition
SOUTH_M2REDUCED use if 2D momentum reduced-physics
SOUTH_M2NUDGING use if 2D momentum passive/active nudging term
SOUTH_M2CLAMPED use if 2D momentum clamped condition
SOUTH_M3GRADIENT use if 3D momentum gradient condition
SOUTH_M3RADIATION use if 3D momentum radiation condition
SOUTH_M3NUDGING use if 3D momentum passive/active nudging term
SOUTH_M3CLAMPED use if 3D momentum clamped condition
SOUTH_KGRADIENT use if TKE fields gradient condition
SOUTH_KRADIATION use if TKE fields radiation condition
SOUTH_TGRADIENT use if tracers gradient condition
SOUTH_TRADIATION use if tracers radiation condition
SOUTH_TNUDGING use if tracers passive/active nudging term
SOUTH_TCLAMPED use if tracers clamped condition

OPTIONS for tidal forcing at open boundaries:

The tidal data is processed in terms of tidal components, classified by period. The tidal forcing is computed for the full horizontal grid. If requested, the tidal forcing is added to the processed open boundary data.

Both tidal elevation and tidal currents are required to force the model properly. However, if only the tidal elevation is available, the tidal currents at the open boundary can be estimated by reduced physics. Only the pressure gradient, Coriolis, and surface and bottom stresses terms are considered at the open boundary. See "u2dbc_im.F" or "v2dbc_im.F" for details. Notice that there is an additional option (FSOBC_REDUCED) for the computation of the pressure gradient term in both Flather or reduced physics conditions (_M2FLATHER, _M2REDUCED).

SSH_TIDES use if imposing tidal elevation
UV_TIDES use if imposing tidal currents
RAMP_TIDES use if ramping (over one day) tidal forcing
FSOBC_REDUCED use if SSH data and reduced physics conditions
ADD_FSOBC use to add tidal elevation to processed OBC data
ADD_M2OBC use to add tidal currents to processed OBC data

OPTIONS for reading and processing of climatological fields:

M2CLIMATOLOGY use if processing 2D momentum climatology
M3CLIMATOLOGY use if processing 3D momentum climatology
TCLIMATOLOGY use if processing tracers climatology
ZCLIMATOLOGY use if processing SSH climatology

OPTIONS to nudge climatology data (primarily in sponge areas):

M2CLM_NUDGING use if nudging 2D momentum climatology
M3CLM_NUDGING use if nudging 3D momentum climatology
TCLM_NUDGING use if nudging tracers climatology
ZCLM_NUDGING use if nudging SSH climatology

Optimal Interpolation (OI) or nudging data assimilation OPTIONS:

The OI assimilation is intermittent whereas nudging is continuous (observations are time interpolated). If applicable, choose only one option for each field to update: either OI assimilation or nudging.

ASSIMILATION_SSH use if assimilating SSH observations
ASSIMILATION_SST use if assimilating SST observations
ASSIMILATION_T use if assimilating tracers observations
ASSIMILATION_UVsur use if assimilating surface current observations
ASSIMILATION_UV use if assimilating horizontal current observations
UV_BAROCLINIC use if assimilating baroclinic currents only
NUDGING_SST use if nudging SST observations
NUDGING_T use if nudging tracers observations
NUDGING_UVsur use if nudging surface current observations
NUDGING_UV use if nudging horizontal currents observations

ROMS/TOMS driver OPTIONS:

ADM_DRIVER use if generic adjoint model driver
AD_SENSITIVITY use if adjoint sensitivity driver

AFT_EIGENMODES use if adjoint finite time eingenmodes driver
ARRAY_MODES use if W4DVAR representer matrix array modes
CLIPPING use if W4DVAR representer matrix clipping analysis
CONVOLUTION use if adjoint convolution driver
CORRELATION use if background-error correlation model driver
ENSEMBLE use if ensemble prediction driver
FORCING_SV use if forcing singular vectors driver
FT_EIGENMODES use if finite time eingenmodes driver: normal modes
INNER_PRODUCT use if tangent linear and adjoint inner product check
IS4DVAR use if incremental 4DVar data assimilation
IS4DVAR_SENSITIVITY use if I4DVar observations sensitivity driver
OPT_OBSERVATIONS use if optimal observations driver
OPT_PERTURBATION use if optimal perturbations driver, singular vectors
PICARD_TEST use if representer tangent linear model test
PSEUDOSPECTRA use if pseudospectra of tangent linear resolvant
R_SYMMETRY use if representer matrix symmetry test
RPM_DRIVER use if generic representers model driver
SANITY_CHECK use if tangent linear and adjoint codes sanity check
SO_SEMI use if stochastic optimals driver, semi-norm
SO_TRACE use if stochastic optimals, randomized trace
STOCHASTIC_OPT use if stochastic optimals
TLM_CHECK use if tangent linear model linearization check
TLM_DRIVER use if generic tangent linear model driver
W4DPSAS use if weak constraint 4DPSAS data assimilation
W4DPSAS_SENSITIVITY use if weak constraint 4DPSAS observation sensitivity
W4DVAR use if Weak constraint 4DVar data assimilation
W4DVAR_SENSITIVITY use if Weak constraint 4DVar observation sensitivity

OPTIONS associated with tangent linear, representer and adjoint models:

AD_IMPULSE use to force adjoint model with intermittent impulses
ADJUST_STFLUX use if including surface tracer flux in 4DVar state
ADJUST_WSTRESS use if including wind-stress in 4DVar state
ARRAY_MODES_SPLIT use to separate analysis due to IC, forcing, and OBC
BALANCE_OPERATOR use if error covariance multivariate balance term
CELERITY_WRITE use if writing radiation celerity in forward file
CLIPPING_SPLIT use to separate analysis due to IC, forcing, and OBC
CONVOLVE use if convolving solution with diffusion operators
DATALESS_LOOPS use if testing convergence of Picard iterations
FORWARD_MIXING use if processing forward vertical mixing coefficient
FORWARD_WRITE use if writing out forward solution, basic state
FORWARD_READ use if reading in forward solution, basic state
FORWARD_RHS use if processing forward right-hand-side terms
IMPLICIT_VCONV use if implicit vertical convolution algorithm
IMPULSE use if processing adjoint impulse forcing
MULTIPLE_TLM use if multiple TLM history files in 4DVAR
NLM_OUTER use if nonlinear model as basic state in outer loop
OBS_IMPACT use if observation impact to 4DVAR data assimilation
OBS_IMPACT_SPLIT use to separate impact due to IC, forcing, and OBC
POSTERIOR_EOFS use if posterior analysis error covariance EOFS
POSTERIOR_ERROR_F use if final posterior analysis error covariance
POSTERIOR_ERROR_I use if initial posterior analysis error covariance
RECOMPUTE_4DVAR use if recomputing 4DVar in analysis algorithms
RPM_RELAXATION use if Picard iterations, Diffusive Relaxation of RPM
SO_SEMI_WHITE use to activate white/red noise processes
SPLINES_VCONV use to activate implicit splines vertical convolution
VCONVOLUTION use to add vertical correlation to 3D convolution
VERIFICATION use if writing out solution at observation locations

ZETA_ELLIPTIC use if SSH elliptic Equation in balance operator

OPTION for processing the full grid range (interior and boundary points) of the state vector in variational data assimilation and generalized stability theory analysis. Otherwise, only interior points are processed.

FULL_GRID use to consider both interior and boundary points

Fennel et al. (2006) biology model OPTIONS:

BIO_FENNEL use if Fennel et al. (2006) nitrogen-based model
BIO_SEDIMENT use to restore fallen material to the nutrient pool
CARBON use to add carbon constituents
DENITRIFICATION use to add denitrification processes
OXYGEN use to add oxygen dynamics
OCMIP_OXYGEN_SC use if Schmidt number from Keeling et al. (1998)
TALK_NONCONSERV use if nonconservative computation of alkalinity

NPZD biology model OPTIONS:

NPZD_FRANKS use if NPZD Biology model, Franks et al. (1986)
NPZD_IRON use if NPZD Biology model with iron limitation
NPZD_POWELL use if NPZD Biology model, Powell et al. (2006)
IRON_LIMIT use if Fe limitation on phytoplankton growth
IRON_RELAX use if nudging Fe over the shelf, h <= FeHmin

Bio-optical EcoSim model OPTIONS:

ECOSIM use if bio-optical EcoSim model

Nemuro lower trophic level ecosystem model OPTIONS:

Need to choose a zooplankton grazing option (HOLLING_GRAZING or IVLEV_EXPLICIT). The default implicit IVLEV algorithm does not work yet.

NEMURO use if Nemuro ecosystem model.
BIO_SEDIMENT use to restore fallen material to the nutrient pool
HOLLING_GRAZING use Holling-type s-shaped curve grazing (implicit)
IVLEV_EXPLICIT use Ivlev explicit grazing algorithm

Sediment transport model OPTIONS:

SEDIMENT use to activate sediment transport model
BEDLOAD_MPM use to activate Meyer-Peter-Mueller bed load
BEDLOAD_SOULSBY use to activate Soulsby wave/current bed load
SED_DENS use to activate sediment to affect equation of state
SED_MORPH use to allow bottom model elevation to evolve
SUSPLOAD use to activate suspended load transport

OPTIONS for two-way coupling to other models:

REFDIF_COUPLING use if coupling to REFDIT wave model
SWAN_COUPLING use if coupling to SWAN wave model
WRF_COUPLING use if coupling to WRF atmospheric model

Nearshore and shallow water model OPTIONS:

WET_DRY use to activate wetting and drying
NEARSHORE_MELLOR use to activate radiation stress terms.

NetCDF input/output OPTIONS:

DEFLATE use to set compression NetCDF-4/HDF5 format files
HDF5 use to create NetCDF-4/HDF5 format files
NO_READ_GHOST use to not include ghost points during read/scatter
NO_WRITE_GRID use if not writing grid arrays
PARALLEL_IO use if parallel I/O via HDF5 or pnetcdf libraries
PERFECT_RESTART use to include perfect restart variables
PNETCDF use if parallel I/O with pnetcdf (classic format)
READ_WATER use if only reading water points data
WRITE_WATER use if only writing water points data
RST_SINGLE use if writing single precision restart fields
OUT_DOUBLE use if writing double precision output fields

Coupling Library OPTIONS:

ESMF_LIB use Earth System Modeling Framework Library
MCT_LIB use Model Coupling Toolkit Library

OPTION to process 3D data by levels (2D slabs) to reduce memory needs in distributed-memory configurations. This option is convenient for large problems on nodes with limited memory.

INLINE_2DIO use if processing 3D IO level by level

OPTION to avoid writing current date and CPP options to NetCDF file

headers. This is used to compare serial and parallel solutions where the UNIX command "diff" is used between NetCDF files. It will only tell us that the binary files are different or not. Finding the parallel bug is complete different story.

DEBUGGING use to activate parallel debugging switch

Idealized Test Problems:

A4DVAR_TOY 4DVAR Data Assimilation Toy
BASIN Big Bad Basin Example
BENCHMARK Benchmark Tests (small, Medium, big grids)
BIO_TOY One-dimension (vertical) Biology Toy
BL_TEST Boundary Layers Test
CANYON Coastal form stress Canyon Test
CHANNEL_NECK Channel with a Constriction
COUPLING_TEST Two-way Atmosphere-Ocean Coupling Test
DOUBLE_GYRE Idealized Double-gyre Example
ESTUARY_TEST Test Estuary for Sediment
FLT_TEST Float Tracking Example
GRAV_ADJ Gravitational Adjustment Example
INLET_TEST Test Inlet Application
KELVIN Kelvin wave test
LAB_CANYON Lab Canyon, Polar Coordinates Example
LAKE_SIGNELL Lake Signell Sediment Test Case

LMD_TEST Test for LMD and KPP

OVERFLOW Gravitational/Overflow Example

RIVERPLUME1 River Plume Example 1

RIVERPLUME2 River plume Example 2 (Hyatt and Signell)

SEAMOUNT Seamount Example

SED_TEST1 Suspended Sediment Test in a Channel

SED_TOY One-dimension (vertical) Sediment Toy

SHOREFACE Shore Face Planar Beach Test Case

SOLITON Equatorial Rossby Wave Example

TEST_CHAN Sediment Test Channel Case

TEST_HEAD Sediment Test Headland Case

UPWELLING Upwelling Example (default)

WEDDELL Idealized Weddell Sea Shelf Application

WINDBASIN Linear Wind-driven Constant Coriolis Basin

Climatological Applications: (See www.myroms.org/Datasets)

DAMEE_4 North Atlantic DAMEE Application, 3/4 degree

Selected Realistic Applications:

ADRIA02 Adriatic Sea Application

NJ_BIGHT New Jersey Bight Application

WC13 California Current System, 1/3 degree resolution

The user needs to choose either a pre-defined application or his/her own application. The application CPP flag to run is activated in the makefile. For example, to activate the upwelling example (UPWELLING) set:

```
ROMS_APPLICATION ?= UPWELLING
```

in the makefile. ROMS will include the associated header file located in the ROMS/Include directory. The application header file name is the lowercase value of ROMS_APPLICATION with the .h extension and passed as ROMS_HEADER definition during C-preprocessing. For example, the upwelling test problem includes the "upwelling.h" header file:

```
ROMS_HEADER="upwelling.h"
```

If building a new application, choose an unique CPP flag for it and create its associated include file (.h) to specify the appropriate configuration options.

APPENDIX C: ROMS MODEL RUNNING OPTIONS

```
-----------------------------------------------------------------------------
 Application tile (string with a maximum of eighty characters) and
 C-preprocessing flag.
-----------------------------------------------------------------------------
  TITLE       Application title.
  MyAppCPP    Application C-preprocession option.
-----------------------------------------------------------------------------
 Variable information file name (string with a maximum of eighty characters).
-----------------------------------------------------------------------------
  VARNAME     Input/Output variable information file name.  This file need to
              be processed first so all information arrays and indices can be
              initialized properly in "mod_ncparam.F".
-----------------------------------------------------------------------------
 Grid dimension parameters.
-----------------------------------------------------------------------------
 These parameters are very important since it determine the grid of the
 application to solve. They need to be read first in order to dynamically
 allocate all model variables.
 WARNING: It is trivial and posible to change these dimension parameters in
 -------  idealized applications via analytical expressions.  However, in
 realistic applications any change to these parameters requires redoing all
 input NetCDF files.
  Lm          Number of INTERIOR grid RHO-points in the XI-direction for
              each nested grid, [1:Ngrids]. If using NetCDF files as
              input, Lm=xi_rho-2 where "xi_rho" is the NetCDF file
              dimension of RHO-points. Recall that all RHO-point
              variables have a computational I-range of [0:Lm+1].
```

Mm Number of INTERIOR grid RHO-points in the ETA-direction for each nested grid, [1:Ngrids]. If using NetCDF files as input, Mm=eta_rho-2 where "eta_rho" is the NetCDF file dimension of RHO-points. Recall that all RHO-point variables have a computational J-range of [0:Mm+1].

N Number of vertical terrain-following levels at RHO-points, [1:Ngrids].

Nbed Number of sediment bed layers, [1:Ngrids]. This parameter is only relevant if CPP option SEDIMENT is activated.

NAT Number of active tracer type variables. Usually, NAT=2 for potential temperature and salinity.

NPT Number of inert (dyes, age, etc) passive tracer type variables to advect and diffuse only. This parameter is only relevant if CPP option T_PASSIVE is activated.

NCS Number of cohesive (mud) sediment tracer type variables. This parameter is only relevant if CPP option SEDIMENT is activated.

NNS Number of non-cohesive (sand) sediment tracer type variables. This parameter is only relevant if CPP option SEDIMENT is activated.

The total of sediment tracers is NST=NCS+NNS. Notice that NST must be greater than zero (NST>0).

Domain tile partition parameters.

Model tile decomposition parameters for serial and parallel configurations which are used to determine tile horizontal range indices (Istr,Iend) and (Jstr,Jend). In some computers, it is advantageous to have tile partitions

in serial applications.

NtileI Number of domain partitions in the I-direction (XI-coordinate).
It must be equal or greater than one.

NtileJ Number of domain partitions in the J-direction (ETA-coordinate).
It must be equal or greater than one.

WARNING: In shared-memory (OpenMP), the product of NtileI and NtileJ must be a MULTIPLE of the number of parallel threads specified with the OpenMP environmental variable OMP_NUM_THREADS. In distributed-memory (MPI), the product of NtileI and NtileJ must be EQUAL to the number of parallel nodes specified during execution with the "mprun" or "mpirun" command.

Time-Stepping parameters.

NTIMES Total number time-steps in current run. If 3D configuration, NTIMES is the total of baroclinic time-steps. If only 2D configuration, NTIMES is the total of barotropic time-steps.

DT Time-Step size in seconds. If 3D configuration, DT is the size of baroclinic time-step. If only 2D configuration, DT is the size of the barotropic time-step.

NDTFAST Number of barotropic time-steps between each baroclinic time step. If only 2D configuration, NDTFAST should be unity since there is not need to splitting time-stepping.

Model iteration loops parameters.

ERstr Starting ensemble run (perturbation or iteration) number.

ERend Ending ensemble run (perturbation or iteration) number.

Nouter Maximum number of 4DVAR outer loop iterations.

Ninner Maximum number of 4DVAR inner loop iterations.

Nintervals Number of time interval divisions for stochastic optimals computations. It must be a multiple of NTIMES. The tangent linear model (TLM) and the adjoint model (ADM) are integrated forward and backward in different intervals. For example, if Nintervals=3,

1 NTIMES/3 2*NTIMES/3 NTIMES

+.....+.....+.....+

<==========> (1)

<==========> (2)

<==========> (3)

In the first iteration (1), the TLM is integrated forward from 1 to NTIMES and the ADM is integrated backward from NTIMES to 1. In the second iteration (2), the TLM is integrated forward from NTIMES/3 to NTIMES and the ADM is integrated backward from NTIMES to NTIMES/3. And so on.

Eigenproblem parameters.

NEV Number of eigenvalues to compute for the Lanczos/Arnoldi problem. Notice that the model memory requirement increases substantially as NEV increases. The GST requires NEV+1 copies of the model state vector. The memory requirements are decreased in distributed-memory applications.

NCV Number of eigenvectors to compute for the Lanczos/Arnoldi problem. NCV must be greater than NEV.

At present, there is no a-priori analysis to guide the selection of NCV relative to NEV. The only formal requirement is that NCV > NEV. However in optimal perturbations, it is recommended to have NCV greater than or equal to 2*NEV. In Finite Time Eigenmodes (FTE) and Adjoint Finite Time Eigenmodes (AFTE) the requirement is to have NCV greater than or equal to 2*NEV+1.
The efficiency of calculations depends critically on the combination of NEV and NCV. If NEV is large (greater than 10 say), you can use NCV=2*NEV+1 but for NEV small (less than 6) it will be inefficient to use NCV=2*NEV+1.
In complicated applications, you can start with NEV=2 and NCV=10. Otherwise, it will iterate for very long time.

Input/Output parameters.

NRREC Switch to indicate re-start from a previous solution. Use NRREC=0 for new solutions. In a re-start solution, NRREC is the time index of the re-start NetCDF file assigned for initialization. If NRREC is negative (said NRREC=-1), the model will re-start from the most recent time record. That is, the initialization record is assigned internally.
Notice that it is also possible to re-start from a history or time-averaged NetCDF files. If a history file is used for re-start, it must contains all the necessary primitive

variables at all levels.

LcycleRST Logical switch (T/F) used to recycle time records in output re-start file. If TRUE, only the latest two re-start time records are maintained. If FALSE, all re-start fields are saved every NRST time-steps without recycling. The re-start fields are written at all levels in double precision.

NRST Number of time-steps between writing of re-start fields.

NSTA Number of time-steps between writing data into stations file. Station data is written at all levels.

NFLT Number of time-steps between writing data into floats file.

NINFO Number of time-steps between print of single line information to standard output. If also determines the interval between computation of global energy diagnostics.

Output history and average files parameters.

LDEFOUT Logical switch (T/F) used to create new output files when initializing from a re-start file, abs(NRREC) > 0. If TRUE and applicable, a new history, average, diagnostic and station files are created during the initialization stage. If FALSE and applicable, data is appended to an existing history, average, diagnostic and station files. See also parameters NDEFHIS, NDEFAVG and NDEFDIA below.

NHIS Number of time-steps between writing fields into history file.

NDEFHIS Number of time-steps between the creation of new history file. If NDEFHIS=0, the model will only process one history file. This feature is useful for long simulations when history files get too large; it creates a new file every NDEFHIS time-steps.

NTSAVG Starting time-step for the accumulation of output time-averaged data.

NAVG Number of time-steps between writing time-averaged data into averages file. Averaged date is written for all fields.

NDEFAVG Number of time-steps between the creation of new average file. If NDEFAVG=0, the model will only process one average file. This feature is useful for long simulations when average files get too large; it creates a new file every NDEFAVG time-steps.

NTSDIA Starting time-step for the accumulation of output time-averaged diagnostics data.

NDIA Number of time-steps between writing time-averaged diagnostics data into diagnostics file. Averaged date is written for all fields.

NDEFDIA Number of time-steps between the creation of new time-averaged diagnostics file. If NDEFDIA=0, the model will only process one diagnostics file. This feature is useful for long simulations when diagnostics files get too large; it creates a new file every NDEFDIA time-steps.

Output tangent linear and adjoint model parameters.

LcycleTLM Logical switch (T/F) used to recycle time records in output tangent linear file. If TRUE, only the latest two time records are maintained. If FALSE, all tangent linear fields are saved every NTLM time-steps without recycling.

NTLM Number of time-steps between writing fields into tangent linear model file.

NDEFTLM Number of time-steps between the creation of new tangent linear file. If NDEFTLM=0, the model will only process one tangent linear file. This feature is useful for long simulations when output NetCDF files get too large; it creates a new file every NDEFTLM time-steps.

LcycleADJ Logical switch (T/F) used to recycle time records in output adjoint file. If TRUE, only the latest two time records are maintained. If FALSE, all tangent linear fields re saved every NADJ time-steps without recycling.

NADJ Number of time-steps between writing fields into adjoint model file.

NDEFADJ Number of time-steps between the creation of new adjoint file. If NDEFADJ=0, the model will only process one adjoint file. This feature is useful for long simulations when output NetCDF files get too large; it creates a new file every NDEFADJ time-steps.

Generalized Stability Theory (GST) analysis parameters.

LrstGST Logical switch (TRUE/FALSE) to restart GST analysis. If TRUE, the check pointing data is read in from the GST restart NetCDF file. If FALSE and applicable, the check pointing GST data is saved and overwritten every NGST iterations of the algorithm.

MaxIterGST Maximum number of GST algorithm iterations.

NGST Number of GST iterations between storing of check pointing data into NetCDF file. The restart data is always saved if MaxIterGST is reached without convergence. It is also saved when convergence is achieved. It is always a good idea to

save the check pointing data at regular intervals so there is a mechanism to recover from an unexpected interruption in this very expensive computation. The check pointing data can be used also to recompute the Ritz vectors by changing some of the parameters, like convergence criteria (Ritz_tol) and number of Arnoldi iterations (iparam(3)).

Ritz_tol Relative accuracy of the Ritz values computed in the GST analysis.

Harmonic/Biharmonic horizontal diffusion for active tracers.

TNU2 Lateral, harmonic, constant, mixing coefficient (m2/s) for active (NAT) and inert (NPT) tracer variables. If variable horizontal diffusion is activated, TNU2 is the mixing coefficient for the largest grid-cell in the domain.

TNU4 Lateral, biharmonic, constant, mixing coefficient (m4/s) for active (NAT) and inert (NPT) tracer variables. If variable horizontal diffusion is activated, TNU4 is the mixing coefficient for the largest grid-cell in the domain.

Harmonic/biharmonic horizontal viscosity coefficients.

VISC2 Lateral, harmonic, constant, mixing coefficient (m2/s) for momentum. If variable horizontal viscosity is activated, UVNU2 is the mixing coefficient for the largest grid-cell in the domain.

VISC4 Lateral, biharmonic, constant mixing coefficient (m4/s) for

momentum. If variable horizontal viscosity is activated, UVNU4 is the mixing coefficient for the largest grid-cell in the domain.

Vertical mixing coefficients for active tracers.

AKT_BAK Background vertical mixing coefficient (m2/s) for active (NAT) and inert (NPT) tracer variables.

Vertical mixing coefficient for momentum.

AKV_BAK Background vertical mixing coefficient (m2/s) for momentum.

Turbulent closure parameters.

AKK_BAK Background vertical mixing coefficient (m2/s) for turbulent kinetic energy.

AKP_BAK Background vertical mixing coefficient (m2/s) for turbulent generic statistical field, "psi".

TKENU2 Lateral, harmonic, constant, mixing coefficient (m2/s) for turbulent closure variables.

TKENU4 Lateral, biharmonic, constant mixing coefficient (m4/s) for turbulent closure variables.

Generic length-scale turbulence closure parameters.

GLS_P Stability exponent (non-dimensional).

GLS_M Turbulent kinetic energy exponent (non-dimensional).

GLS_N Turbulent length scale exponent (non-dimensional).

GLS_Kmin Minimum value of specific turbulent kinetic energy

GLS_Pmin Minimum Value of dissipation.

Closure independent constraint parameters (non-dimensional):

GLS_CMU0 Stability coefficient.

GLS_C1 Shear production coefficient.

GLS_C2 Dissipation coefficient.

GLS_C3M Buoyancy production coefficient (minus).

GLS_C3P Buoyancy production coefficient (plus).

GLS_SIGK Constant Schmidt number (non-dimensional) for turbulent kinetic energy diffusivity.

GLS_SIGP Constant Schmidt number (non-dimensional) for turbulent generic statistical field, "psi".

Suggested values for various parameterizations:

	k-kl	k-epsilon	k-omega	gen
GLS_P =	0.d0	3.0d0	-1.0d0	2.0d0
GLS_M =	1.d0	1.5d0	0.5d0	1.0d0
GLS_N =	1.d0	-1.0d0	-1.0d0	-0.67d0
GLS_Kmin =	5.0d-6	7.6d-6	7.6d-6	1.0d-8
GLS_Pmin =	5.0d-6	1.0d-12	1.0d-12	1.0d-8
GLS_CMU0 =	0.5544d0	0.5477d0	0.5477d0	0.5544d0
GLS_C1 =	0.9d0	1.44d0	0.555d0	1.00d0
GLS_C2 =	0.52d0	1.92d0	0.833d0	1.22d0
GLS_C3M =	2.5d0	-0.4d0	-0.6d0	0.1d0
GLS_C3P =	1.0d0	1.0d0	1.0d0	1.0d0
GLS_SIGK =	1.96d0	1.0d0	2.0d0	0.8d0

GLS_SIGP = 1.96d0 1.30d0 2.0d0 1.07d0

Constants used in the various formulation of surface turbulent kinetic energy flux in the GLS.

CHARNOK_ALPHA Charnok surface roughness,
Zos: (charnok_alpha * u_star**2) / g

ZOS_HSIG_ALPHA Roughness from wave amplitude,
Zos: zos_hsig_alpha * Hsig

SZ_ALPHA Surface flux from wave dissipation,
flux: dt * sz_alpha * Wave_dissip

CRGBAN_CW Surface flux due to Craig and Banner wave breaking,
flux: dt * crgban_cw * u_star**3

Constants used in the computation of momentum stress.

RDRG Linear bottom drag coefficient (m/s).

RDRG2 Quadratic bottom drag coefficient.

Zob Bottom roughness (m).

Zos Surface roughness (m).

Height of atmospheric measurements for bulk fluxes parameterization.

BLK_ZQ Height (m) of surface air humidity measurement. Usually, recorded at 10 m.

BLK_ZT Height (m) of surface air temperature measurement. Usually,

recorded at 2 or 10 m.

BLK_ZW Height (m) of surface winds measurement. Usually, recorded at 10 m.

Wetting and drying parameters.

DCRIT Minimum depth (m) for wetting and drying.

Jerlow Water type.

WTYPE Jerlov water type: an integer value from 1 to 5.

Body-force parameters. Used when CPP option BODYFORCE is activated.

LEVSFRC Deepest level to apply surface momentum stress as a body-force.

LEVBFRC Shallowest level to apply bottom momentum stress as a body-force.

Vertical S-coordinates parameters.

THETA_S S-coordinate surface control parameter, [0 < theta_s < 20].

THETA_B S-coordinate bottom control parameter, [0 < theta_b < 1].

TCLINE Width (m) of surface or bottom boundary layer in which higher vertical resolution is required during stretching.

WARNING: Users need to experiment with these parameters. We have found out that the model goes unstable with

high values of THETA_S. In steep and very tall topography, it is recommended to use THETA_S < 3.0.

Mean Density and background Brunt-Vaisala frequency.

RHO0 Mean density (Kg/m3) used when the Boussinesq approximation is inferred.

BVF_BAK Background Brunt-Vaisala frequency squared (1/s2). Typical values for the ocean range (as a function of depth) from 1.0E-4 to 1.0E-6.

Time Stamps.

DSTART Time stamp assigned to model initialization (days). Usually a Calendar linear coordinate, like modified Julian Day. For Example:

Julian Day = 1 for Nov 25, 0:0:0 4713 BCE
modified Julian Day = 1 for May 24, 0:0:0 1968 CE GMT

It is called truncated or modified Julian day because an offset of 2440000 needs to be added.

TIDE_START Reference time origin for tidal forcing (days). This is the time used when processing input tidal model data. It is needed in routine "set_tides" to compute the correct phase lag with respect ROMS/TOMS initialization time.

TIME_REF Reference time (yyyymmdd.f) used to compute relative time: elapsed time interval since reference-time. The "units"

attribute takes the form "time-unit since reference-time".
This parameter also provides information about the calendar
used:
If TIME_REF = -2, model time and DSTART are in modified Julian
days units. The "units" attribute is:
'time-units since 1968-05-23 00:00:00 GMT'
If TIME_REF = -1, model time and DSTART are in a calendar
with 360 days in every year (30 days each month). The "units"
attribute is:
'time-units since 0000-01-01 00:00:00'
If TIME_REF = 0, model time and DSTART are in a common year
calendar with 365.25 days. The "units" attribute is:
'time-units since 0000-01-01 00:00:00'
If TIME_REF > 0, model time and DSTART are the elapsed time
units since specified reference time. For example,
TIME_REF=20020115.5 will yield the following attribute:
'time-units since 2002-01-15 12:00:00'

Nudging/relaxation time scales, inverse scales will be computed internally.

When passive/active open boundary conditions are activated, these nudging values correspond to the passive (outflow) nudging time scales.

TNUDG Nudging time scale (days) for active tracer variables.
(1:NAT+NPT,1:Ngrids) values are expected.
ZNUDG Nudging time scale (days) for free-surface.
M2NUDG Nudging time scale (days) for 2D momentum.
M3NUDG Nudging time scale (days) for 3D momentum.

OBCFAC Factor between passive (outflow) and active (inflow) open boundary conditions. The nudging time scales for the active (inflow) conditions are obtained by multiplying the passive values by OBCFAC. If OBCFAC > 1, nudging on inflow is stronger than on outflow (recommended).

Linear equation of State parameters.

Ignoring pressure, the linear equation of state is:

rho(:,:,:) = R0 - R0 * TCOEF * (t(:,:,:,:,itemp) - T0)
+ R0 * SCOEF * (t(:,:,:,:,isalt) - S0)

Typical values: R0 = 1027.0 kg/m3
T0 = 10.0 Celsius
S0 = 35.0 PSU
TCOEF = 1.7d-4 1/Celsius
SCOEF = 7.6d-4 1/PSU

R0 Background density value (Kg/m3) used in Linear Equation of State.

T0 Background potential temperature (Celsius) constant.

S0 Background salinity (PSU) constant.

TCOEF Thermal expansion coefficient in Linear Equation of State.

SCOEF Saline contraction coefficient in Linear Equation of State.

Slipperiness parameter.

GAMMA2 Slipperiness variable, either 1.0 (free slip) or -1.0 (no slip).

Adjoint sensitivity parameters.

DstrS Starting day for adjoint sensitivity forcing.

DendS Ending day for adjoint sensitivity forcing.
The adjoint forcing is applied at every time step according to desired state functional stored in the adjoint sensitivity NetCDF file. DstrS must be less or equal to DendS. If both values are zero, their values are reset internally to the full range of the adjoint integration.

KstrS Starting vertical level of the 3D adjoint state variables whose sensitivity is required.

KendS Ending vertical level of the 3D adjoint state variables whose sensitivity is required.

Lstate Logical switches (TRUE/FALSE) to specify the adjoint state variables whose sensitivity is required.
Lstate(isFsur): Free-surface
Lstate(isUbar): 2D U-momentum
Lstate(isVbar): 2D V-momentum
Lstate(isUvel): 3D U-momentum
Lstate(isVvel): 3D V-momentum
Lstate(isTvar): Traces (NT values expected)

Stochastic optimals parameters.

SO_decay Stochastic optimals time decorrelation scale (days) assumed for red noise processes.

SOstate Logical switches (TRUE/FALSE) to specify the state surface forcing variable whose stochastic optimals is required.

SOstate(isUstr): surface u-stress

SOstate(isVstr): surface v-stress

SOstate(isTsur): surface tracer flux (NT values expected)

SO_sdev Stochastic optimals surface forcing standard deviation for dimensionalization.

SO_sdev(isUstr): surface u-stress

SO_sdev(isVstr): surface v-stress

SO_sdev(isTsur): surface tracer flux (NT values expected)

Logical switches (T/F) to activate writing of fields into HISTORY file.

Hout(idUvel) Write out 3D U-velocity component.

Hout(idVvel) Write out 3D V-velocity component.

Hout(idWvel) Write out 3D W-velocity component.

Hout(idOvel) Write out 3D omega vertical velocity.

Hout(idUbar) Write out 2D U-velocity component.

Hout(idVbar) Write out 2D V-velocity component.

Hout(idFsur) Write out free-surface.

Hout(idBath) Write out time-dependent bathymetry.

Hout(idTvar) Write out active (NAT) tracers: temperature and salinity.

Hout(idUsms) Write out surface U-momentum stress.

Hout(idVsms) Write out surface V-momentum stress.

Hout(idUbms) Write out bottom U-momentum stress.

Hout(idVbms) Write out bottom V-momentum stress.

Hout(idUbrs) Write out current-induced, U-momentum stress.

Hout(idVbrs) Write out current-induced, V-momentum stress.

Hout(idUbws) Write out wind-induced, bottom U-wave stress.

Hout(idVbws) Write out wind-induced, bottom V-wave stress.

Hout(idUbcs) Write out bottom maximum wave and current U-stress.

Hout(idVbcs) Write out bottom maximum wave and current V-stress.

Hout(idUbot) Write out wind-induced, bed wave orbital U-velocity.

Hout(idVbot) Write out wind-induced, bed wave orbital V-velocity.

Hout(idUbur) Write out bottom U-velocity above bed.

Hout(idVbvr) Write out bottom V-velocity above bed.

Hout(idW2xx) Write out 2D radiation stress, Sxx component.

Hout(idW2xy) Write out 2D radiation stress, Sxy component.

Hout(idW2yy) Write out 2D radiation stress, Syy component.

Hout(idU2rs) Write out 2D U-radiation stress.

Hout(idV2rs) Write out 2D V-radiation stress.

Hout(idU2Sd) Write out 2D U-Stokes velocity.

Hout(idV2Sd) Write out 2D V-Stokes velocity.

Hout(idW3xx) Write out 3D radiation stress, Sxx component.

Hout(idW3xy) Write out 3D radiation stress, Sxy component.

Hout(idW3yy) Write out 3D radiation stress, Syy component.

Hout(idW3zx) Write out 3D radiation stress, Szx component.

Hout(idW3zy) Write out 3D radiation stress, Szy component.

Hout(idU3rs) Write out 3D U-radiation stress.

Hout(idV3rs) Write out 3D V-radiation stress.

Hout(idU3Sd) Write out 3D U-Stokes velocity.

Hout(idV3Sd) Write out 3D V-Stokes velocity.

Hout(idWamp) Write out wave height.

Hout(idWlen) Write out wave length.

Hout(idWdir) Write out wave direction.

Hout(idTsur) Write out surface net heat and salt flux

Hout(idLhea) Write out latent heat flux.

Hout(idShea) Write out sensible heat flux.

Hout(idLrad) Write out long-wave radiation flux.

Hout(idSrad) Write out short-wave radiation flux.

Hout(idevap) Write out evaporation rate.

Hout(idrain) Write out precipitation rate.

Hout(idDano) Write out density anomaly

Hout(idVvis) Write out vertical viscosity coefficient.

Hout(idTdif) Write out vertical diffusion coefficient of temperature.

Hout(idSdif) Write out vertical diffusion coefficient of salinity.

Hout(idHsbl) Write out depth of oceanic surface boundary layer.

Hout(idHbbl) Write out depth of oceanic bottom boundary layer.

Hout(idMtke) Write out turbulent kinetic energy.

Hout(idMtls) Write out turbulent kinetic energy times length scale.

Hout(inert) Write out extra inert passive tracers.

Hout(idBott) Write out exposed sediment layer properties, 1:MBOTP.

Generic User parameters.

NUSER Number of User parameters to consider (integer).

USER Vector containing user parameters (real array). This array is used with the SANITY_CHECK to test the correctness of the tangent linear adjoint models. It contains information of the model variable and grid point to perturb:

INT(user(1)): tangent state variable to perturb

INT(user(2)): adjoint state variable to perturb

[isFsur=1] free-surface

[isUbar=2] 2D U-momentum

[isVbar=3] 2D V-momentum

[isUvel=4] 3D U-momentum

[isVvel=5] 3D V-momentum

[isTvar=6] Firt tracer (temperature)

[...]

[isTvar=?] Last tracer

INT(user(3)): I-index of tangent variable to perturb

INT(user(4)): I-index of adjoint variable to perturb

INT(user(5)): J-index of tangent variable to perturb

INT(user(6)): J-index of adjoint variable to perturb

INT(user(7)): K-index of tangent variable to perturb, if 3D

INT(user(8)): K-index of adjoint variable to perturb, if 3D

Set tangent and adjoint parameters to the same values if perturbing and reporting the same variable.

Input/output NetCDF file names (string with a maximum of eighty characters).

GRDNAME Input grid file name.

ININAME Input nonlinear initial conditions file name. It can be a

re-start file.

IRPNAME Input representer model initial conditions file name.

ITLNAME Input tangent linear model initial conditions file name.

IADNAME Input adjoint model initial conditions file name.

FRCNAME Input forcing fields file name.

CLMNAME Input climatology fields file name.

BRYNAME Input open boundary data file name.

FWDNAME Input forward solution fields file name.

ADSNAME Input adjoint sensitivity functional file name.

GSTNAME Output GST analysis re-start file name.

RSTNAME Output re-start file name.

HISNAME Output history file name.

TLFNAME Output impulse forcing for tangent linear (TLM and RPM) models.

TLMNAME Output tangent linear file name.

ADJNAME Output adjoint file name.

AVGNAME Output averages file name.

DIANAME Output diagnostics file name.

STANAME Output stations file name.

FLTNAME Output floats file name.

Input ASCII parameters file names.

APARNAM Input assimilation parameters file name.

SPOSNAM Input stations positions file name.

FPOSNAM Input initial drifters positions file name.

BPARNAM Input biological parameters file name.

SPARNAM Input sediment transport parameters file name.

USRNAME USER's input generic file name.